Universität Bremen

Impact of melt water controlled material flux on the sedimentation in the western Baffin Bay and the circum-Greenland marginal seas

Dissertation

Zur Erlangung des Doktorgrades der Naturwissenschaften
- Dr. rer. nat. –

im Fachbereich Geowissenschaften (FB5)
der Universität Bremen

vorgelegt von

Johanna Hingst

MARUM – Zentrum für Marine Umweltwissenschaften

Bremen, März 2023

marum
Zentrum für Marine Umweltwissenschaften
Universität Bremen

Erstgutachterin	Prof. Dr. Simone A. Kasemann MARUM – Zentrum für Marine Umweltwissenschaften, Universität Bremen
Zweitgutachter	Prof. Dr. Cristiano M. Chiessi University of São Paulo

Datum des Promotionskolloquiums: 08. Juni 2023

Versicherung an Eides Statt / *Affirmation in lieu of an oath*

gem. § 5 Abs. 5 der Promotionsordnung vom 18.06.2018 /
according to § 5 (5) of the Doctoral Degree Rules and Regulations of 18 June, 2018

Ich / I, Johanna Hingst_____
(Vorname / First *Name*, Name / *Name*, Anschrift / *Address*, ggf. Matr.-Nr. / *student ID no., if applicable)*

versichere an Eides Statt durch meine Unterschrift, dass ich die vorliegende Dissertation selbständig und ohne fremde Hilfe angefertigt und alle Stellen, die ich wörtlich dem Sinne nach aus Veröffentlichungen entnommen habe, als solche kenntlich gemacht habe, mich auch keiner anderen als der angegebenen Literatur oder sonstiger Hilfsmittel bedient habe und die zu Prüfungszwecken beigelegte elektronische Version (PDF) der Dissertation mit der abgegebenen gedruckten Version identisch ist. / *With my signature I affirm in lieu of an oath that I prepared the submitted dissertation independently and without illicit assistance from third parties, that I appropriately referenced any text or content from other sources, that I sed only literature and resources listed in the dissertation, and that the electronic (PDF) and printed versions of the dissertation are identical.*

Ich versichere an Eides Statt, dass ich die vorgenannten Angaben nach bestem Wissen und Gewissen gemacht habe und dass die Angaben der Wahrheit entsprechen und ich nichts verschwiegen habe*. / I affirm in lieu of an oath that the information provided herein to the best of my knowledge is true and complete.*

Die Strafbarkeit einer falschen eidesstattlichen Versicherung ist mir bekannt, namentlich die Strafandrohung gemäß § 156 StGB bis zu drei Jahren Freiheitsstrafe oder Geldstrafe bei vorsätzlicher Begehung der Tat bzw. gemäß § 161 Abs. 1 StGB bis zu einem Jahr Freiheitsstrafe oder Geldstrafe bei fahrlässiger Begehung. / *I am aware that a false affidavit is a criminal offence which is punishable by law in accordance with § 156 of the German Criminal Code (StGB) with up to three years imprisonment or a fine in case of intention, or in accordance with § 161 (1) of the German Criminal Code with up to one year imprisonment or a fine in case of negligence.*

Bremen,_____ _____
(Ort / *Place*, Datum / *Date*) (Unterschrift / *Signature*)

Preface

This thesis was submitted for the doctoral degree of natural science (Dr. rer. nat.) to the Faculty of Geoscience of the University of Bremen. The PhD project was incorporated into the International Research Group ArcTrain, which aims to study processes and impacts of climate change in the North Atlantic Ocean and the Canadian Arctic. The presented research was supervised by Prof. Dr. Simone A. Kasemann and conducted at the Isotope Geochemistry Lab of MARUM – Center for Marine Environmental Science and the Faculty of Geosciences, University of Bremen, Germany. The thesis was written in a cumulative format, including three manuscripts. Below, a short summary of all chapters is given.

Chapter 1 introduces the project and describes the scientific motivation, the regional setting, the isotope systems used, and the main research aims of this PhD thesis.

Chapter 2 introduces the methodology, including a description of the sample material and the laboratory procedure.

Chapter 3 provides an overview of the manuscripts, including a summary and the different authors' contributions.

Chapter 4 presents the first manuscript *Deglacial and Holocene sediment dynamics and provenances off Lancaster Sound: implications for paleoenvironmental conditions in northern Baffin Bay*. The manuscript discusses variations in sediment deposition at the mouth of Lancaster Sound, northern Baffin Bay, under changing conditions of deglaciation.

Chapter 5 contains the second manuscript *Holocene variability of the northeastern Laurentide Ice Sheet in the Clyde Inlet area, western Baffin Bay, from radiogenic isotope records in marine sediments*. Two marine sediment records from western Baffin Bay reflect changing detrital sediment sources related to deglaciation processes on Baffin Island.

Chapter 6 presents the third manuscript *Marine radiogenic isotope record from Barrow Strait reveals late Pleistocene to early Holocene ice sheet dynamics in the Canadian Arctic Archipelago*, which discuss changing detrital sediment provenances in a sediment core from Barrow Strait that are related to past ice margin fluctuations and variations in meltwater discharge.

Chapter 7 summarizes the main results of the three manuscripts, formulates the main conclusions of this thesis, and shows potential perspectives for future research.

Contents

Abstract

The Arctic is highly sensitive to present climate change and is known to be affected by higher degrees of warming than any other region. Since the Arctic is strongly linked to the global climate system by atmospheric and oceanic circulations, it is crucial to learn more about present and possible future environmental changes in the region. Ice sheets, ice caps, and glaciers play an important role in the Arctic system. In the northern hemisphere, the Greenland Ice Sheet (GIS) and glaciers of the Canadian Arctic comprise most of the glacier ice and act as a large freshwater storage. While the area of glacier ice is already decreasing, future climate warming could accelerate melting and related freshwater input into the oceans, which would significantly affect the sea-level rise and the global ocean circulation system.

To learn more about the sensitivity of ice sheets and glaciers to climate change, the reconstruction of past ice sheet deglaciation patterns is a helpful tool. An interesting research area for ice sheet reconstruction is the Baffin Bay, which is located between Greenland and the Canadian Arctic and connects the Arctic Ocean with the Labrador Sea. During the last glacial cycle, the basin was surrounded by three ice sheets. While the GIS extended onto the western Greenland shelf, the Innuitian Ice Sheet (IIS) covered the Canadian Arctic Archipelago (CAA) in the north of Baffin Bay, and the northeastern Laurentide Ice Sheet (LIS) extended onto the Baffin Island shelf in the west. Many studies focused on the GIS history and related past changes in meltwater discharge and its consequences for ocean circulation. However, detailed reconstructions of ice sheet dynamics in western Baffin Bay are still limited.

Provenance studies on marine sediments from western Baffin Bay can provide insight into past changes in sediment supply and transport pathways and thus give valuable information about regional ice sheet dynamics and palaeoceanographic conditions. This study analyzed the radiogenic Sr, Nd, and Pb isotope composition of the detrital sediment fraction of four sediment cores from western and northern Baffin Bay and the CAA. Radiogenic isotope compositions are imprints of bedrock erosion along the active ice margin and display temporal and spatial variations in meltwater discharge. The data of the four sediment cores are used to trace changes in the detrital sediment provenance and related ice sheet dynamics in three different areas during the late Pleistocene and throughout the Holocene.

The marine sediment cores from northern Baffin Bay (GeoB22336-4) and the CAA (PS72/287-3) give information about the deglaciation of the LIS and IIS and related past environmental changes in northern Baffin Bay. Sedimentological, mineralogical, and radiogenic isotope data of GeoB22336-4 reflect the presence of a grounded ice stream off Lancaster Sound, the ice margin retreat during

the late Pleistocene and early Holocene, and the opening of the Barrow Strait – Lancaster Sound connection after ~ 10.2 ka BP. Radiogenic isotope data from Barrow Strait confirm the landward ice margin retreat after ~ 10 ka BP. The opening of the Arctic gateways and the resultant establishment of an Arctic – Atlantic throughflow influenced the material transport in Baffin Bay. During the mid-Holocene, sedimentological data suggest an increasing input of sea-ice rafted sediment in northern Baffin Bay, probably related to a stronger influence of the West Greenland Current. Additional measurements of the radiogenic isotope composition on sediment leachates of PS72/287-3 indicate a strong influence of leached detrital carbonates on, especially the Pb isotope signatures.

Two sediment cores from the Clyde Inlet (GeoB22346-3 and GeoB22357-3), a fjord on northeastern Baffin Island, provide insights into the late Pleistocene and Holocene deglaciation history of an outlet glacier of the northeastern LIS. Changing radiogenic isotope data within the fjord reflect short-term ice margin fluctuations during the early Holocene. During the mid-Holocene, Sr and Pb isotope data were strongly influenced by changing sediment mineralogy related to changing meltwater intensities after the ice margin retreated from the fjord head. On the shelf in front of the Inlet, radiogenic isotope signatures suggest slight variations in the sediment source of the continental detritus during the early Holocene, likely related to changing sediment transport patterns in western Baffin Bay associated with the onset of the Arctic-Atlantic throughflow.

Overall, this thesis provides new details on the late Pleistocene and Holocene deglaciation history of the LIS and IIS and related changes in sediment transport processes in western and northern Baffin Bay. Further, the identification of changing sediment provenance of detrital material in marine sediment cores from northern Baffin Bay and Barrow Strait helped to determine better the timing of the opening of these Arctic gateways and the inflow of Arctic waters into Baffin Bay.

Kurzfassung

Die Arktis reagiert sehr empfindlich auf den gegenwärtigen Klimawandel und ist von einer stärkeren Erwärmung betroffen als jede andere Region auf der Erde. Da die Arktis über atmosphärische und ozeanische Zirkulationen eng mit dem globalen Klimasystem verbunden ist, ist es von entscheidender Bedeutung, mehr über die heutigen und möglichen zukünftigen Umweltveränderungen in der Region zu erfahren. Eisschilde, Eiskappen und Gletscher spielen eine wichtige Rolle im System der Arktis. In der nördlichen Hemisphäre machen der grönländische Eisschild und die Gletscher der kanadischen Arktis den größten Teil des Gletschereises aus und dienen als großer Süßwasserspeicher. Während die Fläche des Gletschereises bereits rapide abnimmt, könnte die künftige Klimaerwärmung das Abschmelzen und den damit verbundenen Süßwassereintrag in die Ozeane noch beschleunigen, was den Anstieg des Meeresspiegels und das globale Ozeanzirkulationssystem erheblich beeinflussen würde.

Um mehr über die Empfindlichkeit von Eisschilden und Gletschern gegenüber dem Klimawandel zu erfahren, ist die Rekonstruktion des Abschmelzens von vergangenen Eisschilden ein hilfreiches Instrument. Ein interessantes Forschungsgebiet für die Rekonstruktion vergangener Eisschilddynamiken ist die Baffin Bay, die sich zwischen Grönland und der kanadischen Arktis erstreckt und den Arktischen Ozean mit dem Nordatlantik verbindet. Während des letzten Eiszeitzyklus war die Baffin Bay von drei Eisschilden umgeben. Der grönländische Eisschild erstreckte sich auf den westlichen grönländischen Schelf, der Innuitische Eisschild bedeckte das Kanadisch-Arktische Archipel im Norden der Baffin Bay, und der nordöstliche Teil des Laurentidischen Eisschilds erstreckte sich bis auf den Schelf der Baffininsel im Westen. Während sich viele Studien auf die glaziale Geschichte des grönländischen Eisschilds und auf die damit verbundenen früheren Veränderungen im Schmelzwasserabfluss und dessen Folgen auf die Ozeanzirkulation konzentrieren, sind ähnliche Studien in der westlichen Baffin Bay noch begrenzt.

Provenienzstudien an Meeressedimenten aus der westlichen Baffin Bay können Aufschluss über vergangene Veränderungen im Sedimenteintrag und dessen Transportwege geben und somit wertvolle Informationen über die regionale Eisschilddynamik und die paläozeanografischen Bedingungen geben. In dieser Studie wurden die radiogenen Sr-, Nd- und Pb-Isotopenzusammensetzungen der detritischen Sedimentfraktion von vier Sedimentkernen aus der westlichen und nördlichen Baffin Bay und aus dem Kanadisch-Arktische Archipel analysiert. Die radiogene Isotopenzusammensetzung ist geprägt von der Gesteinserosion entlang des aktiven Eisrandes und zeigt zeitliche und räumliche Variationen des Schmelzwasserabflusses an. Die Daten der vier Sedimentkerne werden verwendet, um Veränderungen in der Herkunft der detritischen

Sedimente und damit verbundenen Eisschilddynamiken in drei verschiedenen Gebieten während des späten Pleistozäns und des gesamten Holozäns zu verfolgen.

Die marinen Sedimentkerne aus der nördlichen Baffin Bay (GeoB22336-4) und dem Kanadisch-Arktischen Archipel (PS72/287-3) geben Aufschluss über das Abschmelzschema des Innuitischen und Laurentidischen Eisschilds und die damit verbundenen Umweltveränderungen in der nördlichen Baffin Bay. Die sedimentologischen und mineralogischen Daten, sowie die Untersuchung der radiogenen Isotopen spiegeln das Vorhandensein des Eisstroms vor Lancaster Sound, den Rückzug des Eisrandes während des späten Pleistozäns und frühen Holozäns sowie die Öffnung der Verbindung zwischen Barrow Strait und Lancaster Sound nach ~ 10.2 ka BP wider. Radiogene Isotopendaten aus der Barrow Strait bestätigen den landwärtigen Rückzug des Eisrandes nach ~ 10 ka BP. Die Öffnung dieser Wasserstraßen und die daraus resultierende Etablierung eines arktisch-atlantischen Wasserdurchflusses beeinflussten den Sedimenttransport in der Baffin Bay. Während des mittleren Holozäns deuten sedimentologische Daten auf einen zunehmenden Eintrag von meereistransportierten Sedimenten in die nördliche Baffin Bay hin, was vermutlich auf einen stärkeren Einfluss des Westgrönlandstroms hinweist. Zusätzliche Messungen von radiogenen Isotopenzusammensetzungen an der gelösten Sedimentfraktion in PS72/287-3 deuten auf einen starken Einfluss von gelösten detritischen Karbonaten auf die Pb-Isotopensignaturen hin.

Zwei Sedimentkerne vom Clyde Inlet (GeoB22346-3 und GeoB22357-3), einem Fjord auf der nordöstlichen Baffininsel, geben Aufschluss über die spätpleistozäne und holozäne Abschmelzgeschichte eines Auslassgletschers des nordöstlichen Laurentidischen Eisschilds. Wechselnde radiogene Isotopendaten innerhalb des Fjords spiegeln kurzfristige Schwankungen des Eisrandes während des frühen Holozäns wider. Während des mittleren Holozäns sind die Sr- und Pb-Isotopendaten stark von der sich verändernden Sedimentmineralogie beeinflusst, die wiederum mit den veränderten Schmelzwasserintensitäten zusammenhängt, nachdem sich das Eis aus dem Fjord zurückgezogen hat. Auf dem vorgelagerten Schelf deuten radiogene Isotopensignaturen auf leichte Veränderungen in der Herkunft des detritischen Materials während des frühen Holozäns hin, was wahrscheinlich mit veränderten Sedimenttransportmustern in der westlichen Baffin Bay im Zusammenhang mit dem einsetzenden arktischen-atlantischen Meeresdurchflusses zusammenhängt.

Insgesamt liefert diese Arbeit neue Details über die spätpleistozäne und holozäne Abschmelzgeschichte des Laurentidischen und Innuitischen Eisschilds und die damit verbundenen Veränderungen der Sedimenttransportprozesse in der westlichen Baffin Bay. Darüber hinaus hat die Identifizierung von Veränderungen des Ursprungs von detritischen Material in Sedimentkernen

aus der nördlichen Baffin Bay und der Barrow Strait dazu beigetragen, den Zeitpunkt der Öffnung der arktischen Meeresstraßen besser zu bestimmen.

1. Introduction

1.1 Motivation

The Arctic is a region located at the northernmost part of the Earth, encompassing the Arctic Ocean and parts of Canada, Russia, Alaska, Norway, Finland, Sweden, and Greenland (Denmark). It is defined as the area above the Arctic Circle at 66°33'N, and it is one of the most sensitive environments on the planet. The Arctic is extremely vulnerable to present and projected future climate change (Anisimov et al., 2007). Climate observations and projections show that the Arctic is witnessing higher degrees of warming than any other region in the world (Overland et al., 2019), an effect also known as Arctic amplification. The Arctic amplification is the result of different physical processes, including albedo feedback, sea ice loss, cloud cover, and water vapor (Serreze and Barry, 2011). Albedo feedback, a positive climate feedback, is responsible for the increasing surface temperature due to a decreasing area of sea ice, glaciers, and ice sheets. The increase in the dark snow/ice-free area leads to stronger absorption of solar radiation and higher air temperatures, thus further enhancing ice melting (Serreze and Barry, 2011). Additionally, the diminishing area of sea ice contributes to atmospheric warming, exposing the relatively warm Arctic Ocean surface, resulting in enhanced absorption of solar radiation and increased heat loss to the overlying atmosphere (Serreze and Barry, 2011).

Changes happening in the Arctic due to climate warming will probably have regional but also global consequences. For instance, collapsing permafrost and sea ice retreat strongly affect the Arctic communities' infrastructure (Ford et al., 2021). Due to the north-south heat and water exchange, circulation of the atmosphere and ocean, and the global carbon cycle, the Arctic is directly linked to the global climate system (Overland et al., 2019). Today, the lateral extent of multiyear, thick sea ice in the Arctic Ocean is rapidly decreasing, indicating the dramatic speed of Arctic climate change (Overland et al., 2019). The extent of the multiyear sea ice is today 60 % smaller than in the 1980s (AMAP, 2017). Besides the sea ice loss, climate change has various consequences for the Arctic realm. On land, the thawing of ice-rich permafrost in the Arctic lead to irreversible release of water, CO_2 and methane (Overland et al., 2019). The permafrost degradation is not only accelerated by warmer air temperatures but also sea ice-free coastlines enable higher erosion rates in coastal areas (Overland et al., 2019). Also, the Greenland Ice Sheet (GIS) as well as smaller ice caps and glaciers in the Arctic, which act as important storage of freshwater, have experienced accelerated melting over the last decades (Gardner et al., 2011; Kjeldsen et al., 2015).

Increasing air and ocean temperatures accelerate the retreat of large Greenland outlet glaciers, mainly causing the huge mass loss of the GIS (Andresen et al., 2012). The ice mass loss results in the

lowering of the GIS´s surface elevation and the exposure to the warmer air temperatures of the lower atmosphere and consequently to further increase of melting. This positive feedback, also described as melt-elevation feedback, can be a crucial mechanism for a possible future destabilization of the GIS (Boers and Rypdal, 2021). A destabilization of the GIS and near-complete melting could have global consequences, including a maximum sea-level rise of about 7 m (Church et al., 2013). Besides the influence on the global sea-level, the enhanced release of freshwater in the Arctic can also affect major ocean circulations. The melting of the GIS results in a freshening of the North Atlantic (Bamber et al., 2012), which can affect the formation of the North Atlantic Deep Water (NADW) and influence the Atlantic Meridional Overturning Circulation (AMOC) (Böning et al., 2016). Significant amounts of freshwater from the Arctic Ocean and the melting of the GIS and the glaciers in the high Canadian Arctic are transported through Baffin Bay and Labrador Sea into the North Atlantic. Paleoclimate studies in the North Atlantic investigated that large inputs of meltwater into the Labrador Sea strongly affected the AMOC with significant consequences for the northern Hemisphere climate during the early Holocene (e.g., Alley and Agustsdottir, 2005; Bamberg et al., 2010; Hillaire-Marcel et al., 2007). That highlights the high relevance of the ice sheets and glaciers for the climate system.

1.2 Introduction to the Research Area

The majority of today´s glacier ice in the northern Hemisphere is contained in the GIS and in glaciers of the Canadian Arctic Archipelago (CAA) (Gardner et al., 2013). In addition to the GIS, the Laurentide and Innuitian Ice Sheets (LIS, IIS) covered large parts of North America and the CAA during the Late Quaternary. Therefore, northeastern North America is a perfect area to study the response of past and present ice sheets and glaciers to climate change (Briner et al., 2016).

Baffin Bay is a narrow (approximately 450 km wide, 1300 km long), semi-enclosed ocean basin between Greenland and the Canadian Arctic (Fig. 1-1), with a maximal water depth of 2500 m in its central part (Simon et al., 2014). The basin is the product of the North Atlantic-Labrador Sea rift system (Maclean et al., 1990), resulting in a similar geology on both sides of Baffin Bay. It is connected to the Arctic Ocean in the north via Nares Strait and channels of the CAA and in the south via Davis Strait to the Labrador Sea. The broad west Greenland continental shelf (> 250 km) and the relatively narrow Baffin Island shelf (max. 50 km) (Bennett et al., 2013; Simon et al., 2014) are cut by major cross-shelf troughs, which probably result from glacial erosion by marine-terminating outlet glaciers during full glacial periods of the Quaternary (Batchelor and Dowdeswell, 2014).

Because of its interesting setting and glacial history (cf. 1.2.2), Baffin Bay is highly important for studying past ice sheet dynamics and related oceanographic changes.

1.2.1 Modern Oceanography and Sea Ice extent

Baffin Bay´s modern anti-cyclonic circulation is characterized by the inflow of relatively warm waters via Davis Strait, which compose of cooler polar waters transported southward along the eastern coast of Greenland that merge with warmer and more saline Atlantic waters transported northward by the Irminger Current (Fig. 1-1) (Tang et al., 2004). These waters form in Baffin Bay the West Greenland current and travel northward along the west Greenland margin (Tang et al., 2004). In northern Baffin Bay, the current meets cold Arctic waters, which enter the basin via Nares Strait, Lancaster Sound, Jones Sound, and smaller channels of the CAA and feed the Baffin Current (BC) (Münchow et al., 2015; Tang et al., 2004). The BC transports the relatively cold, fresh waters southward along eastern Baffin Island and through Davis Strait into the Labrador Sea (Tang et al., 2004). Münchow et al. (2015) suggested describing both currents better as current systems since they are characterized by several velocity cores and eddies. Baffin Bay is covered by sea ice most of the year, with maximum ice extent in March and minimum ice extent in August and September (Tang et al., 2004). Icebergs of significant size in Baffin Bay are mainly produced by glaciers of west Greenland and are transported north and south depending on their size (Tang et al., 2004).

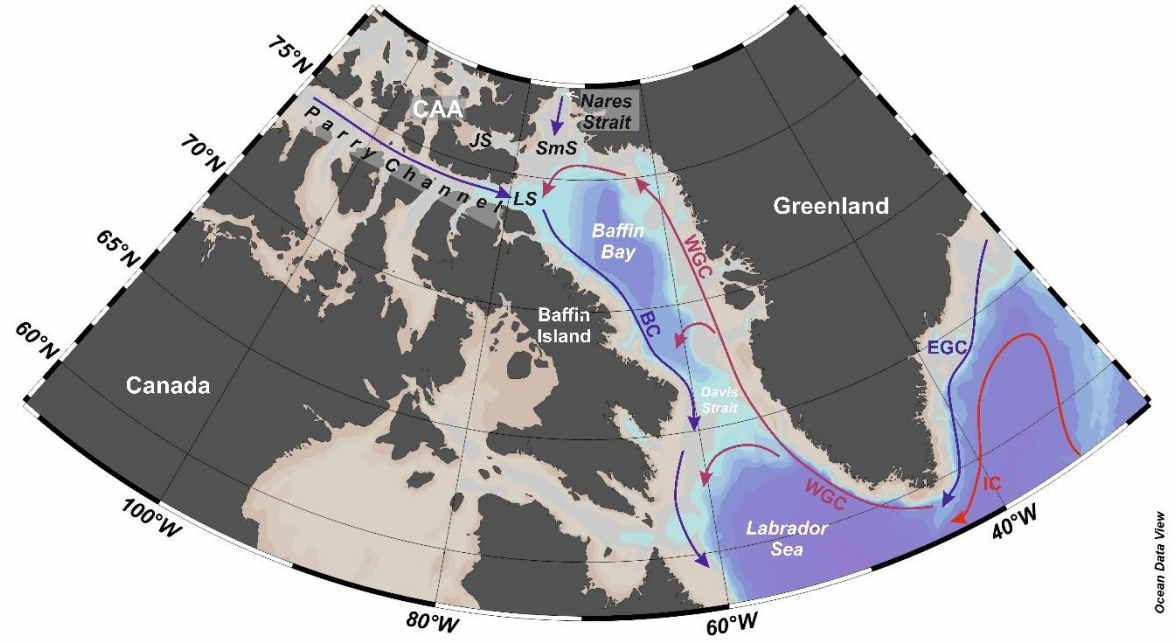

Figure 1-1: Overview map of the research area with simplified modern-day surface ocean circulation (Myers et al., 2009; Tang et al., 2004). Used abbreviations: EGC, East Greenland Current; IC, Irminger Current; WGC, West Greenland Current; BC, Baffin Current; SmS, Smith Sound; JS, Jones Sound; LS, Lancaster Sound; CAA, Canadian Arctic Archipelago. Map created with Ocean Data View (Schlitzer, 2020).

1.2.2 Glacial History

During the Last Glacial Maximum (LGM; locally between ~ 25 and 16 ka BP), Baffin Bay was surrounded by three large ice sheets forming a nearly continuous belt of ice around the basin, draining Greenland and the Canadian Arctic (Dyke et al., 2002; Simon et al., 2014). To the east of Baffin Bay, the GIS extended onto the Greenland shelf, while to the north, the IIS covered the CAA and the northeastern LIS, to the west, extended onto the Baffin Island shelf during the LGM (e.g., Dalton et al., 2020; Dyke et al., 2002; Funder et al., 2011). The confluent ice sheets in the north of Baffin Bay blocked Nares Strait, Lancaster Sound, and smaller channels of the Arctic gateways, preventing the inflow of Arctic waters and ice into Baffin Bay (Dyke et al., 2002; Jennings et al., 2011; Pieńkowski et al., 2014). Marine-terminating grounded ice streams in Lancaster Sound and Smith Sound reached far seaward into northern Baffin Bay and drained the confluent ice sheets in these regions (Li et al., 2011; Margold et al., 2015, 2018). Additionally, there is evidence of a thick ice shelf that covered northern Baffin Bay and affected the stability of regional ice streams (Couette et al., 2022).

The asynchronous deglaciation of the ice sheets can be reconstructed, e.g., using marine sedimentary records from Baffin Bay, which recorded different periods of enhanced meltwater and iceberg release (Jackson et al., 2017). The initial retreat of the west GIS after ~ 15 ka BP (Ó Cofaigh et al., 2013) was not steady but interrupted by ice margin readvances during colder periods like the Younger Dryas (YD; 12.9 to 11.7 ka BP) (Jennings et al., 2014). Afterward, the GIS deglaciated more rapidly during the early Holocene and finally retreated from the shelf between 8.4 and 7.8 ka BP (Jennings et al., 2014; Slabon et al., 2016). The IIS also extended onto the shelf until the end of the YD and retreated steadily during the early Holocene (England et al., 2006). Ice-free sites on Baffin Island indicate the initial recession of the northeastern LIS by around 14 ka BP (Briner et al., 2009). Further deglaciation was interrupted by ice margin stabilization during the YD (Couette et al., 2023). Subsequent rapid deglaciation LIS outlet glaciers on Baffin Island between 12 and 10 ka BP was followed by a slower retreat of the ice margin throughout the Holocene, again interrupted by ice advances, e.g., during the 8.2 ka cold event (Briner et al., 2009; Young et al., 2012).

1.3 Radiogenic Isotopes as tracers for past ice sheet dynamics and oceanographic conditions

Radiogenic isotopes are the final product of a radioactive decay cascade. That means that in contrast to other stable isotopes, the concentrations of radiogenic isotopes increase over time. The ratio of a radiogenic and a stable isotope of the same element, e.g., $^{87}Sr/^{86}Sr$, with ^{87}Sr as the radiogenic isotope, is used in geosciences for tracing different processes. For example, radiogenic

isotope compositions can be used in sedimentary environments to trace the source and transport of detrital material (Banner, 2004). Additionally, they can be used to trace water masses and changes in ocean circulation or to date the timing of the formation of rocks and minerals (Banner, 2004; Frank, 2002).

Depending on their age, formation, and mineralogical composition, continental bedrocks have different Sr, Nd, and Pb isotope signatures ($^{87}Sr/^{86}Sr$, $^{143}Nd/^{144}Nd$, $^{206}Pb/^{204}Pb$, $^{207}Pb/^{204}Pb$, and $^{208}Pb/^{204}Pb$). These signatures can be identified in detrital constituents of marine sediments and therefore help to trace the spatial material input of continental detritus by river or meltwater discharge (e.g., Maccali et al., 2018; Reyes et al., 2014). While the Nd isotope composition is considered a reliable sediment provenance tracer, Sr and Pb isotope compositions can be influenced by additional parameters. For instance, grain-size effects can influence the Sr and chemical weathering the Pb isotope compositions (Eisenhauer et al., 1999; Tütken et al., 2002; von Blanckenburg and Nägler, 2001). Thus, the combination of all three radiogenic isotope systems should be considered for interpreting their ratios regarding sediment provenance. Sr, Nd, and Pb isotope composition in marine sediments from the Arctic Ocean, Baffin Bay, and the North Atlantic have been successfully used to identify the provenance of detrital material and assess associated changes of regional ice sheet dynamics and ocean circulation through time (Colville et al., 2011; Fagel et al., 2004; Fagel et al., 2014; Farmer et al., 2003; Reyes et al., 2014; Tütken et al., 2002).

1.4 Research Objectives

Previous studies using radiogenic isotope compositions for sediment provenance reconstructions in Baffin Bay concentrated on sediment cores from central western Baffin Bay, the central basin, along the western Greenland margin, and Nares Strait (Kirillova, 2017; Madaj, 2021). The studies reconstructed the main ice sheet dynamics around Baffin Bay during the late Pleistocene and Holocene. In particular, their data revealed the ice retreat of local glaciers and ice streams and related changes in sediment transport patterns along the west Greenland coast. Moreover, radiogenic isotope data from the Kane Basin in Nares Strait revealed changes in sediment provenances that help to assess the timing of the Nares Strait opening due to the retreating GIS and IIS. While these studies demonstrated that radiogenic isotopes in Baffin Bay marine sediments are valuable tracers for reconstructing ice sheet dynamics, little is still known about high-frequency ice sheet fluctuations and related sediment provenance changes during the late Pleistocene and Holocene along the Baffin Island coast. Moreover, additional sediment provenance reconstructions in northwestern Baffin Bay could gain new insight into the opening of Lancaster Sound and related changes in sediment transport processes and ocean circulation in western Baffin Bay.

Therefore, this research focuses on the spatial and temporal variations of meltwater discharge and material transport from the CAA and Baffin Island into Baffin Bay under changing conditions during the last deglaciation. Information about freshwater and material input is used to reconstruct past changes in the regional ice sheet and glacier dynamics in response to Holocene climate changes. In this study, we analyzed four high-resolution marine sedimentary records from western and northern Baffin Bay and used the radiogenic isotope composition of the continental detritus to trace the sediment provenance. The data are used to answer the following research questions:

1. Are there spatial and temporal changes in meltwater discharge along the Baffin Island margin that can be associated with high-frequency fluctuations of the northeastern Laurentide Ice Sheet during the last deglaciation?
2. How affected the deglaciation of the Laurentide and Innuitian ice sheets sediment transport pathways in western Baffin Bay?

References

Alley, R., Agustsdottir, A., 2005. The 8k event: cause and consequences of a major Holocene abrupt climate change. Quaternary Science Reviews 24, 1123-1149.

AMAP, 2017. Snow, Water, Ice and Permafrost in the Arctic (SWIPA), Arctic Monitoring Assessment Programme (AMAP), Oslo, Norway.

Andresen, C.S., Straneo, F., Ribergaard, M.H., Bjørk, A.A., Andersen, T.J., Kuijpers, A., Nørgaard-Pedersen, N., Kjær, K.H., Schjøth, F., Weckström, K., Ahlstrøm, A.P., 2012. Rapid response of Helheim Glacier in Greenland to climate variability over the past century. Nature Geoscience 5, 37-41.

Anisimov, O.A., Vaughan, D.G., Callaghan, T.V., Furgal, C., Marchant, H., Prowse, T.D., Vilhjálmsson, H., Walsh, J.E., 2007. Polar regions (arctic and antarctic). Climate change 15, 653-685.

Bamber, J., van den Broeke, M., Ettema, J., Lenaerts, J., Rignot, E., 2012. Recent large increases in freshwater fluxes from Greenland into the North Atlantic. Geophysical Research Letters 39, n/a-n/a.

Bamberg, A., Rosenthal, Y., Paul, A., Heslop, D., Mulitza, S., Rühlemann, C., Schulz, M., 2010. Reduced North Atlantic Central Water formation in response to early Holocene ice-sheet melting. Geophysical Research Letters 37.

Banner, J.L., 2004. Radiogenic isotopes: systematics and applications to earth surface processes and chemical stratigraphy. Earth-Science Reviews 65, 141-194.

Batchelor, C.L., Dowdeswell, J.A., 2014. The physiography of High Arctic cross-shelf troughs. Quaternary Science Reviews 92, 68-96.

Bennett, R., Campbell, D.C., Furze, M.F.A., 2013. The shallow stratigraphy and geohazards of the Northeast Baffin Shelf and Lancaster Sound. Geological Survey of Canada Open File 7355.

Boers, N., Rypdal, M., 2021. Critical slowing down suggests that the western Greenland Ice Sheet is close to a tipping point. PNAS 118.

Böning, C.W., Behrens, E., Biastoch, A., Getzlaff, K., Bamber, J.L., 2016. Emerging impact of Greenland meltwater on deepwater formation in the North Atlantic Ocean. Nature Geoscience 9, 523-527.

Briner, J.P., Davis, P.T., Miller, G.H., 2009. Latest Pleistocene and Holocene glaciation of Baffin Island, Arctic Canada: key patterns and chronologies. Quaternary Science Reviews 28, 2075-2087.

Briner, J.P., McKay, N.P., Axford, Y., Bennike, O., Bradley, R.S., de Vernal, A., Fisher, D., Francus, P., Fréchette, B., Gajewski, K., Jennings, A., Kaufman, D.S., Miller, G., Rouston, C., Wagner, B., 2016. Holocene climate change in Arctic Canada and Greenland. Quaternary Science Reviews 147, 340-364.

Church, J.A., Clark, P.U., Cazenave, A., Gregory, J.M., Jevrejeva, S., Levermann, A., Merrifield, M.A., Milne, G.A., Nerem, R.S., Nunn, P.D., 2013. Sea level change. PM Cambridge University Press.

Colville, E.J., Carlson, A.E., Beard, B.L., Hatfield, R.G., Stoner, J.S., Reyes, A.V., Ullman, D.J., 2011. Sr-Nd-Pb isotope evidence for ice-sheet presence on southern Greenland during the Last Interglacial. Science 333, 620-623.

Couette, P.-O., Lajeunesse, P., Ghienne, J.-F., Dorschel, B., Gebhardt, C., Hebbeln, D., Brouard, E., 2022. Evidence for an extensive ice shelf in northern Baffin Bay during the Last Glacial Maximum. Communications Earth & Environment 3.

Couette, P.-O., Lajeunesse, P., Ghienne, J.-F., Dorschel, B., Gebhardt, C., Hebbeln, D., Brouard, E., 2023. Retreat and stabilization of a marine-based ice margin along a high arctic fjord-cross-shelf trough system. Quaternary Science Reviews 302, 107949.

Dalton, A.S., Margold, M., Stokes, C.R., Tarasov, L., Dyke, A.S., Adams, R.S., Allard, S., Arends, H.E., Atkinson, N., Attig, J.W., Barnett, P.J., Barnett, R.L., Batterson, M., Bernatchez, P., Borns, H.W., Breckenridge, A., Briner, J.P., Brouard, E., Campbell, J.E., Carlson, A.E., Clague, J.J., Curry, B.B., Daigneault, R.-A., Dubé-Loubert, H., Easterbrook, D.J., Franzi, D.A., Friedrich, H.G., Funder, S., Gauthier, M.S., Gowan, A.S., Harris, K.L., Hétu, B., Hooyer, T.S., Jennings, C.E., Johnson, M.D., Kehew, A.E., Kelley, S.E., Kerr, D., King, E.L., Kjeldsen, K.K., Knaeble, A.R., Lajeunesse, P., Lakeman, T.R., Lamothe, M., Larson, P., Lavoie, M., Loope, H.M., Lowell, T.V., Lusardi, B.A., Manz, L., McMartin, I., Nixon, F.C., Occhietti, S., Parkhill, M.A., Piper, D.J.W., Pronk, A.G., Richard, P.J.H., Ridge, J.C., Ross, M., Roy, M., Seaman, A., Shaw, J., Stea, R.R., Teller, J.T., Thompson, W.B., Thorleifson, L.H., Utting, D.J., Veillette, J.J., Ward, B.C., Weddle, T.K., Wright, H.E., 2020. An updated radiocarbon-based ice margin chronology for the last deglaciation of the North American Ice Sheet Complex. Quaternary Science Reviews 234, 106223.

Dyke, A.S., Andrews, J.T., Clark, P.U., England, J.H., Miller, G.H., Shaw, J., Veillette, J.J., 2002. The Laurentide and Innuitian ice sheets during the Last Glacial Maximum.

Eisenhauer, A., Meyer, H., Rachold, V., Tütken, T., Wiegand, B., Hansen, B.T., Spielhagen, R.F., Lindemann, F., Kassens, H., 1999. Grain size separation and sediment mixing in Arctic Ocean sediments: evidence from the strontium isotope systematic. Chemical Geology 158, 173-188.

England, J., Atkinson, N., Bednarski, J., Dyke, A.S., Hodgson, D.A., Ó Cofaigh, C., 2006. The Innuitian Ice Sheet: configuration, dynamics and chronology. Quaternary Science Reviews 25, 689-703.

Fagel, N., Hillaire-Marcel, C., Humblet, M., Brasseur, R., Weis, D., Stevenson, R., 2004. Nd and Pb isotope signatures of the clay-size fraction of Labrador Sea sediments during the Holocene: Implications for the inception of the modern deep circulation pattern. Paleoceanography 19, n/a-n/a.

Fagel, N., Not, C., Gueibe, J., Mattielli, N., Bazhenova, E., 2014. Late Quaternary evolution of sediment provenances in the Central Arctic Ocean: mineral assemblage, trace element composition and Nd and Pb isotope fingerprints of detrital fraction from the Northern Mendeleev Ridge. Quaternary Science Reviews 92, 140-154.

Farmer, G.L., Barber, D., Andrews, J., 2003. Provenance of Late Quaternary ice-proximal sediments in the North Atlantic: Nd, Sr and Pb isotopic evidence. Earth and Planetary Science Letters 209, 227-243.

Frank, M., 2002. Radiogenic isotopes: Tracers of past ocean circulation and erosional input. Reviews of Geophysics 40.

Funder, S., Kjeldsen, K.K., Kjær, K.H., Ó Cofaigh, C., 2011. The Greenland Ice Sheet During the Past 300,000 Years: A Review. 15, 699-713.

Gardner, A.S., Moholdt, G., Cogley, J.G., Wouters, B., Arendt, A.A., Wahr, J., Berthier, E., Hock, R., Pfeffer, W.T., Kaser, G., 2013. A reconciled estimate of glacier contributions to sea level rise: 2003 to 2009. science 340, 852-857.

Gardner, A.S., Moholdt, G., Wouters, B., Wolken, G.J., Burgess, D.O., Sharp, M.J., Cogley, J.G., Braun, C., Labine, C., 2011. Sharply increased mass loss from glaciers and ice caps in the Canadian Arctic Archipelago. Nature 473, 357-360.

Hillaire-Marcel, C., De Vernal, A., Piper, D.J., 2007. Lake Agassiz final drainage event in the northwest North Atlantic. Geophysical Research Letters 34.

Jackson, R., Carlson, A.E., Hillaire-Marcel, C., Wacker, L., Vogt, C., Kucera, M., 2017. Asynchronous instability of the North American-Arctic and Greenland ice sheets during the last deglaciation. Quaternary Science Reviews 164, 140-153.

Jennings, A.E., Sheldon, C., Cronin, T.M., Francus, P., Stoner, J.S., Andrews, J.T., 2011. The Holocene History of Nares Strait. Focus on Geology Special Issue on Arctic Oceanography.

Jennings, A.E., Walton, M.E., Ó Cofaigh, C., Kilfeather, A., Andrews, J.T., Ortiz, J.D., De Vernal, A., Dowdeswell, J.A., 2014. Paleoenvironments during Younger Dryas-Early Holocene retreat of the Greenland Ice Sheet from outer Disko Trough, central west Greenland. Journal of Quaternary Science 29, 27-40.

Kirillova, V., 2017. Radiogenic isotopes on marine sediments from the Baffin Bay: implications for the sediment supply during the last deglaciation. Dissertation, Faculty of Geosciences, University Bremen, Bremen, Germany.

.

Kjeldsen, K.K., Korsgaard, N.J., Bjork, A.A., Khan, S.A., Box, J.E., Funder, S., Larsen, N.K., Bamber, J.L., Colgan, W., van den Broeke, M., Siggaard-Andersen, M.L., Nuth, C., Schomacker, A., Andresen, C.S., Willerslev, E., Kjaer, K.H., 2015. Spatial and temporal distribution of mass loss from the Greenland Ice Sheet since AD 1900. Nature 528, 396-400.

Li, G., Piper, D.J.W., Campbell, D.C., 2011. The Quaternary Lancaster Sound trough-mouth fan, NW Baffin Bay. Journal of Quaternary Science 26, 511-522.

Maccali, J., Hillaire-Marcel, C., Not, C., 2018. Radiogenic isotope (Nd, Pb, Sr) signatures of surface and sea ice-transported sediments from the Arctic Ocean under the present interglacial conditions. Polar Research 37, 1442982.

Maclean, B., Williams, G.L., Srivastava, S.P., 1990. Geology of Baffin Bay and Davis Strait, in: Keen, M.J., Williams, G.L. (Eds.), Geology of Canada No.2: Geology of the continental margin of eastern Canada, Geological Survey of Canada, pp. 293-348.

Madaj, L., 2021. Holocene Ice Sheet Dynamics and Detriral Provenance Shifts Along the West Greenland Margin Recorded by Radiogenic Isotopes. Dissertation, Faculty of Geosciences, University Bremen, Bremen, Germany.

Margold, M., Stokes, C.R., Clark, C.D., 2015. Ice streams in the Laurentide Ice Sheet: Identification, characteristics and comparison to modern ice sheets. Earth-Science Reviews 143, 117-146.

Margold, M., Stokes, C.R., Clark, C.D., 2018. Reconciling records of ice streaming and ice margin retreat to produce a palaeogeographic reconstruction of the deglaciation of the Laurentide Ice Sheet. Quaternary Science Reviews 189, 1-30.

Münchow, A., Falkner, K.K., Melling, H., 2015. Baffin Island and West Greenland Current Systems in northern Baffin Bay. Progress in Oceanography 132, 305-317.

Myers, P.G., Donnelly, C., Ribergaard, M.H., 2009. Structure and variability of the West Greenland Current in summer derived from 6 repeat standard sections. Progress in Oceanography 80, 93-112.

Ó Cofaigh, C., Dowdeswell, J.A., Jennings, A.E., Hogan, K.A., Kilfeather, A., Hiemstra, J.F., Noormets, R., Evans, J., McCarthy, D.J., Andrews, J.T., Lloyd, J.M., Moros, M., 2013. An extensive and dynamic ice sheet on the West Greenland shelf during the last glacial cycle. Geology 41, 219-222.

Overland, J., Dunlea, E., Box, J.E., Corell, R., Forsius, M., Kattsov, V., Olsen, M.S., Pawlak, J., Reiersen, L.-O., Wang, M., 2019. The urgency of Arctic change. Polar Science 21, 6-13.

Pieńkowski, A.J., England, J.H., Furze, M.F.A., MacLean, B., Blasco, S., 2014. The late Quaternary environmental evolution of marine Arctic Canada: Barrow Strait to Lancaster Sound. Quaternary Science Reviews 91, 184-203.

Reyes, A.V., Carlson, A.E., Beard, B.L., Hatfield, R.G., Stoner, J.S., Winsor, K., Welke, B., Ullman, D.J., 2014. South Greenland ice-sheet collapse during Marine Isotope Stage 11. Nature 510, 525-528.

Schlitzer, R., 2020. Ocean Data View, https://odv.awi.de.

Serreze, M.C., Barry, R.G., 2011. Processes and impacts of Arctic amplification: A research synthesis. Global and Planetary Change 77, 85-96.

Simon, Q., Hillaire-Marcel, C., St-Onge, G., Andrews, J.T., 2014. North-eastern Laurentide, western Greenland and southern Innuitian ice stream dynamics during the last glacial cycle. Journal of Quaternary Science 29, 14-26.

Slabon, P., Dorschel, B., Jokat, W., Myklebust, R., Hebbeln, D., Gebhardt, C., 2016. Greenland ice sheet retreat history in the northeast Baffin Bay based on high-resolution bathymetry. Quaternary Science Reviews 154, 182-198.

Tang, C.C.L., Ross, C.K., Yao, T., Petrie, B., DeTracey, B.M., Dunlap, E., 2004. The circulation, water masses and sea-ice of Baffin Bay. Progress in Oceanography 63, 183-228.

Tütken, T., Eisenhauer, A., Wiegand, B., Hansen, B.T., 2002. Glacial-interglacial cycles in Sr and Nd isotopic composition of Arctic marine sediments triggered by the Svalbard/Barents Sea ice sheet. Marine Geology 182, 351-372.

von Blanckenburg, F., Nägler, T.F., 2001. Weathering versus circulation-controlled changes in radiogenic isotope tracer composition of the Labrador Sea and North Atlantic Deep Water. Paleoceanography 16, 424-434.

Young, N.E., Briner, J.P., Rood, D.H., Finkel, R.C., 2012. Glacier extent during the Younger Dryas and 8.2-ka event on Baffin Island, Arctic Canada. Science 337, 1330-1333.

2. Methodology

2.1 Sample Material

In this study, we analyze the radiogenic isotope composition of the detrital sediment fraction of four marine sediment cores from western and northern Baffin Bay and the Canadian Arctic Archipelago (Table 2-1, Fig. 2-1). The GeoB Core Repository at MARUM – Center for Marine Environmental Science, University of Bremen, provided access to gravity cores GeoB22336-4, GeoB22346-3, and GeoB22357-3. The sampling of the working halves of the three GeoB cores was performed in the sampling laboratory of the IODP Bremen Core Repository at MARUM. For isotope and mineral analysis, twelve samples of GeoB22346-3 and Twenty-four samples of GeoB22357-3 with an approximate weight of 5 g for each sample were taken. Thirty-two samples of GeoB22336-4, previously sampled by Emmanuel Okuma, were selected for further isotope analysis. Sixteen sediment samples of PS72/287-3 were provided by Rüdiger Stein and the Alfred Wegener Institute Helmholtz Centre for Polar and Marine Research, Bremerhaven.

Table 2-1: Details of gravity cores analyzed in this study. Cruise reports: MSM 66 (Dorschel et al., 2017), ARK-XXIII/3 (Jokat, 2009).

Core ID	**GeoB22336-4**	**GeoB22346-3**	**GeoB22357-3**	**PS72/287-3**
Cruise	MSM66	MSM66	MSM66	ARK-XXIII/3
Sampling Device	Gravity core	Gravity core	Gravity core	Gravity core
Sampling Date	08 Aug 2017	17 Aug 2017	19 Aug 2017	21 Aug 2008
Sampling Area	Offshore Lancaster Sound	Clyde Inlet fjord	Offshore Clyde Inlet	Barrow Strait
Latitude	74° 04.43´ N	69° 54.18’N	70° 36.28’N	74°15.95’N
Longitude	77° 26.99´ W	70° 13.54’W	67°53.63’W	90°59.09’W
Water Depth [m]	839	203	315	337
Recovery Length [cm]	613	783	902	463

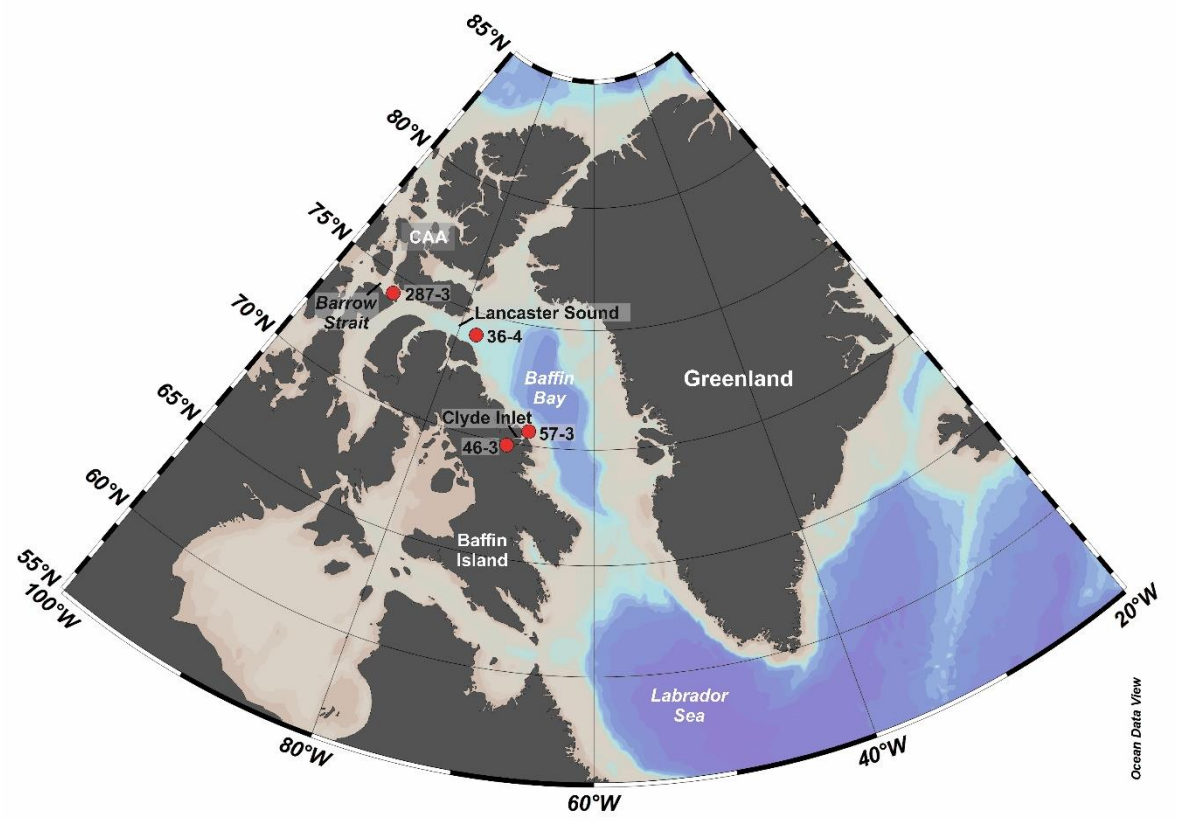

Figure 2-1: Overview Map of Baffin Bay with core locations. Core IDs are shortened: GeoB22336-4 = 36-4, GeoB22346-3 = 46-3, GeoB22357-3 = 57-3, PS72/287-3 = 287-3. Map created with Ocean Data View (Schlitzer, 2020).

2.2 Radiogenic isotope analysis

2.2.1 Sample preparation

Sample preparation was conducted at the laboratory of the Isotope Geochemistry Group at MARUM. Approximately 2 g of wet sediment was transferred into 15 ml centrifuge tubes and washed twice with Milli Q water (18.2 MΩ) to remove residual pore water. Samples were dried after washing at 110 °C and weighed to determine the dry bulk sediment weight. For radiogenic isotope analyses, the fine sediment fraction < 63 µm was separated from the coarse fraction by wet sieving. Both fractions were dried at 110 °C, and the dry weight of each fraction was determined. While the coarse sediment fraction was stored in 2 ml Eppendorf® centrifuge tubes, the fine fraction was homogenized with an agate mortar and transferred again into centrifuge tubes for sediment leaching.

2.2.1.1 Sample leaching

Since the main target of this study is to identify the sediment provenance of the continental detritus in the marine sedimentary records, possible other sediment components like marine carbonates or

authigenic minerals were removed by leaching. The leaching procedure for radiogenic isotope analysis traditionally includes different steps. To remove marine carbonates, samples are usually leached with a 15 % acetic acid solution, buffered with 1 M Na-acetate to pH ~4 (Gutjahr et al., 2007), or with unbuffered 10 % acetic acid (Bayon et al., 2002). In a second leaching step, possible Fe-Mn oxyhydroxide coatings can be extracted by using a solution of hydroxylamine hydrochloride and 15 % acetic acid buffered with NaOH (Gutjahr et al., 2007). Since previous work on marine sediments from Baffin Bay showed that the decarbonated sediment fraction after the first leaching and the potentially detrital fraction after the second leaching show very similar radiogenic isotope compositions (Madaj, 2021), we decided to perform just one leaching step. Moreover, measurements on leachates of Baffin Bay sediments containing possible Fe-Mn oxyhydroxide coatings yielded highly radiogenic Pb isotope values, which were interpreted to reflect the signature of detrital dolomites in the leachates (Kirillova, 2017). To get the option to measure the radiogenic isotope composition of the continental detritus and the potentially separated detrital dolomites in the leachates, we decided to leach the samples with the hydroxylamine hydrochloride solution. Thus, the NaOH buffered solution of hydroxylamine hydrochloride and 15 % acetic acid were added to the samples, which were then shaken for 3 hours on a rotary platform. The leachate was separated from the centrifuged samples and stored for further analysis. The residual detrital/siliciclastic sediment fraction was dried at 110 °C and weighed.

2.2.1.2 Sample dissolution

For the dissolution of the siliciclastic sediment fraction (modified after Höppner et al., 2018), 100 mg of each leached and homogenized sample was transferred into a 15 ml Teflon Savillex® beaker. To destroy the silicate lattice, 3 ml of a concentrated HF-HNO_3 mixture was added to the samples in the first digestion step. The closed Savillex® beakers were placed for at least 48 hours on the hotplate at 140 °C. After drying, samples were redissolved in 3 ml Aqua Regia (3:1, 6 M HCl and concentrated HNO_3) for at least 48 hours at 120 °C. To remove possible residual organic matter, 100 µl H_2O_2 was added four to five times and evaporated at 70 °C after each step before samples were redissolved in 1 ml concentrated HNO_3 at 70 °C overnight. After drying, 3 ml 6 M HCl was added to the dry samples for redissolution at 70 °C overnight. For chemical separation, dried samples were finally dissolved in 1100 µl 2M HNO_3. Samples were centrifuged before the column separation to separate possible residual particles.

For the dissolution of the leachates, samples were transferred into 15 ml Teflon Savillex® beakers. After drying on the hotplate at 85 °C, samples were redissolved three times in 2 ml of concentrated HNO_3 and 6 M HCl, respectively, and dried again after each step at 85 °C. Similar to the siliciclastic sediment fraction, dried samples were redissolved in 1100 µl 2 M HNO_3 for the column chemistry.

2.2.2 Chemical separation and mass spectrometry

To measure the Sr, Nd, and Pb isotope composition in sediment samples by thermal ionization mass spectrometry, prior isolation of these elements from the sample matrix is needed. Therefore, chemical separation using ion exchange chromatographic technique was conducted in a clean environment at the laboratory of the Isotope Geochemistry Group at MARUM.

Sr and Pb were isolated simultaneously on the same column procedure using 70 µl Sr.spec^{TM} resin following a modified method after Deniel and Pin (2001). Sr.spec^{TM} is an extraction chromatographic material that retains Sr as well as Pb, which can be stripped again from the column by adding 0.05 M HNO_3 and 6 M HCl, respectively. Matrix elements eluted during the Sr and Pb separation contain rare earth elements (REE), which can be directly used to isolate Nd in the two following steps. In the first step, REE are loaded onto columns with TRU.spec^{TM} to separate the light rare earth elements (LREE), which are eluted using 0.05 M HNO_3. LREE are then transferred onto Nd columns to separate Nd using LN.spec^{TM} and eluted with 0.25 M HCl (method after Pin et al., 1994). After the chemical separation, 20 µl of 0.1 N H_3PO_4 were added to the isolated Sr, Pb, and Nd samples, which were then dried. For the removal of possible residual resin material, 70 µl of concentrated HNO_3 were added and subsequently evaporated again.

Sr, Nd, and Pb isotope ratios were measured with a Thermo-Fisher Scientific TRITON Plus thermal ionization mass spectrometer (TIMS) at the Isotope Geochemistry Laboratory at MARUM. For the measurements, all samples were transferred onto rhenium filaments by using a drop of 0.1 N H_3PO_4. Sr and Pb were measured on a single filament, using a tantalum and a silicon activator, respectively. Nd was transferred onto double filaments without an additional activator. To increase the vacuum of the instrument for an accurate measurement, liquid nitrogen was filled into the cryopump. All measurements were performed in the static multicollection mode. To correct the instrumental mass fractionation during Sr and Nd isotope analysis, the stable isotope ratios $^{86}Sr/^{88}Sr$ (=0.1194) and $^{146}Nd/^{144}Nd$ (=0.7219) were used, respectively. During Pb isotope analysis, instrumental mass fractionation was corrected by applying a factor of 1.001 per atomic mass unit. The measurement accuracy and external long-term reproducibility were recorded by using reference material NIST SRM 987 was used for $^{87}Sr/^{86}Sr$, NIST SRM 981 for Pb isotope ratios, and JNdi-1 for $^{143}Nd/^{144}Nd$. The values analyzed during this PhD project (Table 9-7) are in the range of values analyzed by TIMS and published in the GeoReM database (http://georem.mpch-mainz.gwdg.de/, query November 2022, March 2023): NIST SRM987: 0.710242 ± 0.000032 ($2SD_{mean}$, n=15), 0.710250 ± 0.000040 (GeoReM; $2SD_{mean}$, n=1711, data <0.7102 and > 0.7103 are discarded); JNdi-1: 0.512113 ± 0.000024 ($2SD_{mean}$, n=12), 0.512107±0.000024 (GeoReM; 2SDmean, n=414, data <0.51204 and >0.51217 are discarded); NIST SRM 981: 16.9004 ± 0.0133 ($^{206}Pb/^{204}Pb$; $2SD_{mean}$, n=12), 16.9211 ± 0.0423

($^{206}Pb/^{204}Pb$; GeoReM; $2SD_{mean,}$ n=290, data >17 are discarded). Nd isotope ratios are commonly presented in the ε_{Nd} notation using the Chondritic Uniform Reservoir (CHUR) value of $^{143}Nd/^{144}Nd$ = 0.512638 (Jacobsen and Wasserburg, 1980).

2.3. X-Ray diffraction

Radiogenic isotope compositions can be influenced by the mineralogical composition of the sediment (e.g., Garçon et al., 2014). To evaluate the potential influence of the mineralogy on the radiogenic isotope compositions, the bulk mineralogical assemblages of twelve GeoB22346-3 and seventeen samples of GeoB22357-3 were determined by X-ray diffraction (XRD) (Tables 9-5 and 9-6). Samples were prepared by wet sieving to separate the fine fraction (< 63 µm). Afterward, the fine sediment material was ground manually with an agate mortar to reach an approximate grain size of < 20 µm for XRD analysis. XRD measurements were performed by Christoph Vogt at the Crystallography Department of Geosciences, University of Bremen, followed by the mineral identification and the semiquantitative evaluation of mineralogical assemblages (e.g., Vogt, 2009).

References

Bayon, G., German, C.R., Boella, R.M., Milton, J.A., Taylor, R.N., Nesbitt, R.W., 2002. An improved method for extracting marine sediment fractions and its application to Sr and Nd isotopic analysis. Chemical Geology 187, 179-199.

Deniel, C., Pin, C., 2001. Single-stage method for the simultaneous isolation of lead and strontium from silicate samples for isotopic measurements. Analytica Chimica Acta 426, 95-103.

Dorschel, B., Allan, E., Bartels, M., Campbell, C., Couette, P.-O., Diekamp, V., Dreutter, S., Duboc, Q., Geils, J., Greco, M., Lenz, K.-F., Lübben, B., Lütjens, M., Madaj, L., Perez, L., Recinos, B., Saini, J., Schade, T., Täuber, F., Ulner, L.-C., Warnke, F., Weiser, J., 2017. WESTBAFF - Reconstruction of the Laurentide Ice sheet drainage into the northwest Baffin Bay and the palaoceanography of the west Baffin Bay, Cruise No. MSM66, 22nd of July 2017 - 28th of August 2017, Nuuk (Greenland) - Reykjavik (Iceland). MARIA S. MERIAN-Berichte, Gutachterpanel Forschungsschiffe MSM66.

Garçon, M., Chauvel, C., France-Lanord, C., Limonta, M., Garzanti, E., 2014. Which minerals control the Nd–Hf–Sr–Pb isotopic compositions of river sediments? Chemical Geology 364, 42-55.

Gutjahr, M., Frank, M., Stirling, C.H., Klemm, V., van de Flierdt, T., Halliday, A.N., 2007. Reliable extraction of a deepwater trace metal isotope signal from Fe–Mn oxyhydroxide coatings of marine sediments. Chemical Geology 242, 351-370.

Höppner, N., Lucassen, F., Chiessi, C.M., Sawakuchi, A.O., Kasemann, S.A., 2018. Holocene provenance shift of suspended particulate matter in the Amazon River basin. Quaternary Science Reviews 190, 66-80.

Jacobsen, S.B., Wasserburg, G.J., 1980. Sm-Nd Isotopic Evolution of Chondrites. Earth and Planetary Science Letters 50, 139-155.

Jokat, W., 2009. The Expedition of Research Vessel "Polarstern" to the Arctic in 2008 (ARK-XXIII/3), in: Jokat, W. (Ed.), Reports of Polar and Marine Research. Alfred-Wegener-Institute für Polar- und Meeresforschung, Bremerhaven, Germany.

Kirillova, V., 2017. Radiogenic isotopes on marine sediments from the Baffin Bay: implications for the sediment supply during the last deglaciation. Dissertation, Faculty of Geosciences, University Bremen, Bremen, Germany.

Madaj, L., 2021. Holocene Ice Sheet Dynamics and Detriral Provenance Shifts Along the West Greenland Margin Recorded by Radiogenic Isotopes. Dissertation, Faculty of Geosciences, University Bremen, Bremen, Germany.

Pin, C., Briot, D., Bassin, C., Poitrasson, F., 1994. Concomitant separation of strontium and samarium-neodymium for isotopic analysis in silicate samples, based on specific extraction chromatography. Analytica Chimica Acta 298, 209-217.

Schlitzer, R., 2020. Ocean Data View, https://odv.awi.de.

Vogt, C., 2009. Data report: semiquantitative determination of detrital input to ACEX sites based on bulk sample X-ray diffraction data, Proc. IODP| Volume, p. 2.

3. Outline of manuscripts

This dissertation contains three manuscripts that are in different stages of publication. All manuscripts discuss changes in sediment processes related to the ice sheet retreat around Baffin Bay during the last deglaciation. This overview includes a summary of each manuscript and indicates the contributions of all authors and my own.

3.1 First Manuscript (Chapter 4)

Deglacial and Holocene sediment dynamics and provenances off Lancaster Sound: implications for paleoenvironmental conditions in northern Baffin Bay

Emmanuel Okuma[a], Johanna Hingst[a], Jens Weiser[a], Lina Madaj[b], Jürgen Titschack[a,c], Christoph Vogt[a], Markus Kienast[d], Claude Hillaire-Marcel[e], Dierk Hebbeln[a], and Simone A. Kasemann[a]

[a]MARUM - Centre for Marine Environmental Science and Faculty of Geoscience, University of Bremen, Germany
[b]Department of Earth Sciences, Vrije Universiteit Amsterdam, Amsterdam, The Netherlands
[c]Senckenberg am Meer, Marine Research Department, Wilhelmshaven, Germany
[d]Department of Oceanography, Dalhousie University, Halifax, Canada
[e]Geotop - Centre de recherche sur la dynamique du système Terre, Université du Québec à Montréal, Canada

Submitted to Quaternary Science Reviews in January 2023, under revision

(Manuscript Number: JQSR-D-23-00050)

Summary

This manuscript includes sedimentological, mineralogical, and geochemical data of the sediment core GeoB22336-4 from the mouth of Lancaster Sound, northern Baffin Bay. The data are used to discuss the changing sedimentation patterns influenced by the retreating ice sheets and the opening of the Arctic gateways. Till deposits at the core bottom are evidence of a grounded ice stream at the core site before ~ 14.3 ka BP. A change in sediment provenance, traced by the radiogenic isotope composition of the detrital material, is caused by the openings of Lancaster Sound and Nares Strait at ~ 10.2 to 9.8 ka BP and 8.5 to 8.2 ka BP, respectively. Moreover, the enhanced deposition of fine-grained material during the early Holocene is probably related to enhanced sea ice melting due to a stronger West Greenland Current.

Authors contributions

Emmanuel Okuma and Johanna Hingst contributed equally to this manuscript. Emmanuel Okuma performed sedimentological analyses and developed the age model and figures in the manuscript. Further, he wrote the original draft and included all comments and suggestions in the final version. All authors contributed to the writing, reviewing, and editing process. Moreover, Jens Weiser supported the data visualization, and Lina Madaj provided radiogenic data for sediment provenance

discussion. Jürgen Titschack, Claude Hillaire-Marcel, Markus Kienast, Dierk Hebbeln, and Simone A. Kasemann further supervised the project and provided access to resources. Christoph Vogt performed XRD analysis and the following mineral identification and quantitative evaluation of the mineralogical compositions of the core. Dierk Hebbeln and Simone A. Kasemann were part of the project conceptualization, funding acquisition, and administration.

Detailed own contributions

I prepared the sediment samples for radiogenic isotope analysis, including grain-size separation, leaching, and dissolution. Further, I conducted the Sr, Nd, and Pb isotope separation and the measurements of isotope ratios using the Thermo-Fisher Scientific TRITON Plus thermal ionization mass spectrometer. With the advice of the co-authors, I discussed the radiogenic isotopes and prepared the figures for sediment provenance discussion. Together with Emmanuel Okuma, I designed the first manuscript of the draft. All co-authors contributed to the development of the final manuscript, while all comments and suggestions were incorporated into the manuscript by Emmanuel Okuma and myself.

3.2 Second Manuscript (Chapter 5)

Holocene variability of the northeastern Laurentide Ice Sheet in the Clyde Inlet area, western Baffin Bay, from radiogenic isotope records in marine sediments

Johanna Hingst[a], Claude Hillaire-Marcel[b], Friedrich Lucassen[a], Christoph Vogt[a], Emmanuel Okuma[a], Simone A. Kasemann[a]

[a]MARUM – Centre for Marine Environmental Science and Faculty of Geoscience, University of Bremen, Germany
[b]Geotop – Centre de recherche sur la dynamique du système Terre, Université du Québec à Montréal, Canada

Manuscript in preparation

Summary

This manuscript discusses the radiogenic isotope composition of the detrital sediment fraction and mineralogical composition of the bulk sediment of two marine sediment cores retrieved from the Clyde Inlet fjord head (GeoB22346-3) and the shelf in front of the inlet (GeoB22357-3), respectively. The data are used to trace sediment provenance changes and reconstruct related past meltwater and ice margin fluctuations of an outlet glacier of the northeastern Laurentide Ice Sheet (LIS). The changing mineralogical composition of the sediment strongly influences the radiogenic Sr and Pb isotope ratios at the fjord head. However, they reflect short-term ice sheet fluctuations during the early to mid-Holocene and changing meltwater dynamics after the ice margin retreated from the fjord head. On the shelf, variable radiogenic isotope data reflect the retreat of the ice margin from

the shelf during the early Holocene and an enhanced input of sediments originating from northern Baffin after the opening of Lancaster Sound.

Authors contributions

All authors contributed to the discussion and interpretation of the data. Additionally, Simone Kasemann, Claude Hillaire-Marcel, and Friedrich Lucassen supervised the project and contributed to the conceptualization of the manuscript. Emmanuel Okuma took samples for AMS ^{14}C ages, which were measured at the Alfred Wegener Institute (AWI) in Bremerhaven, Germany, and developed the age models of both cores. Further, he provided feedback on the method part of the manuscript and helped visualize the age model. Christoph Vogt performed XRD analysis and the following mineral identification and semiquantitative evaluation of the mineralogical compositions of both cores.

Detailed own contributions

I took the sediment samples of the two sediment cores and prepared the samples for radiogenic isotope analysis, including grain-size separation, leaching, and dissolution. Additionally, I conducted the Sr, Nd, and Pb isotope separation and the measurements of isotope ratios using the Thermo-Fisher Scientific TRITON Plus thermal ionization mass spectrometer. Samples for XRD analysis were prepared by myself. With the advice of the co-authors, I discussed the radiogenic isotopes and prepared the figures for the manuscript. Finally, I developed the manuscript draft.

3.3 Third Manuscript (Chapter 6)

Marine radiogenic isotope record from Barrow Strait reveals late Pleistocene to early Holocene ice sheet dynamics in the Canadian Arctic Archipelago

Johanna Hingst[a], Claude Hillaire-Marcel[b], Friedrich Lucassen[a], Rüdiger Stein[a], and Simone A. Kasemann[a]

[a]MARUM – Center for Marine Environmental Science and Faculty of Geosciences, University of Bremen, Germany
[b]Geotop – Centre de recherche sur la dynamique du système Terre, Université du Québec à Montréal, Canada

Manuscript in preparation

Summary

This manuscript discusses the radiogenic isotope data obtained from the sediment core PS72/287-3 from Barrow Strait. Radiogenic Sr, Nd, and Pb isotope data of the siliciclastic sediment fraction are used to trace changes in sediment provenances related to the retreating Laurentide and Innuitian ice sheets during the last deglaciation and the Holocene. The data suggest the recession of the ice margins towards land-terminating positions and, with that, the complete opening of

Barrow Strait by around 10 ka BP. Further, radiogenic Pb isotope ratios achieved from the sediment leachate fraction seem to be characteristic of the detrital carbonates in the Canadian Arctic Archipelago. The identification of their radiogenic isotope signatures can be used for future studies to trace the input of detrital carbonates into Baffin Bay and the Arctic Ocean during periods of rapid deglaciation of the northeastern Laurentide and Innuitian ice sheets.

Authors contributions

All authors contributed to the data discussion and interpretation. Additionally, Simone Kasemann, Claude Hillaire-Marcel, and Friedrich Lucassen supervised the project and contributed to the conceptualization of the manuscript. Rüdiger Stein provided access to the sediment core and took the samples for radiogenic isotope analysis.

Detailed own contributions

I prepared the samples for radiogenic isotope analysis, including grain-size separation, leaching, and dissolution. Additionally, I performed the Sr, Nd, and Pb isotope separation and the measurements of isotope ratios using the Thermo-Fisher Scientific TRITON Plus thermal ionization mass spectrometer. I discussed the radiogenic isotopes and prepared the figures for the manuscript in cooperation with the co-authors. Further, I developed the manuscript draft.

4. Deglacial and Holocene sediment dynamics and provenances off Lancaster Sound: implications for paleoenvironmental conditions in northern Baffin Bay

Emmanuel Okuma[a*], Johanna Hingst[a*], Jens Weiser[a], Lina Madaj[b], Jürgen Titschack[a,c], Christoph Vogt[a], Markus Kienast[d], Claude Hillaire-Marcel[e], Dierk Hebbeln[a], and Simone A. Kasemann[a]

[*]contributed equally to this manuscript

[a]MARUM - Centre for Marine Environmental Science and Faculty of Geoscience, University of Bremen, Germany
[b]Department of Earth Sciences, Vrije Universiteit Amsterdam, Amsterdam, The Netherlands
[c]Senckenberg am Meer, Marine Research Department, Wilhelmshaven, Germany
[d]Department of Oceanography, Dalhousie University, Halifax, Canada
[e]Geotop - Centre de recherche sur la dynamique du système Terre, Université du Québec à Montréal, Canada

Originally published in Quaternary Science Reviews, 2023, Volume 309, doi:10.1016/j.quascirev.2023.108101

Abstract

Since the last deglaciation, Baffin Bay between Greenland and Canada developed from an isolated marginal sea to a major Arctic-Atlantic throughflow closely linked to the North Atlantic circulation. While the initial steps of gateway openings through Lancaster Sound and Nares Strait to northern Baffin Bay are reasonably well documented, far less is known about related regional deglacial-to-Holocene changes in sediment sources and depositional processes due to a lack of continuous and well-dated paleoenvironmental records from northern Baffin Bay. Sedimentological, mineralogical, and radiogenic isotope data of the well-dated sediment core GeoB22336-4 from the mouth of Lancaster Sound provide new insights on the impacts of ice sheet retreat and opening of the gateways to the Arctic Ocean on the depositional setting. Basal subglacial till deposits point to a grounded ice stream at the mouth of Lancaster Sound before ~14.3 ka BP. Subsequent glaciomarine sedimentation is characterized by the input of ice-rafted detritus (IRD), bioturbation traces, and foraminifera shells. Decreasing sediment supply and input of IRD through time reflects a period of ice sheets recession to predominantly land-terminating positions during the Early Holocene. Changes in radiogenic isotope signatures reveal the openings of Lancaster Sound between ~10.2 – 9.8 ka BP and of Nares Strait between 8.5 and 8.2 ka BP, in alignment with earlier studies. The rapid mid-Holocene (up to ~5.6 ka BP) deposition of fine-grained sediments is most likely caused by enhanced sea ice-rafted sediment input released under a strong West Greenland Current influence.

Finally, a slight increase in IRD input during the last ~2 ka BP is linked to the neoglacial re-advance of regional glaciers.

Keywords: Deglaciation, Holocene, Baffin Bay, Lancaster Sound, Sedimentology, Computed tomography, X-ray diffraction, Detrital carbonate, Radiogenic Isotopes

4.1 Introduction

Today, Baffin Bay serves as a major Arctic-Atlantic throughflow, between Greenland and Canada, and constitutes an important component of the North Atlantic circulation (Holland et al., 2001; Tang et al., 2004; Jennings et al., 2019). Due to its high latitude setting, it is a perfectly suited area to study ice margin and sea ice dynamics and their coupling to changes in late Quaternary climate and oceanography (e.g., Aksu and Piper, 1987; Andrews et al., 1998; Simon et al., 2014). During the Last Glacial Maximum (LGM), Baffin Bay was partly surrounded by grounded glacial ice of the extended Laurentide (LIS), Innuitian (IIS), and Greenland (GIS) ice sheets (England, 1999; Dyke et al., 2002; Zreda et al., 1999; Dalton et al., 2020). The margins of the LIS, IIS, and GIS persisted on Baffin Bay shelves into the early Holocene and formed a continuous belt of ice over the Lancaster Sound, Nares Strait, and other smaller channels of the Canadian Arctic Archipelago (CAA) north of Baffin Bay (Fig. 4-1; Dalton et al., 2020). The blocking of these Arctic gateways prevented the inflow of Arctic Ocean water and ice into Baffin Bay (Dyke et al., 2002; Knudsen et al., 2008; Jennings et al., 2011; Pieńkowski et al., 2012, 2014).

Past climate warming and the increasing influence of relatively warm Atlantic waters in the region likely forced the final collapse of the LIS, IIS, and GIS and their retreat from marine-terminating portions during the early Holocene (Dyke et al., 2002; Kaufman et al., 2004; Jennings et al., 2014, 2017; Dalton et al., 2020). Eventually, this led to the reconnection of the Arctic Ocean to Baffin Bay. The final separation of the coalescent LIS and IIS in the central Barrow Strait was probably completed between 10.6 and 10.4 ka BP (Pieńkowski et al., 2012, 2014; Kelleher et al., 2022), whereas the eventual severance of the IIS and GIS and the resulting opening of Nares Strait likely occurred much later between 8.5 and 8.2 ka BP (Knudsen et al., 2008; Jennings et al., 2011, 2019, 2022; Georgiadis et al., 2018; Kelleher et al., 2022). The deglaciation of these northern gateways controlled the connectivity of Baffin Bay to the Arctic Ocean (e.g., Jennings et al., 2011; Pieńkowski et al., 2012, 2014) and probably the sedimentary dynamics, particularly in northern Baffin Bay during the Early Holocene.

While the deglaciation pattern and subsequent opening of the Arctic gateways are fairly well documented based on marine geophysical and sediment core data (e.g., Zreda et al., 1999; England et al., 2006; Harrison et al., 2011a; Li et al., 2011; Jennings et al., 2011; Pieńkowski et al., 2012,

2014; Bennett et al., 2014; MacLean et al., 2017; Furze et al., 2018; Georgiadis et al., 2018; Kelleher et al., 2022), the impacts of ice-ocean interactions on paleoenvironmental and paleoceanographic conditions, especially in northern Baffin Bay, remain, in part, enigmatic. This is partly due to the lack of continuous records from northern Baffin Bay documenting environmental and oceanographic developments since the last deglaciation and throughout the Holocene. Previous studies reconstructing such developments in northern Baffin Bay are largely based on sediment records covering either the Holocene only (e.g., Ledu et al., 2008; Knudsen et al., 2008; St-Onge and St-Onge, 2014; Caron et al., 2019; Jennings et al., 2019; Stevenard et al., 2021) or the late Pleistocene to early Holocene (Furze et al., 2018; Kelleher et al., 2022). For instance, a recently published paleoenvironmental reconstruction from northern Baffin Bay partly based on core 49PC (Kelleher et al., 2022), taken close to the core location presented here (Fig. 4-1), suffers from an incomplete record and lacking radiocarbon age control for the most likely middle to late-Holocene sediment sequence. Thus, a continuous well-dated sedimentary record capturing the environmental conditions since the retreat of ice streams from the marine realm and the opening of Arctic gateways is so far unavailable.

In the last decades, the analyses of the mineral composition of Baffin Bay late Quaternary sediments have proven to be very useful in the differentiation of sediment provenance and the reconstruction of ice sheet dynamics around Baffin Bay (e.g., Andrews and Eberl, 2011; Andrews et al., 2018; Andrews and Piper, 2022). In addition to the mineral assemblage, the Sr and Nd radiogenic isotope composition of the detrital sediment fraction can serve as a reliable tracer for sediment source areas, especially when mineralogical evidence proves ambiguous. Indeed, the analyses of the radiogenic isotope composition of sediment cores from Baffin Bay and Labrador Sea provided additional insights into the history of LIS and GIS (Farmer et al., 2003; Colville et al., 2011; Reyes et al., 2014; Andrews et al., 2015). Similarly, radiogenic isotope analyses of a sediment core from Nares Strait revealed new information on the deglaciation pattern of this Arctic gateway (Madaj, 2021). Although radiogenic isotope studies in northern Baffin Bay have the potential to increase our understanding of glacial erosion and sediment transport processes during past glacial and interglacial cycles, such studies are still rare in this region.

This study focuses on the impacts of the retreat of Lancaster Sound ice stream and surrounding ice margins, the reconnection of the Arctic Ocean and Baffin Bay after the opening of Barrow and Nares Straits, and the establishment of modern oceanographic circulation, on environmental conditions and the sediment routing system in northern Baffin Bay. To investigate temporal changes in (i) sedimentation pattern and (ii) sediment provenances, we analyzed the sedimentological characteristics (computerized tomography and grain size) and mineralogical and radiogenic isotope

compositions from a new well radiocarbon-dated sediment core (spanning the last ~14 ka BP) recovered from northern Baffin Bay (GeoB22336-4; Fig. 4-1).

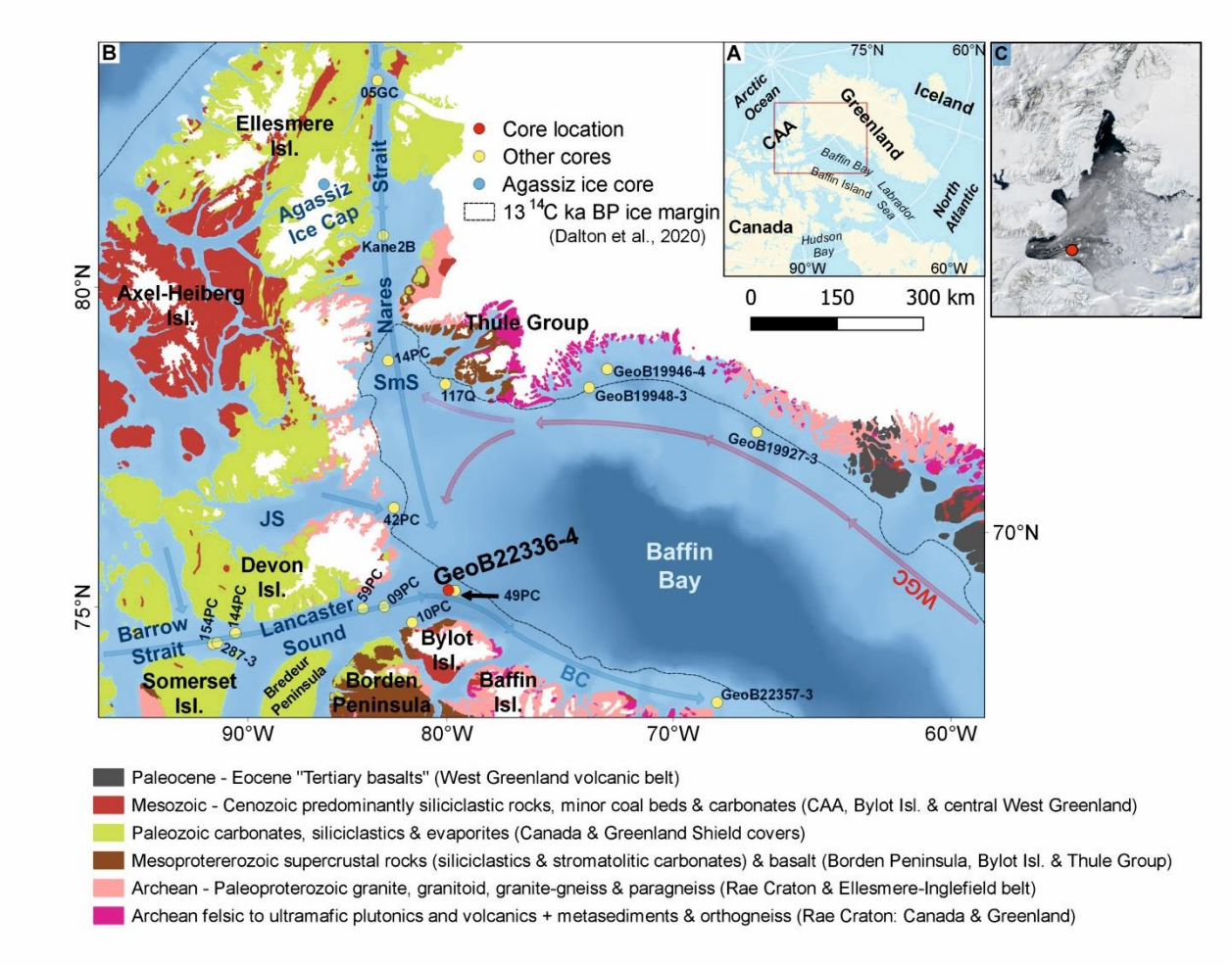

Figure 4-1: (A) Map showing the location of Baffin Bay with the Canadian Arctic Archipelago (CAA) bordering it to the north and (B) the main oceanographic currents interacting in northern Baffin Bay and the adjacent channels, and the bedrock geology of the bordering hinterlands (after Harrisson et al., 2011). (C) Moderate Resolution Imaging Spectroradiometer (MODIS) image showing regional sea-ice distribution and the areal extent of the North Water Polynya in June 2001 (https://visibleearth.nasa.gov/images/56201). Blue arrows represent cold Arctic surface waters entering the northern Baffin Bay through Smith Sound and Lancaster Sound, eventually forming the Baffin Current (BC). Red arrows indicate the path of warmer Atlantic waters partly transported via the West Greenland Current (WGC). Isl. = Island; JS = Jones Sound; SmS = Smith Sound. The black dashed line indicates the 13 14C ka ice margin positions (adapted from Dalton et al., 2020). White-colored areas mark the present-day ice cover of which the blue circle indicates the Agassiz Ice Cap location. The red circle indicates the location of core GeoB22336-4 investigated in this study. Yellow circles represent the locations of other cores discussed or data shown in this study.

4.2 Regional Setting

4.2.1 Environment and Oceanography

Baffin Bay is a narrow, semi-enclosed ocean basin between west Greenland and northeastern Canada (Fig. 4-1). The basin is bordered by islands of the CAA at its northern end and to the south by the Davis Strait, an ocean passage connecting Baffin Bay to the Labrador Sea and the North Atlantic Ocean. The CAA channels, namely Lancaster Sound linked to Barrow Strait, Jones Sound (JS), and Smith Sound (SmS) linked to Nares Strait, connect the northern Baffin Bay to the Arctic Ocean.

In the northern Baffin Bay, the northward-flowing West Greenland Current (WGC), partly transporting relatively warm and saline Atlantic waters, meets the south-flowing cold Arctic surface waters that form the Baffin Current (BC; Fig. 4-1). The latter is dominated by relatively fresh water (and ice) coming from the Arctic Ocean through the CAA gateways. A majority of the WGC is deflected west- and southward in northern Baffin Bay to join the BC´s southward flow (Tang et al., 2004; Dunlap and Tang, 2006; Münchow et al., 2015). The interaction of these ocean currents influences the formation and extent of sea ice (Tang et al., 2004), as well as the formation and endurance of the highly productive North Water Polynya (NOW) in the northernmost Baffin Bay (Melling et al., 2001; Ingram et al., 2002; Jackson et al., 2021). In addition, the formation of the NOW also depends on the presence of the northern and southern ice arches (or bridges) across Nares Strait (Barber and Massom, 2007; Jennings et al., 2011; Ren et al., 2022). Today, sea ice covers almost all of northern Baffin Bay in winter (Tang et al., 2004). Between April and July, however, strong northerly winds, occasionally causing upwelling of warmer Atlantic water transported via the WGC near the Greenland coast, and the southward-flowing currents maintain the thin-ice-cover to open-water areas of the NOW (Fig. 4-1b) until September, when most of northern Baffin Bay is ice-free (Melling et al., 2001; Tang et al., 2004; Barber and Massom, 2007).

Besides the reoccurring NOW in the surface waters of northern Baffin Bay, another prominent feature is a complex submarine sediment fan system fed by former ice streams in the Lancaster, Jones, and Smith Sounds (Dyke et al., 2002; Harrison et al., 2011a). Particularly, the Lancaster Sound Trough Mouth Fan (TMF) is a large sediment fan formed by the delivery of glacially eroded materials by shelf-crossing Lancaster Sound ice streams during the Pleistocene (Harrison et al., 2011a; Li et al., 2011; Bennett et al., 2014; MacLean et al., 2017). These sediments and seafloor erosion patterns indicated by subglacial bedforms provide insights into the history of glacial erosion of surrounding landmasses and CAA channels Li et al., 2011; Simon et al., 2014, 2016; Furze et al., 2018). Modern

sediment transport mechanisms to Baffin Bay are primarily through fluvial and meltwater plumes, icebergs and sea-ice rafting (Andrews, 1990; Andrews et al., 2018).

4.2.2 Surrounding geology and related radiogenic isotope signatures

The bedrock geologic units of the surrounding hinterlands bordering Baffin Bay and the channels of the CAA vary in age from Archean to (early) Cenozoic (Fig. 4-1; Harrison et al., 2011b). Archean to Paleoproterozoic crystalline shield rocks (mainly granite, granite-gneiss, and paragneiss), hence rich in quartz, plagioclase, K-feldspar, and clay minerals like mica and illites, are exposed in the ice-free areas of the still mostly glaciated west Greenland margin. Similar bedrocks are found on the Canadian side of Baffin, Bylot, Devon, and southeastern Ellesmere islands, which, together with the Greenland side, constitute the Rae Craton (Harrison et al., 2011b). Parts of this crystalline basement are still covered by several CAA glaciers and ice caps. Mesoproterozoic siliciclastics (including red beds and shales), carbonates, and volcanic (basalt) rocks of the Borden Peninsula, Bylot Island, and the Thule Group overlie parts of the Rae Craton (Harrison et al., 2011b). Extensive Paleozoic carbonates (dolostones and limestones), siliciclastics, and evaporites crop out on the adjacent land areas on either side of Barrow Strait to Lancaster Sound, Jones Sound, and northern Nares Strait and cover much of the Precambrian basement (Scott and de Kemp, 1998; Harrison et al., 2011b). In addition, Mesozoic to Cenozoic siliciclastics (with minor coal beds and carbonates) are found on the western side of Bylot and Ellesmere islands, and the so-called “Tertiary basalts” (e.g., Simon et al., 2014) occur along the shores of central west Greenland.

Information on the radiogenic isotope composition of the bedrocks bordering northern Baffin Bay and the CAA channels is rare, but measurements made on nearby fluvial and marine sediments (including sediment cores) provide a range of Nd (expressed in ε_{Nd} values; see section 4.3.5) and Sr isotope values, which are used as a reference to characterize these geological terrains. Generally, the old bedrock of the Rae Craton would correspond to unradiogenic ε_{Nd} values and more radiogenic Sr isotope signatures. For example, radiogenic isotope data from shelf sediments off northwest Greenland, bordered by Archean to Paleoproterozoic rocks, reveal ε_{Nd} and $^{87}Sr/^{86}Sr$ values ranging from -36 to -21 and 0.73 to 0.77, respectively (Madaj, 2021). Also, stream sediment (silts) data from the southwest and central west Greenland near Precambrian bedrock yield ε_{Nd} values between -41 and -15 and $^{87}Sr/^{86}Sr$ values between 0.70 and 0.74 (Colville et al., 2011; Reyes et al., 2014). Composite bedrock data from the crystalline basement on eastern Baffin Island show an ε_{Nd} value of -32 and a $^{87}Sr/^{86}Sr$ value of 0.76 (McCulloch and Wasserburg, 1978). Younger rocks are usually characterized by more radiogenic ε_{Nd} and relatively unradiogenic Sr isotope signatures, as reflected by higher ε_{Nd} (-19 to -12) and lower $^{87}Sr/^{86}Sr$ (0.72 to 0.74) values observed in surface sediments from around the CAA (Maccali et al., 2018).

4.3 Material and Methods

4.3.1 Sediment core and location

This study is based on gravity core GeoB22336-4 (74° 04.43´ N, 77° 26.99´ W; water depth: 839 m; core length: 613 cm) retrieved from the mouth of Lancaster Sound approximately 50 km off Bylot Island in northern Baffin Bay during cruise MSM 66 onboard RV Maria S. Merian in 2017 (Dorschel et al., 2017, Fig. 4-1). This core site is ideally situated to record the influence of Arctic gateways (mainly the Lancaster Sound and Nares Strait) on sedimentation patterns and sediment provenance in northern Baffin Bay. According to the initial visual core description, the sediment consists of an upper olive-brown to olive-grey silty mud and transitions to a light brownish-grey, silty-muddy sand interval and a dark brownish-grey, sandy mud at the bottom of the core (Dorschel et al., 2017).

4.3.2 Chronology

4.3.2.1 Radiocarbon dating

Chronostratigraphic control for core GeoB22336-4 is achieved by obtaining several Accelerator Mass Spectrometry (AMS) ^{14}C-datings from mixed planktic and benthic foraminifera and ostracods conducted at the MICADAS (MIni CArbon Dating System) ^{14}C laboratory, Alfred Wegener Institute (AWI) in Bremerhaven, Germany. Since biogenic carbonate was rare, especially in the upper part of the sediment core, several subsamples at different adjacent depths were required to obtain sufficient material for dating. Foraminifera (and ostracods) were picked from the >150 µm size fraction after the original samples were freeze-dried and wet-sieved. AMS ^{14}C measurements were carried out on 13 samples (Table 4-1). Depending on the available amount of carbonate (hence C content) in the samples, the AMS measurements were performed using either the graphitization (samples with >200 µg C) or acid hydrolysis (CO_2 gas; samples with <200 µg C) method (for details on both methods, see Mollenhauer et al., 2021).

4.3.2.2 Age model and calibration

The 13 AMS ^{14}C dates were calibrated using the open-source software UNDATABLE in MATLAB (Lougheed and Obrochta, 2019; settings: nsim = 10^5, bootpc = 30, xfactor = 0.1), which considers age-depth uncertainty in its rapid Bayesian approach in determining the best possible downcore age-depth relationship, applying the Marine20 calibration curve (Heaton et al., 2020). In addition, we applied a regional marine reservoir age correction (ΔR) of 220 ± 20 years, proposed for NE Baffin Island by Coulthard et al. (2010), for the calibration of mid and late-Holocene ages (Table 4-1), assuming largely similar oceanographic conditions for these periods. For the calibration of early Holocene and deglacial dates, we adopted the regional ΔR values calculated from benthic and planktic paired dates according to Kelleher et al. (2022). They calibrated ^{14}C dates from benthic

organisms between 10.2 and 8.1 ka using linearly decreasing ΔR values from 550 to 235 years, and a constant ΔR value of 550 years for dates older than this interval, as employed here. For ^{14}C dates obtained here from mixed benthic and planktic organisms, we used the mean value between planktic ΔR (220 years) and the corresponding benthic ΔR values. Furthermore, we use linear extrapolation to extend the age model outside ^{14}C-dated intervals.

It further has to be mentioned that the applicability of the Marine20 global-average calibration curve is rather limited for samples from polar regions as it does not consider extreme local fluctuations in marine ^{14}C pools in response to rapid shifts in climatic and oceanographic conditions (Heaton et al., 2020). Applying this calibration curve and the assumption of a constant ΔR over time potentially introduces unquantified uncertainty in the age model (Butzin et al., 2017). The appropriate regional marine reservoir offset (ΔR) values through time may differ from those used here (e.g., Pieńkowski et al., 2022), and thus the calibrated ages presented in this study should be used as best estimates, however, taken with caution.

Table 4-1. List of AMS ^{14}C dates obtained from core GeoB22336-4. All ^{14}C ages were calibrated within the age-modeling UNDATABLE software (Lougheed and Obrochta, 2019) using Marine20 dataset (Heaton et al., 2020) and applying a regional reservoir correction (ΔR) of 220 ± 20 years (after Coulthard et al., 2010) for mid and late-Holocene ages and variable ΔR values, described in the text, for older ages (after Kelleher et al., 2022). Calibrated ages are the median probability ages and 95% confidence interval (minimum and maximum age) based on Calib 8.20 (Stuiver and Reimer, 1993). Abbreviations: MBF, mixed benthic foraminifera; MBPF, mixed benthic and planktic foraminifera; O, ostracods.

Lab ID	Depth interval	Material	^{14}C Age		ΔR	Calibrated age (yrs BP)		
AWI-	(cm)		(yrs)	±	(yrs)	Min.	Max.	Median
6220.1.1	65–69	MBF	2513	65	220 ± 20	1520	1940	1730
5488.1.1	108–109	MBPF	3736	69	220 ± 20	2999	3442	3233
5489.1.1	109.5–110.5	MBPF	3640	69	220 ± 20	2879	3338	3113
5490.1.1	198–199	MBPF	6004	79	220 ± 20	5754	6222	6001
5491.1.1	258–259	MBPF	7111	79	220 ± 20	6982	7413	7205
5492.1.1	273–274	MBPF	7493	84	220 ± 20	7359	7771	7561
1724.1.1	290–291	MBF	7729	120	220 ± 20	7510	8084	7787
6221.1.1	323–324	MBPF	8696	92	273 ± 50	8487	9117	8804
5493.1.1	353–354	MBPF	9655	84	345 ± 50	9599	10204	9928
7625.1.1	443–444	MBF	10904	126	550 ± 50	10991	11828	11376
5494.1.1	473–474	MBF & O	10945	104	550 ± 50	11107	11805	11425
1725.1.1	498–499	MBF	11811	136	550 ± 50	12220	12933	12609
5495.1.1	568–569	MBPF	12968	119	385 ± 50	13611	14517	14033

4.3.3 Sedimentological analyses

4.3.3.1 Computed tomography

To gain insights into downcore variability in lithofacies characteristics, the archive halves of core GeoB22336-4 were scanned using a Philips computer tomography (CT) Brilliance iCT Elite 256 at the hospital Klinikum Bremen-Mitte, Bremen, Germany. This CT device is equipped with an X-ray source voltage of 120 kV and a current of 300 mA. Core scanning was done at a resolution of 0.293 mm in the *x* and *y* directions and 0.625 mm resolution in the *z*-direction (0.3 mm reconstruction interval). The scans were reconstructed using the filtered Back Projection (fBP) mode and a bone kernel (YB (Enhanced)) and exported as DICOM data.

Further processing of the CT data was performed using the ZIB edition of the Amira software (version 2021.08; Stalling et al., 2005), partly following the processing approach previously described in Bartels et al. (2017). Similar x-ray density threshold values of >1500, 601 to 1499, 1 to 600, and <1 Hounsfield units (HU) were used for the segmentation of the >1 mm dense constituents (including iceberg-rafted debris (IRD) and lithified/pyritized bioturbation traces), open bioturbation (air- and water-filled) traces, matrix sediments, and the surrounding background (air and water), respectively. For the core interval 580 to 613 cm, the uppermost threshold value had to be adjusted to a slightly lower value (HU=1400) to properly segment the dense constituents from the matrix sediments. For the separation of the dense constituents into lithified/pyritized bioturbation traces and lithic clasts (IRDs), shape information had to be considered. Dense constituents with lengths >3 mm, a length/width ratio >2.6, and a length/volume ratio >0.1 are considered lithified bioturbation traces (parameters were calculated with the *Label Analysis* module and filtered with the *AnalysisFilter* module). Subsequently, touching IRD clasts were separated by running the *ContourTreeSegmentation* module (persistence mode: adaptive; persistent values: 0.003) on the distance map of the IRD segmentation (*DistanceMap* module). Afterwards, all IRD particles within and touching an ~1 cm thick analyzing window (33 CT slices) were automatically counted and divided by the total sediment volume within the respective interval to obtain IRD clasts cm^{-3}. The analyzing window was moved slice by slice, and the obtained results were written to a spreadsheet at the central slice position. In addition, each sediment constituent (IRD, bioturbation traces, and matrix sediments) was quantified using the *MaterialStatistics* module (volume per slice). Finally, the whole core (archive half) X-ray density of the matrix sediment (unit: HU) was computed with the *MaterialStatistics* module (statistic per slice and label).

4.3.3.2 Grain-size analysis

Grain-size measurements were performed every 10 cm on ~0.5 ml bulk sediment in the Particle-Size Laboratory at MARUM – Center for Marine Environmental Sciences, University of Bremen,

using a Beckman Coulter Laser Diffraction Particle Size Analyzer LS 13320. Sample preparation and measurements were carried out with deionized, degassed, and filtered water (filter mesh size: 0.2 µm) to reduce the potential influence of gas bubbles or particles within the water. Following the protocol outlined in McGregor et al. (2009), sample preparation to isolate the terrigenous sediment fractions entail a stepwise removal of organic carbon, biogenic carbonate, and biogenic opal by boiling the samples (in about 200 ml water) with 10 ml of H_2O_2 (35 %; until the reaction stopped), 10 ml of HCl (10 %; 1 min) and 6 g of NaOH (10 min). Finally, ~ 0.3 g of tetrasodium diphosphate decahydrate ($Na_4P_2O_7 * 10H_2O$) was added to the samples and then boiled for 3 min to disaggregate the remaining particles. After each preparation step, the samples were diluted with water (dilution factor: > 25). Prior to the measurements, each sample was sieved to remove the >2 mm sediment fraction. The grain-size distributions obtained with the particle size analyzer range from 0.04 to 2000 µm and are divided into 116 size classes. The calculation of the grain-size range is based on the polarization intensity differential scattering (PIDS; particles from 0.04 to 0.4 µm) and the Fraunhofer diffraction theory (particles from 0.4 to 2000 µm). The repeatability is checked regularly through replicate analyses of three internal glass-bead standards and is found to be better than ±0.7 µm for the mean and ±0.6 µm for the median grain size (1 SD). The average standard deviation integrated over all size classes is better than ±4 vol.% (note that the standard deviation of the individual size classes is not distributed uniformly). Downcore particle size distributions and statistical parameters (including mean grain sizes) were derived by using geometric statistics.

4.3.4 X-ray diffraction (XRD) mineral assemblage and pattern analyses

To determine the mineral composition of core GeoB22336-4, X-ray diffraction pattern analyses were conducted on pulverized sediment samples (~6 g of <20 µm particle size, every 20 cm) in the laboratory of the Crystallography Research Group (Faculty of Geosciences, University of Bremen). The samples were measured on a Bruker D8 Discover diffractometer equipped with a Cu-tube (k-alpha 1.541, 40 kV, 40 mA), a fixed divergence slit of ¼°, and a monochromator (via Linxeye detector system). The measurements involve a continuous scan from 3 – 65° 2θ, with a calculated step size of 0.016°. Mineral identification was performed utilizing the Philips software X'Pert HighScore™, and identification of sheet silicates was done with the freely available Apple MacIntosh X-ray diffraction interpretation software MacDiff 4.25 (http://www.geologie.uni-frankfurt.de/Staff/Homepages/Petschick/Rainer.html#MacDiff; Petschick et al., 1996). This was followed by a full quantification of mineral assemblages of the bulk fraction via the QUAX full pattern method (c.f. Vogt et al., 2002). The main mineral composition (and relative errors) of the samples include carbonates (±1 wt.%), quartz (±1 wt.%), feldspars (±2 to 5 wt.%), and clay minerals (±5 wt.%).

4.3.5 Radiogenic isotope analyses

Radiogenic isotope ratios of Sr and Nd were analyzed in the laboratories of the Isotope Geochemistry Group at MARUM – Center for Marine Environmental Sciences, University of Bremen. Approximately 2 g of wet sediment samples (taken at 10 to 40 cm intervals) were initially washed twice with Milli Q water (18.2 MΩ) to remove the soluble fraction and residual pore water and wet-sieved to obtain the <63 µm grain-size fraction used for further analysis. To remove carbonate from the silicate fraction and dissolve potential authigenic Fe-Mn oxyhydroxide coatings on the sediment, samples were leached with a solution of hydroxylamine hydrochloride and 15 % acetic acid, buffered with NaOH (for 3 hours; adapted from Gutjahr et al., 2007). The remaining detrital samples were washed with Milli Q water (twice) and dried, after which 100 mg of the siliciclastic fraction was transferred into 15 ml Teflon Savillex® beakers for sample digestion in several steps (modified after Höppner et al., 2018). Samples were dissolved in 3 ml of a concentrated HF:HNO_3 (5:1) mixture at 140 °C (at least 48 hours), dried, and re-dissolved in 3 ml of aqua regia (3:1, 6 N HCl: concentrated HNO_3) at 120 °C for two days. To remove organic matter, 100 µl of H_2O_2 was added to the samples (4 to 5 times) until the reaction stopped. Afterwards, 1 ml of concentrated HNO_3 was added to each sample, and the samples were placed on the hotplate (70 °C) overnight to dissolve again, dried, and re-dissolved in 3 ml 6 N HCl. Finally, the samples were dried and re-dissolved in 1100 µl 2N HNO_3 for further chemical separation. Column chemistry was performed to separate Nd and Sr from the sample matrix. Sr was separated using 70 µl of Sr.spec™ resin, following a modified method after Deniel and Pin (2001). Nd was isolated in two steps using TRU.spec™ for light rare earth elements and LN.spec™ for Nd separation (Eichrom®) (method after Pin et al., 1994).

Isotope ratios were measured with a Thermo-Fisher Scientific TRITON Plus thermal ionization mass spectrometer (TIMS). Sr isotope composition was measured using a single filament, a Ta activator, and the static multicollection mode, whereas Nd isotope composition was analyzed on double filaments in a static multicollection mode. The stable ratio of $^{86}Sr/^{88}Sr$ (= 0.1194) was used to correct the instrumental mass fractionation that occurs during Sr isotope analysis. To assess the analytical accuracy and repeatability of the $^{87}Sr/^{86}Sr$ data, the reference material NIST SRM 987 was used with an analyzed value of 0.710246 ± 0.000018 ($2SD_{mean}$, n = 5), which is within the range of values analyzed by TIMS and published in the GeoRem database of 0.710250±0.000034 ($2SD_{mean}$, n= 1711, data <0.7102 and >0.7103 are discarded) (http://georem.mpch-mainz.gwdg.de/, 2022). During Nd analysis, instrumental mass fractionation was corrected to $^{146}Nd/^{144}Nd$ (= 0.7219). The analytical accuracy and repeatability for $^{143}Nd/^{144}Nd$ were monitored by the reference material JNdi-1, which yielded a value of 0.512111 ± 0.000022 ($2SD_{mean}$, n = 3) and agrees with the published values of

0.512107±0.000024 ($2SD_{mean}$, n= 414, data <0.51204 and >0.51217 are discarded) analyzed by TIMS (GeoRem database, http://georem.mpch-mainz.gwdg.de/, 2022). The $^{143}Nd/^{144}Nd$ ratio is reported in the ε_{Nd} notation relative to the Chondritic Uniform Reservoir (CHUR) value ($^{143}Nd/^{144}Nd$ = 0.512638; Jacobsen and Wasserburg, 1980) to emphasize changes in radiogenic Nd isotope composition.

4.3.6 Characterization of sediment provenance based on radiogenic isotope signatures

For sediment provenance reconstructions, the obtained Sr and Nd isotopic signatures from core GeoB22336-4 are compared with available reference data describing the characteristic radiogenic isotope composition of adjacent geological terrains. Due to the paucity of reference radiogenic isotope data, especially from the CAA and Baffin Island regions, we incorporate two additional data sets from sediment cores from Barrow Strait (PS72/287-3; Table 9-4) and the Baffin Island shelf (GeoB22357-3; Table 9-3; Fig.4-1). These additional samples were analyzed in the laboratories of the Isotope Geochemistry Group at MARUM, following similar preparation and analytical steps described above (section 4.3.5). The radiogenic isotope data from the Holocene part of the core PS72/287-3 form a distinct cluster and are representative of sediments deposited in this area under postglacial conditions. For sediment provenance discussion, they are used here as an end-member to track sediments from the Barrow Strait area. Additionally, the radiogenic isotope data obtained from core GeoB22357-3 from Baffin Island shelf are grouped with the data from cores GeoB19927-3 and GeoB19946-4 from the northwestern Greenland shelf (Madaj, 2021), also analyzed at MARUM following similar procedure as mentioned above, to represent the Sr and Nd isotope signatures of the proximal Rae Craton (Archean and Archean to Paleoproterozoic are differentiated).

4.4 Results

4.4.1 Age model and sedimentation rates

The final age-depth model of sediment core GeoB22336-4 is based on 13 calibrated AMS ^{14}C dates and indicates that the entire core record extends to ~14.3 ka BP, spanning from the last deglaciation through the Holocene (Fig. 4-2). The sedimentation rates between calibrated ages primarily range from 27 to 75 cm ka^{-1}. Exceptions are the lowest (21 cm ka^{-1}) and highest (612 cm ka^{-1}) values observed near a turbidite interval, which was identified in the deglacial part of this core (see section 4.4.2). The deglacial period is characterized by a moderate sedimentation rate of 49 cm ka^{-1} to over 62 cm ka^{-1}, followed by a drop to lower rates of 27 to 32 cm ka^{-1} during the early Holocene. During the mid-Holocene, sedimentation rates increased to moderate to high values of 42 to 75 cm ka^{-1},

and during the neoglacial period (late-Holocene), the rates dropped again towards lower values of ~31 cm ka^{-1}.

4.4.2 Computed tomography and stratigraphic units

Analyses of the CT-scans of core GeoB22336-4 reveal downcore changes in sediment characteristics, which in relation to the age model, allow the differentiation of five main stratigraphic units (Fig. 4-2): Unit 1: the lowermost unit characterized by high IRD content and a very high matrix sediment density from 613 to 580 cm (> ~14.3 ka BP); Unit 2: a rapidly deposited deglacial IRD-rich unit from 580 to 370 cm (~14.3 – 10.1 ka BP); Unit 3: a slowly accumulated early-Holocene transitional unit with significantly reduced IRD contents from 370 to 309 cm (10.1 – 8.4 ka BP); Uni 4: a mid-Holocene rapidly deposited IRD-free interval between 309 and 189 cm (8.4 – 5.6 ka BP); and Unit 5: a heavily bioturbated, slowly accumulated, and low IRD neoglacial sediment interval in the upper 189 cm of the core (< 5.6 ka BP).

The basal interval from 613 to 580 cm (Unit 1; > ~14.3 ka BP) constitutes a relatively dense and IRD-rich interval with many clasts reaching gravel size (Fig. 4-2). Maximum mean matrix sediment densities (MSD) (~1400 HU) and IRD concentrations (mean: 11.4 vol.%; 120.3 clasts cm^{-3}) are recorded here. This massive (unstratified) and over-compacted unit lacks any bioturbation, although some internal cracks are visible, which appear to be an artifact of the coring or subsequent processing of these dense deposits. Based on these observations, the basal sediments are classified as till deposits. Throughout Unit 2, between 580 and 370 cm (14.3 – 10.1 ka BP), there is a continuous trend (although with some fluctuations) toward decreasing MSDs and IRD contents (mean: 985 HU; 2.6 vol.%; 21.8 clasts cm^{-3}). Thin cross- to planar-bedded sediment layers with an erosional basal contact visible in the CT data between 495 and 474 cm having low quantities of IRD are classified as turbidite (Fig. 4-2). Bioturbation is enhanced in low-IRD layers in the older and denser part of Unit 2, but in the younger part bioturbation is typically low even when IRD content is low (mean: 0.4 vol.%). In Unit 3, the IRD contributions are low in an even less dense matrix (mean: 762 HU; 0.3 vol.%; 4.2 clasts cm^{-3}), while volume percentages of bioturbation portray an increasing trend (mean: 0.4 vol.%). Bioturbation is only marginally increased in Unit 4 (mean: 0.7 vol.%), where hardly any IRD is observed. The uppermost Unit 5 displays an over three-fold higher bioturbation content (mean: 2.2 vol.%) and shows rare occurrences of isolated IRD mainly towards the core top. The lowest MSD values are obtained in the upper Units 4 and 5 (decreasing from 710 to 552 HU). In the following sections, subsequent data from core GeoB22336-4 are presented exclusively against calibrated ages.

4.4.3 Grain-size distributions

The grain-size distributions of the <2 mm terrigenous sediment fraction of core GeoB22336-4 are polymodal and can generally be classified as sandy to silty mud, showing an upward fining sequence (Fig. 4-3). Multiple modes can be observed in the silt- and sand-sized fractions (8 to 0 ϕ) with the volume percentages of the sand-sized modes largely decreasing towards the core top. A finer mode of ~7.5 ϕ (~5.4 µm) is relatively stable and remained present in all samples downcore. Based on the grain-size distributions, the 6 ϕ (~16 µm) line is used to separate the unimodal <16 µm (fine) fraction from the polymodal >16 µm (coarse) fraction (orange demarcation line in Fig. 4-3).

In general, downcore changes in the proportion of the fine-grained sediments (and inversely of the coarse fraction), as well as the calculated mean-grain sizes, largely fit the previously defined units (Units 1 – 5; Fig. 4-3). The lowermost section of the core (Unit 1; > ~14.3 ka BP) is associated with a rather stable mean grain size of around 19 µm and consistently low contents of fine-grained material (FGM) (~ 45 vol.%). The following Unit 2 (14.3 – 10.1 ka BP) is initially characterized by strong fluctuations in mean grain size (mean: 10.5 µm), mirrored by variable FGM contents (mean: 62 vol.%). Above the turbidite, the record is marked by a less variable mean grain size (mean: 4.6 µm) but more variable and higher FGM contents (mean: 79 vol.%). In Unit 3 (10.1 – 8.4 ka BP), a very slight increase in the mean grain size (mean: 4.9 µm) and a drop in the FGM content (mean: 78 vol.%) indicate slightly coarser sediments. A fining-upward trend is reflected by the decreasing mean grain sizes and increasing FGM contents towards the upper part of this unit. This trend continues into Unit 4 (8.4 – 5.6 ka BP), which shows the finest sediments with the smallest mean grain sizes (mean: 3.7 µm) and highest FGM contents (mean: 87 vol.%). The transition to Unit 5 (< 5.6 ka BP) is marked by a small decrease in FGM contents (mean: 83 vol.%). Across this unit, the overall rather stable grain-size distribution is overlain by a weak long-term trend towards slightly coarser compositions, which becomes most obvious during the last 2 ka by increasing mean grain size (mean: 4.4 µm) and decreasing FGM contents (mean: 82 vol.%).

4.4.4 Mineralogical association

The XRD analyses of the sediments in core GeoB22336-4 show that, on average, carbonates (dolomite and calcite), quartz, K-feldspar, plagioclase, and clay minerals (mica and illites) constitute 81% of the total mineral assemblages. The remaining background composition is dominated by chlorite, kaolinite, pyroxene, and smectites. The basal till unit shows a mixed mineral composition with higher and lower contents of total carbonates (dolomite and calcite; mean: 34 wt.%), SIM (sum of illites and mica; mean: 16 wt.%), and SQF (sum of quartz, plagioclase, and K-feldspars; mean: 36 wt.%; Fig. 4-3). In the overlying units, the XRD data reveal an anti-correlation of detrital dolomite and SIM. This anti-correlation demonstrates a pronounced shift from dolomite-dominated deglacial

deposits (Unit 2; mean: dolomite = 31 wt.%, SIM = 12 wt.%), through transitional Unit 3 (mean: dolomite = 26 wt.%, SIM = 20 wt.%), to SIM-rich mid-late Holocene sediments (Unit 4 and 5; mean: dolomite = 20 wt.%, SIM = 24 wt.% and dolomite = 22 wt.%, SIM = 21 wt.%, respectively). In addition, Unit 2 sediments are associated with relatively high calcite (mean: 11 wt.%) and variable SQF (mean: 34 wt.%) contents. In Unit 3, calcite abundance steadily decreases from 11 wt.% mean value, observed in the lower unit, to ~1 wt.% at the top of this unit, while SQF content shows only a slight relative drop (mean: 28 wt.%). Calcite remained nearly absent (mostly below 1 wt.%) in Units 4 and 5 sediments. SQF values gradually increase from the onset of Unit 4 up to about 37 wt.% at ~6.6 ka BP. The SQF values stay around this level until the core top except for the central part in Unit 5 (4.5 to 2 ka BP), when these decrease to <32 wt.%.

4.4.5 Radiogenic Nd and Sr isotope composition

Varying radiogenic Nd and Sr isotope compositions of the <63 µm siliciclastic sediment fraction of core GeoB22336-4 (Fig. 4-3; Table 9-1) reflect variable contributions of source rocks, which have different ages and mineral compositions. The $^{87}Sr/^{86}Sr$ versus ε_{Nd} plot (Fig. 4-4) sets the isotope signatures into context with potential source areas. The radiogenic isotope data of the siliciclastic sediment fraction show uniform compositions in the basal Unit 1 (>14.3 ka BP), having $^{87}Sr/^{86}Sr$ and ε_{Nd} values of 0.738 and ~26.6, respectively (Fig. 4-3). The highest variability with both the highest and lowest $^{87}Sr/^{86}Sr$ and ε_{Nd} values is recorded in Unit 2. Within this unit, $^{87}Sr/^{86}Sr$ values range from 0.733 to 0.747 and ε_{Nd} values from -28.6 to -18.8. The most extreme $^{87}Sr/^{86}Sr$ and ε_{Nd} values occur within or close to the turbidite layer. The Sr-Nd isotope plot (Fig. 4-4) also reveals a larger scatter in Unit 2. However, the majority of the data points of units 1 and 2 are in close agreement with reference data representing the old (Archean to Paleoproterozoic) granitic and metamorphic rocks of the Rae Craton exposed along the Canadian and Greenland coasts of Baffin Bay (Fig. 4-1). In Unit 3, the isotope patterns of Sr and Nd change significantly to relatively stable values around 0.74 and -21, respectively (Fig. 4-3). Data from this unit form a more defined cluster in the Sr-Nd isotope plot, which is closest to the Holocene isotope signatures of core PS72/287-3, however still on the 'mixing line' between reference data from Barrow Strait and the Rae Craton (Fig. 4-4). At the onset of Unit 4, $^{87}Sr/^{86}Sr$ (ε_{Nd}) values slightly increase (decrease) toward relatively uniform compositions within this unit, concentrating around 0.742 and -22.6, respectively (Fig. 4-3). This unit also shows a well-defined cluster in the Sr-Nd isotope plot (Fig. 3-4), but differs from the previous unit since the data plot again closer to the radiogenic isotope signature of the Rae Craton, similar to Units 1 and 2. Within the uppermost Unit 5, the $^{87}Sr/^{86}Sr$ ratios show a continuous upward decrease from ~0.742 to 0.737 (Fig. 4-3). This change toward lesser radiogenic Sr values is initially gradual and becomes more pronounced after ~2.2 ka BP. In contrast, until ~2.2 ka BP, ε_{Nd} values remain largely (with one

exception at the beginning of this unit at ~4.7 ka BP) at Unit 4 levels (-22) before values decrease to around -25. These youngest Nd isotope signatures are in a similar range as observed in the much older Units 1 and 2, being again close to the reference data from the Rae Craton (Fig. 4-4).

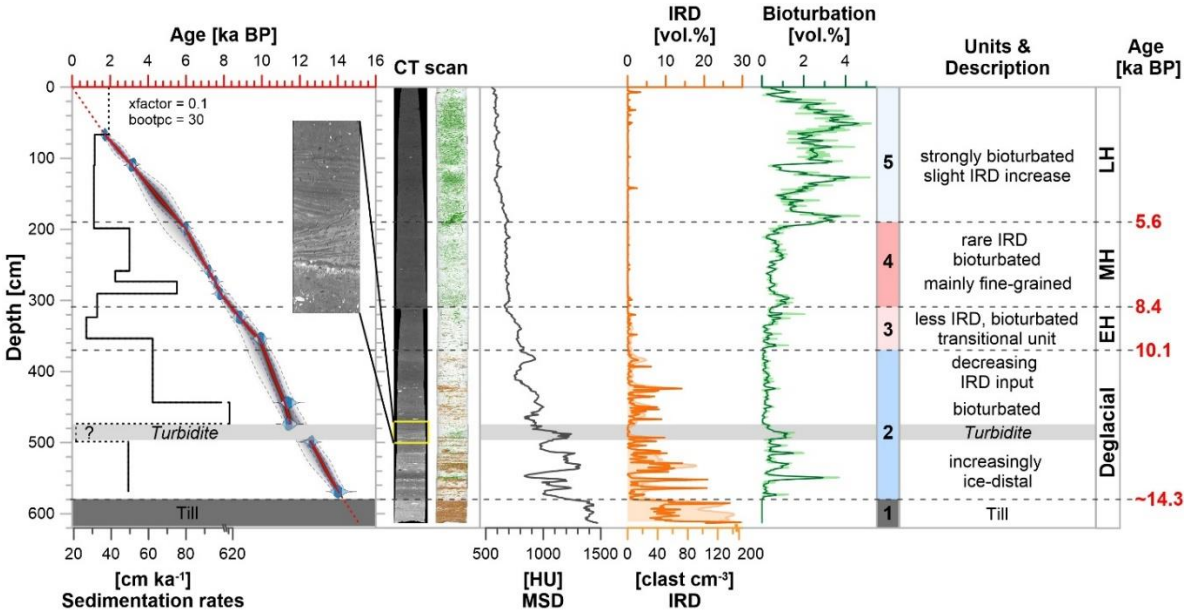

Figure 4-2: Age-depth model and calculated sedimentation rates (left) and processed CT scan and associated downcore quantification of the mean matrix sediment density (MSD) and ice-rafted debris (IRD) and bioturbation content (right) with a brief description of stratigraphic units 1-5 of core GeoB22336-4. Left to right: the solid black step line represents the sedimentation rates between calibrated ages; the solid red line connects the median probability ages (dashed red lines show depths outside radiocarbon-dated intervals where linear extrapolation is applied), and the blue and grey dashed lines represent the 68% (1σ) and 95% (2σ) probability intervals; the yellow rectangle on the CT scan marks the turbidite interval enlarged to the right; the brown, green and light-grey colors on the interpreted CT image respectively highlight IRD (clasts > 1 mm), bioturbation, and the matrix sediments.

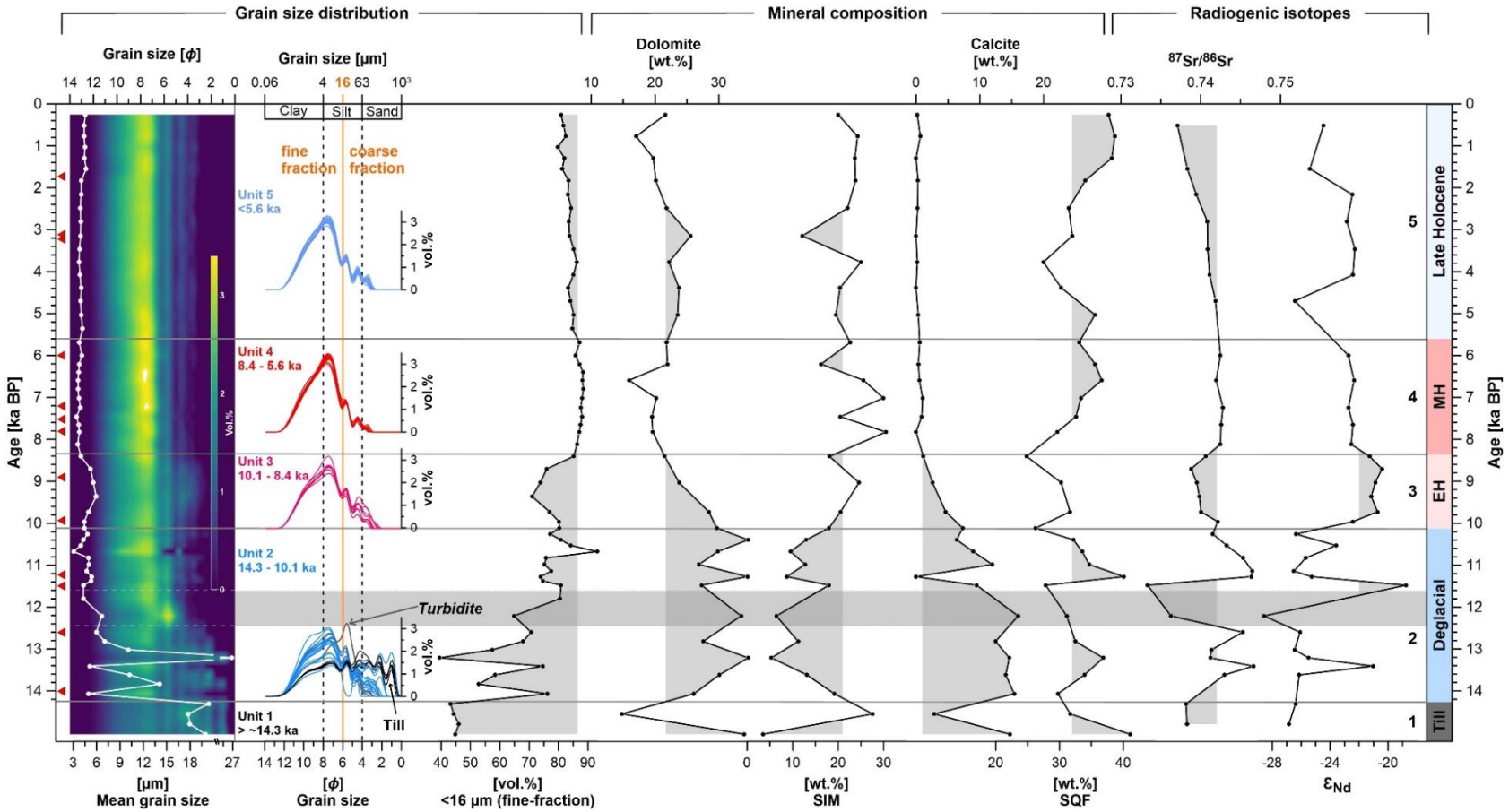

Figure 4-3: Contour plot of the downcore grain-size distributions overlain by the mean grain size (white line), grain-size distribution of individual samples associated with stratigraphic units 1–5 (orange line separates the fine and coarse fractions), downcore abundance of the fine-grained (<16 µm) fraction, as well as mineralogical and radiogenic isotope composition of core GeoB22336-4. Grey lines mark the boundary of the different units; red triangles indicate intervals with age control; SIM (sum of illites and mica), SQF (sum of quartz, plagioclase, and K-feldspars); grey shaded areas indicate intervals of higher or lower values in grain size, mineralogical and radiogenic isotope composition; EH (early-Holocene); MH (mid-Holocene).

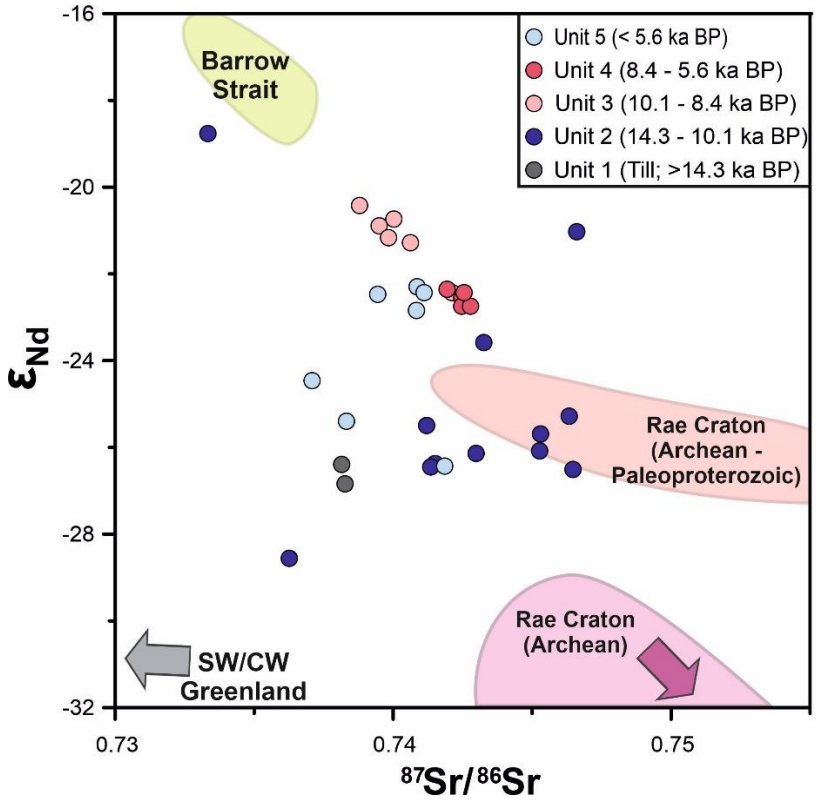

Figure 4-4: The $^{87}Sr/^{86}Sr$ versus ε_{Nd} isotope plot for core GeoB22336-4. Data points have colors corresponding to their age and the five stratigraphic units identified in the text. Background isotope signatures from different geological terrains are shown for comparison. The colors of the background data are adapted to the colors used in Figure 4-1. Background data are from marine sediment analyses of different studies: Rae Craton (Archean – Paleoproterozoic; light pink): sediment core (GeoB19927-3) from the western Greenland shelf (Madaj, 2021), Rae Craton (Archean; dark pink): sediment core (GeoB19946-4) from the northwestern Greenland shelf (Madaj, 2021) as well as from the northeastern Baffin Island shelf (data from GeoB22357-3, Table 9-3), Barrow Strait (light green): Holocene isotope signatures of core PS72/287-3 (Table 9-4), and southwest (SW) and central west (CW) Greenland: stream sediment data (Colville et al., 2011; Reyes et al., 2014).

4.5 Discussion

Variations in sedimentological properties and mineralogical and radiogenic isotopic composition of the five stratigraphic units of core GeoB22336-4 (Fig. 4-2, 4-3) provide a continuous record of the changing depositional and environmental conditions and sediment provenances in northern Baffin Bay since the last deglaciation. These are discussed in the following sections from paleoclimatic and palaeoceanographic perspectives.

4.5.1 Ice stream retreat and deglacial sediment dynamics (~14.3 to 10.1 ka BP)

During the LGM, the LIS, IIS, and GIS advanced across the continental shelves surrounding Baffin Bay (England, 1999; Dyke et al., 2002; England et al., 2006; MacLean et al., 2017). The coalescing of

the LIS and GIS with the IIS formed marine-terminating grounded ice shelves blocking the connections between the Arctic Ocean and Baffin Bay, which presently exist (mainly) through Lancaster Sound and Nares Strait (Blake et al., 1996; England, 1999; Dyke, 1999; Dyke et al., 2002; Niessen et al., 2010; MacLean et al., 2017; Dalton et al., 2020). The glacial-ice stream draining the coalescent LIS and IIS advanced eastward into Baffin Bay and was grounded on the seabed approximately 270 km from the mouth of Lancaster Sound in ~1300 m water depth (Li et al., 2011; Harrison et al., 2011a; Bennett et al., 2014). The glacial-ice margins were likely buttressed by an ice shelf that extended partly (Jennings et al., 2018; Couette et al., 2022) or entirely across Baffin Bay (Gibb et al., 2015; Simon et al., 2016).

In core GeoB22336-4, the massive, very dense, highly homogenized, and burrow-free gravelly and sandy mud in the oldest Unit 1 (> ~14.3 ka BP) are indicative of subglacial till deposits (Figs. 4-2, 4-3). The variability and composition in mineral assemblages of the till unit suggest highly mixed sediment provenances (Fig. 4-3), probably materials eroded from northeastern Baffin and Devon Islands and adjacent channels transported by the Lancaster Sound ice stream toward the core site. In contrast, the radiogenic isotope signatures in the till unit are rather stable, also pointing to a mixture of various source regions (Fig. 4-4). The presence of these till deposits indicates that the Lancaster Sound ice stream was still grounded at the mouth of Lancaster Sound until 14.3 ka BP.

In contrast, based on three ^{14}C-dated sediment cores (incl. core 49PC collected ~11 km from our core site), Kelleher et al. (2022) suggested that the ice stream had already retreated to central Lancaster Sound (to site 59PC; Fig. 4-1) by ~15.3 ka BP, much earlier than previously thought (e.g., Dyke et al., 2002; MacLean et al., 2017; Furze et al., 2018; Dalton et al., 2020). However, this interpretation is based on linear age extrapolations for sediments older than ~11.6 and 11.1 ka BP, without considering probable higher sedimentation rates in the older parts of the cores deposited under more ice proximal conditions, which would support younger lift-off ages. As the presence of the Lancaster Sound ice stream at site GeoB22336-4 until ~14.3 ka BP (last calibrated ^{14}C age of 14 ka BP obtained 10 cm above the till) is also consistent with an extensive ice margin close or even seaward of our core site around ~13 ^{14}C ka (~14 ka BP; Dalton et al. (2020); Fig. 4-1), there is clear evidence that grounded ice indeed extended to the outer Lancaster Sound until the end of the Bølling/Allerød interstadial.

These basal till deposits are overlain by a slightly bioturbated, gravel-bearing sandy-silty mud with an intercalated turbidite (Unit 2; 14.3 – 10.1 ka BP; Figs. 4-2, 4-3), suggesting variable sediment delivery also by iceberg rafting and mass-wasting. Decreasing but variable IRD input at the core site and nearby site 49PC (Kelleher et al., 2022) probably reflects the change from ice proximal to increasingly distal glaciomarine sedimentation. Ice-proximal sediments containing abundant large

clasts have been widely described along Baffin Bay surrounding shelves and slopes (e.g., Ó Cofaigh et al., 2013a, 2013b; Dowdeswell et al., 2014; Jennings et al., 2017; Jenner et al., 2018; Kelleher et al., 2022). In addition, some bioturbation traces in our core (Fig. 4-2) and the presence of foraminifera (available for radiocarbon dating and also found in cores 49PC and 10PC; Furze et al., 2018; Kelleher et al., 2022) point to more open water conditions. These glaciomarine conditions prevailed until ~10.1 ka BP, as also found in other cores in the region (Bennett et al., 2014; Kelleher et al., 2022).

Decreasing sedimentation rates between 14.3 and 10.1 ka BP (in addition to decreasing IRD inputs, Fig. 4-2) probably reflect the fast westward recession of the Lancaster Sound ice stream (e.g., Dyke, 1999; Pieńkowski et al., 2014; MacLean et al., 2017). In addition to the maximum northern latitude summer insolation at that time (Berger and Loutre, 1991; Laskar et al., 2004), the ice stream recession might have been accelerated by the gradual strengthening northward flow of comparably warm Atlantic Water via the WGC at this time (Fig. 4-5; Weiser et al., 2021). Strengthened Atlantic Water influence inferred from foraminifera assemblages has been reported from several sites along the west Greenland shelf (e.g., Sheldon et al., 2016; Jennings et al., 2014, 2017) up to northern Baffin Bay (e.g., Knudsen et al., 2008; Jennings et al., 2019; Jackson et al., 2021) and into Lancaster Sound and the CAA channels (e.g., Pieńkowski et al., 2012, 2013, 2014; Furze et al., 2018; Kelleher et al., 2022). During this time, the Arctic Ocean-Baffin Bay connections through the Lancaster Sound, Nares Strait, and other CAA channels remained shut by grounded glacial ice (England, 1999; Dyke et al., 1991, 2003; England et al., 2006), permitting an enhanced northward penetration of warm Atlantic Water as the dominant water mass in Baffin Bay, besides meltwater input from surrounding ice sheets.

The moderate to rapid deposition of this ~2-m thick IRD-rich deglacial interval (Unit 2), also rich in carbonates (mean: ~42 wt.%; Figs. 4-2, 4-5), points to a high sediment input from ice stream activities in Lancaster Sound transporting regional Paleozoic carbonates to site GeoB22336-4, as well as sites 49PC and 59PC (Kelleher et al., 2022). Significant amounts of SQF and radiogenic ε_{Nd} values ranging mainly between ~-24 and -28 and $^{87}Sr/^{86}Sr$ isotope signatures between 0.741 and 0.747 (Fig. 4-3), further indicate a significant contribution of older Archean to Paleoproterozoic granitic and gneissic rocks of the Rae Craton, probably from nearby eastern Devon Island and/or the west coast of Smith Sound (Figs. 4-1, 4-4). Despite the lack of Sr and Nd isotope reference data from sites proximal to the core site, the general bedrock lithology of eastern Devon Island and the west coast of Smith Sound is similar to that of the Rae Craton on Greenland and Baffin Island and, thus, is expected to provide comparable Sr and Nd isotopic signatures. Furthermore, ε_{Nd} values

between -32.1 and -30.8 measured in samples from rivers draining Bylot Island (Grenier et al., 2022) could argue for Bylot Island as an additional source area for parts of Unit 2 sediments.

4.5.2 Early-Holocene postglacial transition and the establishment of Arctic-Atlantic throughflow (10.1 to 8.4 ka BP)

A marked shift from deglacial conditions to the early-Holocene transitional environment is recorded in Unit 3 (10.1 – 8.4 ka BP). This transition is characterized by a pronounced drop in sedimentation rates suggesting largely reduced sediment delivery to the core site (Fig. 4-2), accompanied by a strong increase in ε_{Nd} values and a less pronounced decrease in $^{87}Sr/^{86}Sr$ values and SQF mean content (Fig. 4-3). In addition, coarse-grained sediments (>16 µm) still make up almost a quarter (on average) of the grain-size distributions during this interval (Fig. 4-3). The very low amounts of large iceberg-rafted clasts in this interval and decreasing contents of detrital carbonates (Fig. 4-5) might signify a switch from tidewater to predominately land-terminating glaciers during the late stage of LIS and IIS retreat (onset of postglacial conditions). This transition is similarly reflected in the largely reduced IRD input and decreasing detrital carbonate content in northern Baffin Bay cores 49PC and 59PC around this time (Kelleher et al., 2022). However, still recognizable IRD inputs and enhanced contents of coarse-grained sediments in core GeoB22336-4 point to at least an occasional occurrence of iceberg rafting. The transition to postglacial conditions happens during a period of potentially high northward-heat transport by the early-Holocene WGC-speed maximum occurring synchronously with decreasing but high Agassiz meltwater release and high summer insolation (Fig. 4-5; Laskar et al., 2004; Fisher et al., 2012; Weiser et al., 2021). Still, reconstructions of summer sea-surface temperatures (SSTs) and seasonal sea ice conditions suggest mean sea surface temperatures <2.5°C and sea ice coverage for around 9.5 months at that time in northwestern Baffin Bay (Fig. 4-5; Ledu et al., 2008, 2010). Similarly, cold sea-surface conditions with extensive (spring) sea-ice cover is reconstructed for northeastern Baffin Bay (Fig. 4-5; Saini et al., 2020, 2022). Nevertheless, increasing bioturbation in core GeoB22336-4 hints at slightly more extensive (prolonged) open surface waters. The decrease in sediment delivery (sedimentation rates) during this period appears to be of a regional scale, which is observed in several records from Barrow Strait, Smith Sound, and Northern Baffin Bay (Pieńkowski et al., 2012, 2013; Jennings et al., 2019; Jackson et al., 2021; Fig. 4-S1).

In addition, the shift of Sr and Nd isotope compositions towards lower and higher values (Fig. 4-3), respectively, and their placement between the Barrow Strait and Rae Craton isotope signature range (Fig. 4-4) indicates a weaker influence of sediments from proximal Devon Island and west coast of Smith Sound (i.e., Rae Craton) and a stronger input from the Barrow Strait area during this interval. The radiogenic ε_{Nd} signature of the Barrow Strait region indicated by sediment core

PS72/287-3 (Table 9-4) is further supported by radiogenic ε_{Nd} values of -15.1 and -16.1 obtained from river samples draining into Barrow Strait (Grenier et al., 2022). However, the dolomite content indicating the detrital carbonate input, which is also seen as an indicator for material coming from the Barrow Strait region, continues to decrease at the same time in core GeoB22336-4 (Fig. 4-3) and other cores (e.g., 49PC; Kelleher et al., 2022), thus, seemingly contradicting the interpretation of increased sediment delivery from this region. The long-term decrease in dolomite coincides with a similar reduction in IRD input (Fig. 4-5), pointing to a predominant iceberg transport of the dolomite. Thus, with the transition from tidewater to land-terminating glaciers, the dolomite input to the Lancaster Trough Mouth fan decreased, giving space for the delivery of finer materials of different mineralogies from Barrow Strait and the wider CAA. Consequently, the observed shift in sediment provenance and the marked drop in sedimentation rates at our core site (and others, also in Barrow Strait; Fig. 4-S1) is interpreted as the final deglaciation of Lancaster Sound and Barrow Strait and the establishment of an open marine connection between the Arctic Ocean and Baffin Bay via the main channels of the CAA around this time. According to our results, this opening happened approximately between 10.2 and 9.8 ka BP in agreement with previous studies (e.g., Pieńkowski et al., 2012, 2014).

A shift in trend towards increased contribution of fine-grained sediments (with increasing SIM and SQF contents), higher $^{87}Sr/^{86}Sr$, and decreasing ε_{Nd} values at the core site started at ~8.5 ka BP at the end of Unit 3 (Fig. 4-3). The timing coincides with the opening of the Nares Strait connection between the Arctic Ocean and Baffin Bay, fully unblocked between 8.5 and 8.2 ka BP (Dyke et al., 2002; Jennings et al., 2011, 2019, 2022; Georgiadis et al., 2018; Kelleher et al., 2022). The potential link between Nares Strait deglaciation and a reorganization of the sediment routing system in northern Baffin Bay is discussed in the following section.

4.5.3 Rapid fine-grained sedimentation in Northern Baffin Bay during the HTM (8.4 to 5.6 ka BP)

The most conspicuous feature of Unit 4 (8.4 – 5.6 ka BP) is the rapid deposition of predominantly fine-grained sediments (up to 75 cm ka^{-1}) and the virtual absence of IRD that follows slight changes in sediment composition (highest mean SIM and SQF contents, lowest dolomite content) in this interval (Figs. 4-2, 4-3). Just after 8.5 ka BP, also a shift towards consistently lower ε_{Nd} and higher $^{87}Sr/^{86}Sr$ values (Fig. 4-3) point to a relatively pronounced input of material originating from the Rae Craton. Since the timing of the transition roughly fits the opening of Nares Strait between 8.5 and 8.2 ka BP (Dyke et al., 2002; Jennings et al., 2011, 2019, 2022; Georgiadis et al., 2018; Kelleher et al., 2022), these shifts in our records might point to a reconfiguration of the sediment routing system. A change in surface ocean circulation due to additional Arctic waters entering northern

Baffin Bay via Nares Strait could cause intensive sediment transport from the mouth of Jones Sound to the core site. Enhanced sediment input from eastern Devon Island or the west coast of Smith South, which originate predominantly from rocks of the Rae craton, could potentially drive Nd and Sr isotope composition towards the values observed in Unit 4 (Fig. 4-4).

While at first glance, such a change in provenance also might be a reason for the observed increase in sediment accumulation, this appears rather unlikely here as, towards the end of Unit 4, sedimentation rates decrease by ~50 % without any major change in sediment composition (Figs. 4-3, 4-5). Consequently, the sedimentation rates of Unit 4, which are associated with over 85 vol.% of fine-grained sediments, most likely reflect a change in the dominant sedimentation process. Interestingly, such increases in sedimentation rates by 2 to >5 fold are a common feature in northern Baffin Bay during this time window (Fig. 4-S1), which roughly coincided with the regional Holocene Thermal Maximum (HTM; broadly spanning from ~8.5 to ~5 ka BP; Kaufman et al., 2004; Jennings et al., 2011; Gajewski, 2015; Briner et al., 2016). Accordingly, St-Onge and St-Onge (2014) interpreted similar observations of predominately fine-grained sediments in core 42PC to be caused by warmer and wetter Arctic conditions during the mid-Holocene (Thomas et al., 2018; Chen et al., 2022). Such environmental conditions would have favored increased terrestrial freshwater runoffs, resulting in enhanced delivery of suspended sediments (suspension cloud) mainly to the nearby fjords and shelves around northern Baffin Bay, as observed today along the west Greenland coastline (Overeem et al., 2017). However, the bordering LIS, IIS, and GIS approached their minimum areal extent after 8.5 ka BP (Dyke et al., 2003; Funder et al., 2011; Dalton et al., 2020), coinciding with decreasing Arctic summer solar insolation (Laskar et al., 2004) and low melting rates (e.g., Agassiz melt record, Fisher et al., 2012) (Fig. 4-5). Thus, resulting low amounts of meltwater and, hence, reduced sediment discharge is clearly in conflict with the above interpretation.

Recent model simulations revealed that reduced meltwater input to Baffin Bay results in the thinning of the freshwater lens capping the underlying warmer WGC waters and, consequently, in the weakening of water-column stratification (weaker halocline), which would allow for enhanced vertical heat flux and ocean-atmosphere heat exchange (Castro de la Guardia et al., 2015). Even today, with a much weaker WGC (Weiser et al., 2021), wind-driven upwelling of warmer WGC water along the northwestern Greenland shelf (Melling et al., 2001) can provide heat to melt sea ice and cause the prolongation of sea ice melt season in northern Baffin Bay as observed in recent decades (Ballinger et al., 2022).

Such a scenario can also be assumed for the period between ~8.5 and 5.6 ka BP, a time during which a strong WGC, forced by a strong AMOC, transported latent heat northward (Ritz et al., 2013; Weiser et al., 2021), that probably due to a weak halocline contributed to decreasing sea-ice cover

(increasing SSTs) in northwestern (Ledu et al., 2010) and northeastern (Saini et al., 2020, 2022) Baffin Bay and increasing air temperatures in the eastern Canadian Arctic (Gajewski, 2015) (Fig. 4-5). These conditions most likely favored very high turnover of sediment-laden sea ice (= sea-ice melting rate) and the release of fine-grained sediments entrained in the sea ice (Nürnberg et al., 1994; Eicken et al., 2000; Dethleff, 2005). Consequently, this scenario could explain the regional pattern of high sedimentation rates in Northern Baffin Bay observed for several sites (Fig. 4-S1). In contrast, the relatively low and stable postglacial sedimentation rates in Barrow Strait (sites 144PC and 154PC; Pieńkowski et al., 2012, 2014) and Nares Strait (sites 05GC and Kane2B; Jennings et al., 2011; Georgiadis et al., 2018; Fig. 4-S1) accordingly could be explained by a much weaker influence of the WGC at these locations far off the northern Baffin Bay, which likely resulted in more extensive (permanent) sea ice cover.

Independent evidence for this scenario is provided from a comparable setting in the eastern Fram Strait, where sea-ice-covered Arctic Waters meet the relatively warm waters (>0 °C) of the West Spitsbergen Current (Hebbeln, 2000). Sediment trap studies (1987-1990) revealed a four- to six-fold increase in particle flux that was attributed to the release of sea ice-rafted debris, mainly sediment particles <40 µm (Hebbeln, 2000). This observation is in line with the observed increase in sedimentation rates as well as the predominance of fine-grained sediments in core GeoB22336-4 (Fig. 4-5). Interestingly, the seabed accumulation rates of ~30 g cm^{-2} ka^{-1} extrapolated from the sediment trap study in the Fram Strait are almost in the same order of magnitude to the observed accumulation rates of 40 to 75 g cm^{-2} ka^{-1} in our core GeoB22336-4 (assuming a dry bulk density of ~1 g cm^{-3}). Thus, for the period from 8.5 to 5.6 ka BP, a relatively strong heat supply via the WGC, predominantly controlled by the AMOC (Weiser et al., 2021), probably enabled the intense melting of sea ice due to a weak halocline, resulting in the enhanced sediment accumulation of sea ice-transported fine-grained sediment (<16 µm) at our core site.

4.5.4 Reduced sedimentation during the Late Holocene (< 5.6 ka BP)

The decrease of the fine-grained sediment input at the onset of Unit 5 (~5.6 ka BP) towards pre-HTM levels coincides with a significant reduction in sedimentation rates to ~31 cm ka^{-1} (Fig. 4-5). At the same time, the amount of bioturbation in the sediments shows an ~3-fold increase. This suggests a sudden decline in the input of sea ice-rafted fine-grained sediments at site GeoB22336-4 (see section 4.5.3), probably triggered by the weakening of the WGC, controlled by the AMOC strength, after ~6 ka BP (Fig. 4-5; see Weiser et al., 2021). As neither regional SSTs nor sea ice cover data show any marked shift at ~5.6 ka BP (Ledu et al., 2008, 2010; Saini et al., 2020, 2022), the observed increase in bioturbation might be, at least partly, related to the decrease in sedimentation rates resulting in prolonged exposure of surface sediments to bioturbating organisms. A decreasing

influence of Atlantic-sourced waters at this time is further supported by a strong increase in relative abundances of agglutinated foraminifera in core 117Q from northern Baffin Bay (Fig. 4-5; Jackson et al., 2021).

During the following millennia, sedimentation in northern Baffin Bay showed little variation. Most notable are long-term trends in the mineralogical and radiogenic isotope composition and the IRD input. Less radiogenic ε_{Nd} and Sr signatures and high SQF values, especially for the last ~2 ka BP (Fig. 4-3), suggest an increased influence of sediments originating from the rocks of the Rae Craton of eastern Devon Island and the west coast of Smith Sound. For the same period, a slight coarsening of the sediments (Fig. 4-3) and an increase in IRD (Fig. 4-5) point to glacier advance and an increasing number of tidewater glaciers in the region, which might be sourced rather proximal, e.g., eastern Devon Island, as suggested by the radiogenic isotope and SQF data. The suggested glacier advance is likely linked to the Neoglacial cooling, an Arctic-wide shift in paleoclimatic and paleoceanographic conditions documented in numerous terrestrial- and marine records and climate simulations (e.g., Miller et al., 2005; Briner et al., 2009, 2016; McKay et al., 2018). In northern Baffin Bay, these conditions are most prominently expressed over the last 3 ka BP (e.g., Briner et al., 2016). The shift toward cooler conditions in this region has been explained (e.g., Briner et al., 2016) as a response to (i) the minimum Artic summer insolation at ~3 ka BP (Laskar et al., 2004) and (ii) the decline in northward oceanic heat transport via the AMOC-controlled WGC (Ritz et al., 2013; Weiser et al., 2021; Fig. 4-5). Deteriorating conditions linked to this cooling also might have reduced productivity, as indicated by decreasing bioturbation observed in core GeoB22336-4 (Fig. 4-5). However, the chronostratigraphy in the upper 60 cm (the last ~2 ka) of this core is weak due to the lack of datable material (age control), which hampers more detailed reconstructions.

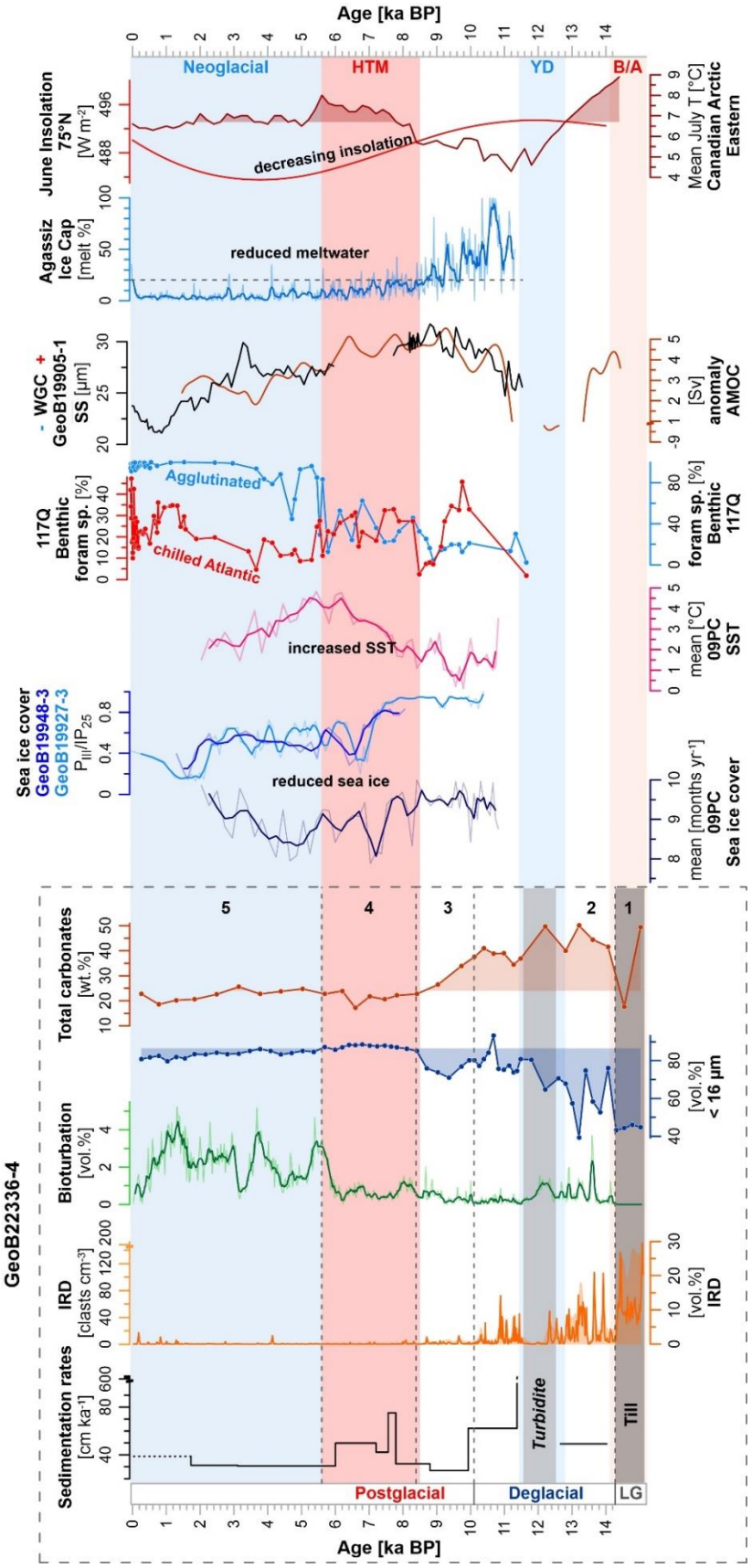

Figure 4-5: Comparison of selected proxies from core GeoB22336-4 with other paleoenvironmental data from northern Baffin Bay. From left to right: Core GeoB22336-4 data on sedimentation rates, contents ice-rafted debris (IRD), bioturbation traces, fine material <16µm and total carbonate (= sum of dolomite and calcite).

The black numbers 1-5 indicate the five units discussed in the text. The grey dashed line marks the transition from deglacial to postglacial conditions in core GeoB22336-4. Further paleoenvironmental data include Holocene sea-ice conditions and sea surface temperatures in northern Baffin Bay from core 09PC (Ledu et al., 2010) and cores GeoB19948-3 and GeoB19927-3 (Saini et al., 2020, 2022) and benthic foraminifera abundance in core 117Q (Jackson et al., 2021), reconstructed Atlantic Meridional Overturning Circulation (AMOC) anomaly (Ritz et al., 2013), West Greenland Current (WGC) strength from mean sortable silt record in core GeoB19905-1 (Weiser et al., 2021), the melt record from the Agassiz Ice Cap (Fisher et., 2012), mean July temperatures for the eastern Canadian Arctic (Gajewski, 2015), and the June solar insolation at 75°N (Laskar et al., 2004). LG = Late Glacial; B/A = Bølling/Allerød; YD = Younger Dryas; HTM = Holocene Thermal Maximum.

4.6 Conclusions

Based on the radiocarbon-dated sediment core GeoB22336-4, we investigated ice sheet dynamics and changing oceanographic conditions in northern Baffin Bay for the last ~14.3 ka. For the time prior to 14.3 ka BP, the sediment record provides evidence for grounded glacial ice at the mouth of Lancaster Sound. This reconstruction puts the grounding line of the Lancaster Sound ice stream farther out of Lancaster Sound at this time, contrary to a tentative inner Lancaster Sound position at ~15.3 ka BP as previously suggested. The prevailing proximity of the ice stream between 14.3 and 10.1 ka BP enabled efficient delivery of IRD, which comprised a substantial portion of materials from regional Paleozoic carbonates accompanied by materials from the proximal eastern Devon and southeastern Ellesmere Islands. The early Holocene postglacial interval is marked by the opening of the Barrow Strait-Lancaster Sound gateway between ~10.2 and 9.8 ka BP resulting in an initial Arctic-Atlantic throughflow documented by enhanced sediment supply from Barrow Strait. After the Nares Strait opening at ~8.5 ka BP, the mid-Holocene interval (up to 5.6 ka BP) witnessed the rapid deposition of fine-grained, sea-ice-rafted sediments. Reduced meltwater input to northern Baffin Bay after the ice sheets had reached their Holocene minimum extent likely led to a weaker halocline, allowing the heat supplied by a strong WGC to trigger intense melting of sediment-laden sea ice during this time. The weakening WGC influence in the region around ~5.6 ka BP resulted in a reduced input of sea-ice-rafted material and a corresponding significant drop in sedimentation rates, which probably enabled the strong bioturbation of the late Holocene sediments deposited thereafter. During the last ~ 2 ka BP, increasing IRD inputs and continuously changing source areas suggest regional glacier re-advances, probably in response to Neoglacial cooling.

Acknowledgements

We gratefully acknowledge the master and crew of the R/V Maria S. Merian for their work during cruise MSM66. Sample material has been provided by the GeoB Core Repository at the MARUM – Center for Marine Environmental Sciences, University of Bremen, Germany. We gratefully acknowledge Klinikum Bremen-Mitte and Christian Timann and Arne-Jörn Lemke for supporting the CT measurements in their facilities. Thanks to Ruediger Stein and the Alfred Wegener Institute Helmholtz Centre for Polar and Marine Research for providing sediment samples from Core PS72/287-3 recovered during Polarstern Expedition ARK-XXIII/3 in 2008. This project was supported by the Deutsche Forschungsgemeinschaft (DFG) through the International Research Training Group "Processes and impacts of climate change in the North Atlantic Ocean and the Canadian Arctic" (IRTG 1904 ArcTrain).

Data availability

All data presented here are available at the PANGAEA online data repository (https://www.pangaea.de/).

References

Aksu, A.E., Piper, D.J.W., 1987. Late Quaternary sedimentation in Baffin Bay. Canadian Journal of Earth Sciences 24, 14.

Andrews, J.T., 1990. Fiord to Deep Sea Sediment Transfers along the Northeastern Canadian Continental Margin: Models and Data. Géographie physique et Quaternaire 44, 55-70.

Andrews, J.T., Bjork, A.A., Eberl, D.D., Jennings, A.E., Verplanck, E.P., 2015. Significant differences in late Quaternary bedrock erosion and transport: East versus West Greenland ~70°N - evidence from the mineralogy of offshore glacial marine sediments. Journal of Quaternary Science 30, 452-463.

Andrews, J.T., Eberl, D.D., 2011. Surface (sea floor) and near-surface (box cores) sediment mineralogy in Baffin Bay as a key to sediment provenance and ice sheet variations. Canadian Journal of Earth Sciences 48, 1307-1328.

Andrews, J.T., Kirby, M.E., Aksu, A., Barber, D.C., Messe, D., 1998. Late quaternary detrital carbonate (DC-) layers in Baffin Bay marine sediments (67°-74°N): Correlation with Heinrich event in the North Atlantic? Quaternary Science Reviews 17, 1125-1137.

Andrews, J.T., Klein, A.J., Jenner, K.A., Jennings, A.E., Campbell, C., 2018. The variability of Baffin Bay seafloor sediment mineralogy: the identification of discrete glacial sediment sources and application to Late Quaternary downcore analysis. Canadian Journal of Earth Sciences 55, 620-639.

Andrews, J.T., Piper, D.J.W., 2022. Late Quaternary changes in sediment sources in the Labrador Sea. Canadian Journal of Earth Sciences 0026, 1-25.

Ballinger, T.J., Moore, G.W.K., Garcia-Quintana, Y., Myers, P.G., Imrit, A.A., Topál, D., Meier, W.N., 2022. Abrupt Northern Baffin Bay Autumn Warming and Sea-Ice Loss Since the Turn of the Twenty-First Century. Geophysical Research Letters 49.

Barber, D.G., Massom, R.A., 2007. Chapter 1 The Role of Sea Ice in Arctic and Antarctic Polynyas, Polynyas: Windows to the World, pp. 1-54.

Bartels, M., Titschack, J., Fahl, K., Stein, R., Seidenkrantz, M.-S., Hillaire-Marcel, C., Hebbeln, D., 2017. Atlantic Water advection vs. glacier dynamics in northern Spitsbergen since early deglaciation. Climate of the Past 13, 1717-1749.

Bennett, R., Campbell, D.C., Furze, M.F.A., 2014. The shallow stratigraphy and geohazards of the Northeast Baffin Shelf and Lancaster Sound. Bulletin of Canadian Petroleum Geology 62, 217-231.

Berger, A., Loutre, M.F., 1991. Insolation values for the climate of the last 10 million years. Quaternary Science Reviews 10, 297-317.

Blake, W., Jr, Jackson, H., Currie, C., 1996. Seafloor evidence for glaciation, northernmost Baffin Bay. Bulletin of the Geological Society of Denmark 43, 157-168.

Briner, J.P., Davis, P.T., Miller, G.H., 2009. Latest Pleistocene and Holocene glaciation of Baffin Island, Arctic Canada: key patterns and chronologies. Quaternary Science Reviews 28, 2075-2087.

Briner, J.P., McKay, N.P., Axford, Y., Bennike, O., Bradley, R.S., de Vernal, A., Fisher, D., Francus, P., Fréchette, B., Gajewski, K., Jennings, A., Kaufman, D.S., Miller, G., Rouston, C., Wagner, B., 2016. Holocene climate change in Arctic Canada and Greenland. Quaternary Science Reviews 147, 340-364.

Butzin, M., Köhler, P., Lohmann, G., 2017. Marine radiocarbon reservoir age simulations for the past 50,000 years. Geophysical Research Letters 44, 8473-8480.

Caron, M., Rochon, A., Montero-Serrano, J.C., St-Onge, G., 2019. Evolution of sea-surface conditions on the northwestern Greenland margin during the Holocene. Journal of Quaternary Science 34, 569-580.

Castro de la Guardia, L., Hu, X., Myers, P.G., 2015. Potential positive feedback between Greenland Ice Sheet melt and Baffin Bay heat content on the west Greenland shelf. Geophysical Research Letters 42, 4922-4930.

Chen, J., Zhang, Q., Kjellström, E., Lu, Z., Chen, F., 2022. The Contribution of Vegetation-Climate Feedback and Resultant Sea Ice Loss to Amplified Arctic Warming During the Mid-Holocene. Geophysical Research Letters 49.

Colville, E.J., Carlson, E.A., Beard, L.B., Hatfield, G.R., Stoner, S.J., Alberto V. Reyes, V.A., Ullman, J.D., 2011. Sr-Nd-Pb Isotope Evidence for Ice-Sheet Presence on Southern Greenland During the Last Interglacial. Science 333, 620-623.

Couette, P.-O., Lajeunesse, P., Ghienne, J.-F., Dorschel, B., Gebhardt, C., Hebbeln, D., Brouard, E., 2022. Evidence for an extensive ice shelf in northern Baffin Bay during the Last Glacial Maximum. Communications Earth & Environment 3.

Coulthard, R.D., Furze, M.F.A., Pieńkowski, A.J., Chantel Nixon, F., England, J.H., 2010. New marine ΔR values for Arctic Canada☆. Quaternary Geochronology 5, 419-434.

Dalton, A.S., Margold, M., Stokes, C.R., Tarasov, L., Dyke, A.S., Adams, R.S., Allard, S., Arends, H.E., Atkinson, N., Attig, J.W., Barnett, P.J., Barnett, R.L., Batterson, M., Bernatchez, P., Borns, H.W., Breckenridge, A., Briner, J.P., Brouard, E., Campbell, J.E., Carlson, A.E., Clague, J.J., Curry, B.B., Daigneault, R.-A., Dubé-Loubert, H., Easterbrook, D.J., Franzi, D.A., Friedrich, H.G., Funder, S., Gauthier, M.S., Gowan, A.S., Harris, K.L., Hétu, B., Hooyer, T.S., Jennings, C.E., Johnson, M.D., Kehew, A.E., Kelley, S.E., Kerr, D., King, E.L., Kjeldsen, K.K., Knaeble, A.R., Lajeunesse, P., Lakeman, T.R., Lamothe, M., Larson, P., Lavoie, M., Loope, H.M., Lowell, T.V., Lusardi, B.A., Manz, L., McMartin, I., Nixon, F.C., Occhietti, S., Parkhill, M.A., Piper, D.J.W., Pronk, A.G., Richard, P.J.H., Ridge, J.C., Ross, M., Roy, M., Seaman, A., Shaw, J., Stea, R.R., Teller, J.T., Thompson, W.B., Thorleifson, L.H., Utting, D.J., Veillette, J.J., Ward, B.C., Weddle, T.K., Wright, H.E., 2020. An updated radiocarbon-based ice margin chronology for the last deglaciation of the North American Ice Sheet Complex. Quaternary Science Reviews 234.

Deniel, C., Pin, C., 2001. Single-stage method for the simultaneous isolation of lead and strontium from silicate samples for isotopic measurements. Analytica Chimica Acta 426, 95-103.

Dethleff, D., 2005. Entrainment and export of Laptev Sea ice sediments, Siberian Arctic. Journal of Geophysical Research 110, 1-17.

Dorschel, B., Allan, E., Bartels, M., Campbell, C., Couette, P.-O., Diekamp, V., Dreutter, S., Duboc, Q., Geils, J., Greco, M., Lenz, K.-F., Lübben, B., Lütjens, M., Madaj, L., Perez, L., Recinos, B., Saini, J., Schade, T., Täuber, F., Ulner, L.-C., Warnke, F., Weiser, J., 2017. WESTBAFF Reconstruction of the

Laurentide Ice sheet drainage into the northwest Baffin Bay and the palaoceanography of the west Baffin Bay. MSM66 Cruise Report.

Dowdeswell, J.A., Hogan, K.A., Ó Cofaigh, C., Fugelli, E.M.G., Evans, J., Noormets, R., 2014. Late Quaternary ice flow in a West Greenland fjord and cross-shelf trough system: submarine landforms from Rink Isbrae to Uummannaq shelf and slope. Quaternary Science Reviews 92, 292-309.

Dunlap, E., Tang, C.C.L., 2006. Modelling the Mean Circulation of Baffin Bay. Atmosphere-Ocean 44, 99-109.

Dyke, A., 1999. Last Glacial Maximum and deglaciation of Devon Island, Arctic Canada: support for an Innuitian Ice Sheet. Quaternary Science Reviews 18, 393-420.

Dyke, A.S., Andrews, J.T., Clark, P.U., England, J.H., Miller, G.H., Shaw, J., Veillette, J.J., 2002. The Laurentide and Innuitian ice sheets during the Last Glacial Maximum. Quaternary Science Reviews 21, 9-31.

Dyke, A.S., Moore, A., Robertson, L., 2003. Deglaciation of North America. Geological Survey of Canada, Ottawa, Ontario, Canada, Open file 1574.

Dyke, A.S., Morris, T.F., Green, D.E.C., 1991. Postglacial Tectonic and Sea Level History of the Central Canadian Arctic. Geological Survey of Canada, Bulltin 397, Ottawa, Canada, pp. 63.

Eicken, H., Kolatschek, J., Freitag, J., Lindemann, F., Kassens, H., Dmitrenko, I., 2000. A key source area and constraints on entrainment for basin-scale sediment transport by Arctic sea ice. Geophysical Research Letters 27, 1919-1922.

England, J., 1999. Coalescent Greenland and Innuitian ice during the Last Glacial Maximum: Revising the Quaternary of the Canadian High Arctic. Quaternary Science Reviews 18, 421-456.

England, J., Atkinson, N., Bednarski, J., Dyke, A.S., Hodgson, D.A., Ó Cofaigh, C., 2006. The Innuitian Ice Sheet: configuration, dynamics and chronology. Quaternary Science Reviews 25, 689-703.

Farmer, G.L., Barber, D., Andrews, J., 2003. Provenance of Late Quaternary ice-proximal sediments in the North Atlantic: Nd, Sr and Pb isotopic evidence. Earth and Planetary Science Letters 209, 227-243.

Fisher, D., Zheng, J., Burgess, D., Zdanowicz, C., Kinnard, C., Sharp, M., Bourgeois, J., 2012. Recent melt rates of Canadian arctic ice caps are the highest in four millennia. Global and Planetary Change 84-85, 3-7.

Funder, S., Kjeldsen, K.K., Kjær, K.H., Ó Cofaigh, C., 2011. The Greenland Ice Sheet During the Past 300,000 Years: A Review, Quaternary Glaciations - Extent and Chronology - A Closer Look, pp. 699-713.

Furze, M.F.A., Pieńkowski, A.J., McNeely, M.A., Bennett, R., Cage, A.G., 2018. Deglaciation and ice shelf development at the northeast margin of the Laurentide Ice Sheet during the Younger Dryas chronozone. Boreas 47, 271-296.

Gajewski, K., 2015. Quantitative reconstruction of Holocene temperatures across the Canadian Arctic and Greenland. Global and Planetary Change 128, 14-23.

Georgiadis, E., Giraudeau, J., Martinez, P., Lajeunesse, P., St-Onge, G., Schmidt, S., Massé, G., 2018. Deglacial to postglacial history of Nares Strait, Northwest Greenland: a marine perspective from Kane Basin. Climate of the Past 14, 1991-2010.

Gibb, O.T., Steinhauer, S., Fréchette, B., de Vernal, A., Hillaire-Marcel, C., 2015. Diachronous evolution of sea surface conditions in the Labrador Sea and Baffin Bay since the last deglaciation. The Holocene 25, 1882-1897.

Grenier, M., Brown, K.A., Colombo, M., Belhadj, M., Baconnais, I., Pham, V., Soon, M., Myers, P.G., Jeandel, C., François, R., 2022. Controlling factors and impacts of river-borne neodymium isotope signatures and rare earth element concentrations supplied to the Canadian Arctic Archipelago. Earth and Planetary Science Letters 578.

Gutjahr, M., Frank, M., Stirling, C.H., Klemm, V., van de Flierdt, T., Halliday, A.N., 2007. Reliable extraction of a deepwater trace metal isotope signal from Fe–Mn oxyhydroxide coatings of marine sediments. Chemical Geology 242, 351-370.

Harrison, J.C., Brent, T.A., Oakey, G.N., 2011a. Chapter 40 Baffin Fan and its inverted rift system of Arctic eastern Canada: stratigraphy, tectonics and petroleum resource potential. Geological Society, London, Memoirs 35, 595-626.

Harrison, J.C., St Onge, M.R., Petrov, O.V., Strelnikov, S.I., Lopatin, B.G., Wilson, F.H., Tella, S., Paul, D., Lynds, T., Shokalsky, S.P., Hults, C.K., Bergman, S., Jepsen, H.F., Solli, A., 2011b. Geological map of the Arctic; Geological Survey of Canada, Map 2159A, scale 1/5 000 000.

Heaton, T.J., Köhler, P., Butzin, M., Bard, E., Reimer, R.W., Austin, W.E.N., Bronk Ramsey, C., Grootes, P.M., Hughen, K.A., Kromer, B., Reimer, P.J., Adkins, J., Burke, A., Cook, M.S., Olsen, J., Skinner, L.C., 2020. Marine20—The Marine Radiocarbon Age Calibration Curve (0–55,000 cal BP). Radiocarbon 62, 779-820.

Hebbeln, D., 2000. Flux of ice-rafted detritus from sea ice in the Fram Strait. Deep-Sea Research Part II: Topical Studies in Oceanography 47, 1773-1790.

Holland, M.M., Bitz, C.M., Eby, M., Weaver, A.J., 2001. The role of ice-ocean interactions in the variability of the North Atlantic thermohaline circulation. J Climate 14, 656-675.

Höppner, N., Lucassen, F., Chiessi, C.M., Sawakuchi, A.O., Kasemann, S.A., 2018. Holocene provenance shift of suspended particulate matter in the Amazon River basin. Quaternary Science Reviews 190, 66-80.

Ingram, R.G., Bâcle, J., Barber, D.G., Gratton, Y., Melling, H., 2002. An overview of physical processes in the North Water. Deep-Sea Research Part II: Topical Studies in Oceanography 49, 4893-4906.

Jackson, R., Kvorning, A.B., Limoges, A., Georgiadis, E., Olsen, S.M., Tallberg, P., Andersen, T.J., Mikkelsen, N., Giraudeau, J., Masse, G., Wacker, L., Ribeiro, S., 2021. Holocene polynya dynamics and their interaction with oceanic heat transport in northernmost Baffin Bay. Sci Rep 11, 10095.

Jacobsen, B.S., Wasserburg, G.J., 1980. Sm-Nd isotopic evolution of chondrites. Earth and Planetary Science Letters 50, 139-155.

Jenner, K.A., Campbell, D.C., Piper, D.J.W., 2018. Along-slope variations in sediment lithofacies and depositional processes since the Last Glacial Maximum on the northeast Baffin margin, Canada. Marine Geology 405, 92-107.

Jennings, A., Reilly, B., Andrews, J., Hogan, K., Walczak, M., Jakobsson, M., Stoner, J., Mix, A., Nicholls, K.W., O'Regan, M., Prins, M.A., Troelstra, S.R., 2022. Modern and early Holocene ice shelf sediment facies from Petermann Fjord and northern Nares Strait, northwest Greenland. Quaternary Science Reviews 283.

Jennings, A., Sheldon, C., Cronin, T., Francus, P., Stoner, J., Andrews, J., 2011. The Holocene History of Nares Strait: Transition from Glacial Bay to Arctic-Atlantic Throughflow. Oceanography 24, 26-41.

Jennings, A.E., Andrews, J.T., Ó Cofaigh, C., Onge, G.S., Sheldon, C., Belt, S.T., Cabedo-Sanz, P., Hillaire-Marcel, C., 2017. Ocean forcing of Ice Sheet retreat in central west Greenland from LGM to the early Holocene. Earth and Planetary Science Letters 472, 1-13.

Jennings, A.E., Andrews, J.T., Ó Cofaigh, C., St-Onge, G., Belt, S., Cabedo-Sanz, P., Pearce, C., Hillaire-Marcel, C., Calvin Campbell, D., 2018. Baffin Bay paleoenvironments in the LGM and HS1: Resolving the ice-shelf question. Marine Geology 402, 5-16.

Jennings, A.E., Andrews, J.T., Oliver, B., Walczak, M., Mix, A., 2019. Retreat of the Smith Sound Ice Stream in the Early Holocene. Boreas 48, 825-840.

Jennings, A.E., Walton, M.E., Ó Cofaigh, C., Kilfeather, A., Andrews, J.T., Ortiz, J.D., De Vernal, A., Dowdeswell, J.A., 2014. Paleoenvironments during Younger Dryas-Early Holocene retreat of the Greenland Ice Sheet from outer Disko Trough, central west Greenland. Journal of Quaternary Science 29, 27-40.

Kaufman, D.S., Ager, T.A., Anderson, N.J., Anderson, P.M., Andrews, J.T., Bartlein, P.J., Brubaker, L.B., Coats, L.L., Cwynar, L.C., Duvall, M.L., Dyke, A.S., Edwards, M.E., Eisner, W.R., Gajewski, K., Geirsdóttir, A., Hu, F.S., Jennings, A.E., Kaplan, M.R., Kerwin, M.W., Lozhkin, A.V., MacDonald, G.M., Miller, G.H., Mock, C.J., Oswald, W.W., Otto-Bliesner, B.L., Porinchu, D.F., Rühland, K., Smol, J.P., Steig, E.J., Wolfe, B.B., 2004. Holocene thermal maximum in the western Arctic (0–180°W). Quaternary Science Reviews 23, 529-560.

Kelleher, R., Jennings, A., Andrews, J., Brooks, N.K.S., Marchitto, T., Feng, S., Woelders, L., Normandeau, A., Jenner, K., Bennett, R., Brookins, S., 2022. Late glacial retreat of the Lancaster Sound Ice Stream and early Holocene onset of Arctic/Atlantic throughflow in the Arctic Island channels. Arctic, Antarctic, and Alpine Research 54, 395-427.

Knudsen, K.L., Stabell, B., Seidenkrantz, M.-S., EirÍKsson, J., Blake, W., 2008. Deglacial and Holocene conditions in northernmost Baffin Bay: sediments, foraminifera, diatoms and stable isotopes. Boreas 37, 346-376.

Laskar, J., Robutel, P., Joutel, F., Gastineau, M., Correia, A.C.M., Levrard, B., 2004. A long-term numerical solution for the insolation quantities of the Earth. Astronomy & Astrophysics 428, 261-285.

Ledu, D., Hollings, P., Rochon, A., de Vernal, A., St-Onge, G., 2008. Palynological evidence of Holocene climate change in the eastern Arctic: a possible shift in the Arctic oscillation at the millennial time scale. This article is one of a series of papers published in this Special Issue on the theme Polar Climate Stability Network. Canadian Journal of Earth Sciences 45, 1363-1375.

Ledu, D., Rochon, A., de Vernal, A., Barletta, F., St-Onge, G., 2010. Holocene sea ice history and climate variability along the main axis of the Northwest Passage, Canadian Arctic. Paleoceanography 25.

Li, G., Piper, D.J.W., Calvin Campbell, D., 2011. The Quaternary Lancaster Sound trough-mouth fan, NW Baffin Bay. Journal of Quaternary Science 26, 511-522.

Lougheed, B.C., Obrochta, S.P., 2019. A Rapid, Deterministic Age-Depth Modeling Routine for Geological Sequences With Inherent Depth Uncertainty. Paleoceanography and Paleoclimatology 34, 122-133.

Maccali, J., Hillaire-Marcel, C., Not, C., 2018. Radiogenic isotope (Nd, Pb, Sr) signatures of surface and sea ice-transported sediments from the Arctic Ocean under the present interglacial conditions. Polar Research 37.

MacLean, B., Blasco, S., Bennett, R., Lakeman, T., Pieńkowski, A.J., Furze, M.F.A., Hughes Clarke, J., Patton, E., 2017. Seafloor features delineate Late Wisconsinan ice stream configurations in eastern Parry Channel, Canadian Arctic Archipelago. Quaternary Science Reviews 160, 67-84.

Madaj, L., 2021. Holocene Ice Sheet Dynamics and Detriral Provenance Shifts Along the West Greenland Margin Recorded by Radiogenic Isotopes. Dissertation, Faculty of Geosciences, University Bremen, Bremen Germany.

McGregor, H.V., Dupont, L., Stuut, J.-B.W., Kuhlmann, H., 2009. Vegetation change, goats, and religion: a 2000-year history of land use in southern Morocco. Quaternary Science Reviews 28, 1434-1448.

McKay, N.P., Kaufman, D.S., Routson, C.C., Erb, M.P., Zander, P.D., 2018. The Onset and Rate of Holocene Neoglacial Cooling in the Arctic. Geophysical Research Letters 45, 12,487-412,496.

Melling, H., Gratton, Y., Ingram, G., 2001. Ocean circulation within the North Water polynya of Baffin Bay. Atmosphere-Ocean 39, 301-325.

Miller, G.H., Wolfe, A.P., Briner, J.P., Sauer, P.E., Nesje, A., 2005. Holocene glaciation and climate evolution of Baffin Island, Arctic Canada. Quaternary Science Reviews 24, 1703-1721.

Mollenhauer, G., Grotheer, H., Gentz, T., Bonk, E., Hefter, J., 2021. Standard operation procedures and performance of the MICADAS radiocarbon laboratory at Alfred Wegener Institute (AWI), Germany. Nuclear Instruments and Methods in Physics Research Section B: Beam Interactions with Materials and Atoms 496, 45-51.

Münchow, A., Falkner, K.K., Melling, H., 2015. Baffin Island and West Greenland Current Systems in northern Baffin Bay. Progress in Oceanography 132, 305-317.

Niessen, F., Matthiessen, J., Stein, R., 2010. Sedimentary environment and glacial history of the northwest passage (Canadian arctic archipelago) reconstructed from high-resolution acoustic data. Polar Research 79, 65-80.

Nürnberg, D., Wollenburg, I., Dethleff, D., Eicken, H., Kassens, H., Letzig, T., Reimnitz, E., Thiede, J., 1994. Sediments in Arctic sea ice: Implications for entrainment, transport and release. Marine Geology 119, 185-214.

Ó Cofaigh, C., Andrews, J.T., Jennings, A.E., Dowdeswell, J.A., Hogan, K.A., Kilfeather, A.A., Sheldon, C., 2013a. Glacimarine lithofacies, provenance and depositional processes on a West Greenland trough-mouth fan. Journal of Quaternary Science 28, 13-26.

Ó Cofaigh, C., Dowdeswell, J.A., Jennings, A.E., Hogan, K.A., Kilfeather, A., Hiemstra, J.F., Noormets, R., Evans, J., McCarthy, D.J., Andrews, J.T., Lloyd, J.M., Moros, M., 2013b. An extensive and dynamic ice sheet on the West Greenland shelf during the last glacial cycle. Geology 41, 219-222.

Overeem, I., Hudson, B.D., Syvitski, J.P.M., Mikkelsen, A.B., Hasholt, B., van den Broeke, M.R., Noël, B.P.Y., Morlighem, M., 2017. Substantial export of suspended sediment to the global oceans from glacial erosion in Greenland. Nature Geoscience 10, 859-863.

Petschick, R., Kuhn, G., Gingele, F., 1996. Clay mineral distribution in surface sediments of the South Atlantic: sources, transport, and relation to oceanography. Marine Geology 130, 203-229.

Pieńkowski, A.J., Coulthard, R.D., Furze, M.F.A., 2022. Revised marine reservoir offset (ΔR) values for molluscs and marine mammals from Arctic North America. Boreas.

Pieńkowski, A.J., England, J.H., Furze, M.F.A., Blasco, S., Mudie, P.J., MacLean, B., 2013. 11,000 yrs of environmental change in the Northwest Passage: A multiproxy core record from central Parry Channel, Canadian High Arctic. Marine Geology 341, 68-85.

Pieńkowski, A.J., England, J.H., Furze, M.F.A., MacLean, B., Blasco, S., 2014. The late Quaternary environmental evolution of marine Arctic Canada: Barrow Strait to Lancaster Sound. Quaternary Science Reviews 91, 184-203.

Pieńkowski, A.J., England, J.H., Furze, M.F.A., Marret, F., Eynaud, F., Vilks, G., Maclean, B., Blasco, S., Scourse, J.D., 2012. The deglacial to postglacial marine environments of SEBarrow Strait, Canadian Arctic Archipelago. Boreas 41, 141-179.

Pin, C., Briot, D., Bassin, C., Poitrasson, F., 1994. Concomitant separation of strontium and samarium-neodymium for isotopic analysis in silicate samples, based on specific extraction chromatography. Analytica Chimica Acta 298, 209-217.

Ren, H., Shokr, M., Li, X., Zhang, Z., Hui, F., Cheng, X., 2022. Estimation of Sea Ice Production in the North Water Polynya Based on Ice Arch Duration in Winter During 2006–2019. Journal of Geophysical Research: Oceans 127.

Reyes, A.V., Carlson, A.E., Beard, B.L., Hatfield, R.G., Stoner, J.S., Winsor, K., Welke, B., Ullman, D.J., 2014. South Greenland ice-sheet collapse during Marine Isotope Stage 11. Nature 510, 525-528.

Ritz, S.P., Stocker, T.F., Grimalt, J.O., Menviel, L., Timmermann, A., 2013. Estimated strength of the Atlantic overturning circulation during the last deglaciation. Nature Geoscience 6, 208-212.

Saini, J., Stein, R., Fahl, K., Weiser, J., Hebbeln, D., Hillaire-Marcel, C., de Vernal, A., 2020. Holocene variability in sea ice and primary productivity in the northeastern Baffin Bay. arktos.

Saini, J., Stein, R., Fahl, K., Weiser, J., Hebbeln, D., Madaj, L., 2022. Holocene variability in sea-ice conditions in the eastern Baffin Bay-Labrador Sea – A north–south biomarker transect study. Boreas 51, 553-572.

Scott, D.J., de Kemp, E.A., 1998. Bedrock geology compilation, Northern Baffin Island and northern Melville Peninsula, Northwest Territories. Geological Survey of Canada, Open File 3633.

Sheldon, C., Jennings, A., Andrews, J.T., Ó Cofaigh, C., Hogan, K., Dowdeswell, J.A., Seidenkrantz, M.-S., 2016. Ice stream retreat following the LGM and onset of the west Greenland current in Uummannaq Trough, west Greenland. Quaternary Science Reviews 147, 27-46.

Simon, Q., Hillaire-Marcel, C., St-Onge, G., Andrews, J.T., 2014. North-eastern Laurentide, western Greenland and southern Innuitian ice stream dynamics during the last glacial cycle. Journal of Quaternary Science 29, 14-26.

Simon, Q., Thouveny, N., Bourlès, D.L., Nuttin, L., Hillaire-Marcel, C., St-Onge, G., 2016. Authigenic 10Be/9Be ratios and 10Be-fluxes (230Thxs-normalized) in central Baffin Bay sediments during the last glacial cycle: Paleoenvironmental implications. Quaternary Science Reviews 140, 142-162.

St-Onge, M.-P., St-Onge, G., 2014. Environmental changes in Baffin Bay during the Holocene based on the physical and magnetic properties of sediment cores. Journal of Quaternary Science 29, 41-56.

Stalling, D., Westerhoff, M., Hege, H.-C., 2005. Amira: A Highly Interactive System for Visual Data Analysis. Visualization Handbook, 749-767.

Stein, R., Niessen, F., Matthiessen, J., 2009: Marine Geology.- In: W. Jokat (ed), The Expedition of the Research Vessel “Polarstern” to the Arctic in 2008 (ARK-XXIII/3), Rep. Polar Mar, Res. 597: 12-15.

Stevenard, N., Montero-Serrano, J.C., Eynaud, F., St-Onge, G., Zaragosi, S., Copland, L., 2021. Lateglacial and Holocene sedimentary dynamics in northwestern Baffin Bay as recorded in sediment cores from Cape Norton Shaw Inlet (Nunavut, Canada). Boreas 51, 532-552.

Stuiver, M., Reimer, P.J., 1993. Extended ^{14}C Data Base and Revised CALIB 3.0 ^{14}C Age Calibration Program. Radiocarbon 35, 215-230.

Tang, C.C.L., Ross, C.K., Yao, T., Petrie, B., DeTracey, B.M., Dunlap, E., 2004. The circulation, water masses and sea-ice of Baffin Bay. Progress in Oceanography 63, 183-228.

Thomas, E.K., Castañeda, I.S., McKay, N.P., Briner, J.P., Salacup, J.M., Nguyen, K.Q., Schweinsberg, A.D., 2018. A Wetter Arctic Coincident With Hemispheric Warming 8,000 Years Ago. Geophysical Research Letters 45, 10,637-610,647.

Vare, L.L., Massé, G., Gregory, T.R., Smart, C.W., Belt, S.T., 2009. Sea ice variations in the central Canadian Arctic Archipelago during the Holocene. Quaternary Science Reviews 28, 1354-1366.

Vogt, C., Lauterjung, J., Fischer, R.X., 2002. Investigation of the Clay Fraction (<2 µm) of the Clay Minerals Society Reference Clays. Clays and Clay Minerals 50, 388-400.

Weiser, J., Titschack, J., Kienast, M., McCave, I.N., Lochte, A.A., Saini, J., Stein, R., Hebbeln, D., 2021. Atlantic water inflow to Labrador Sea and its interaction with ice sheet dynamics during the Holocene. Quaternary Science Reviews 256.

Zreda, M., England, J., Phillips, F., Elmore, D., Sharma, P., 1999. Unblocking of the Nares Strait by Greenland and Ellesmere ice-sheet retreat 10,000 years ago. Nature 398, 139-142.

Supplement

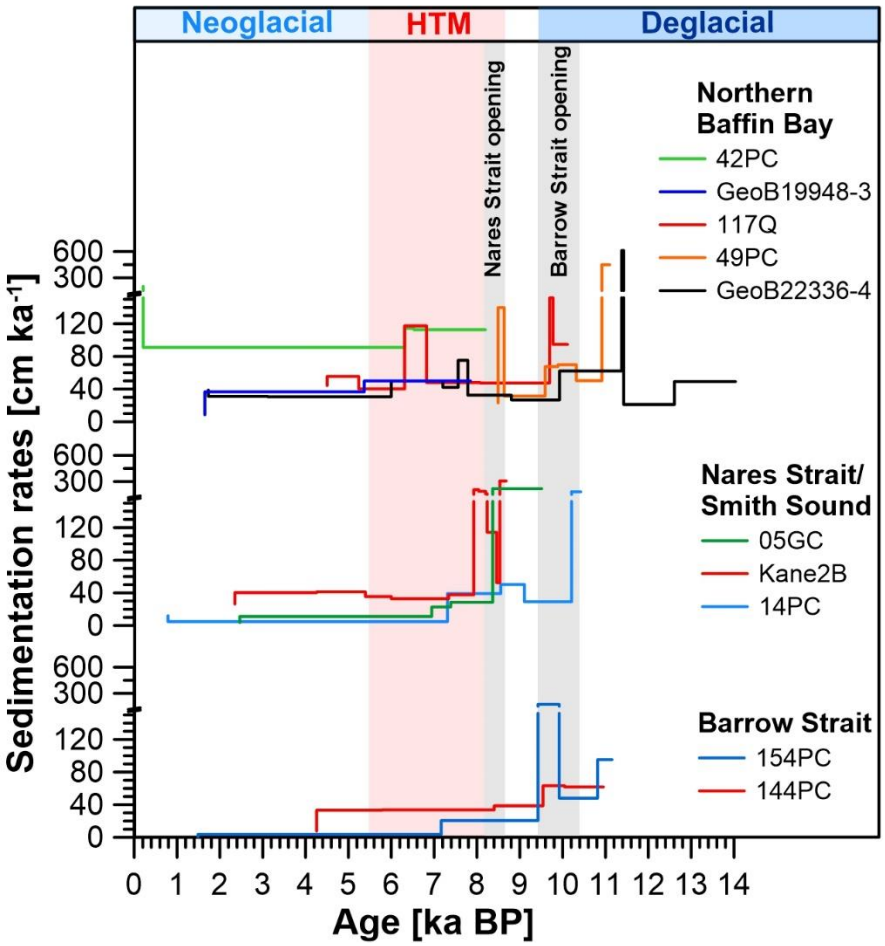

Figure 4-S1: Compilation of sedimentation rates from published sediment cores from Barrow Strait: 144PC (Pieńkowski et al., 2012), 154PC (Pieńkowski et al., 2014); Nares Strait: Kane2B (Georgiadis et al., 2018), 05GC (Jennings et al., 2011); Smith Sound: 14PC (Jennings et al., 2019); and Northern Baffin Bay: GeoB22336-4 (this study), 49PC (Jenner at al., 2018; Kelleher et al., 2022), 42PC (St-Onge & St-Onge, 2014), 117Q (Jackson et al., 2021), GeoB19948-3 (Saini et al., 2022). Grey bars indicate the entire interval for Barrow and Nares Straits opening based on the sediment records. HTM = Holocene Thermal Maximum (see Fig. 4-1 for core locations).

5. Holocene variability of the northeastern Laurentide Ice Sheet in the Clyde Inlet area, western Baffin Bay, from radiogenic isotope records in marine sediments

Johanna Hingst[a], Emmanuel Okuma[a], Claude Hillaire-Marcel[b], Friedrich Lucassen[a], Christoph Vogt[a], Simone A. Kasemann[a]

[a]MARUM – Centre for Marine Environmental Science and Faculty of Geoscience, University of Bremen, Germany
[b]Geotop – Centre de recherche sur la dynamique du système Terre, Université du Québec à Montréal, Canada

Manuscript in preparation

Abstract

The reconstruction of ice sheet fluctuations during the last deglaciation and the Holocene helps understand the response of past and present ice sheets to a changing climate. While the large-scale spatial and temporal variations of the Fox Basin-Baffin Island ice dome (NE Laurentide Ice Sheet, Canada) have been well documented, information on short-term Holocene fluctuations and its final decay is still restricted. Therefore, we reconstructed ice margin fluctuations of one of its eastern outlet glaciers in the Clyde Inlet fjord, northeastern Baffin Island, using two marine sediment cores retrieved within and off the Clyde Inlet (GeoB22346-3, GeoB22357-3). We analyzed the radiogenic isotope composition (Sr-Pb-Nd) and mineral assemblage of the siliciclastic sediment fraction, which reflect bedrock erosion along the active ice margin. Thus, the data can be used to reconstruct ice margin fluctuations and spatial and temporal variations in meltwater discharge into Baffin Bay. Changes in mineralogical and radiogenic isotope compositions in the sediment record from the fjord head suggest ice margin fluctuations rather than a constant retreat throughout the Holocene. Moreover, the data indicate variable meltwater discharge after the ice margin retreated out of the fjord and the advance of alpine glaciers in the research area during the late Holocene. Most variable radiogenic isotope compositions on the shelf occur in subglacial deposits at the core bottom, deposited during the late Pleistocene. Subsequent stable radiogenic isotope signatures are related to relatively homogenized Baffin Island inputs after the ice margin retreated from the shelf. Early Holocene data suggest ice-distal conditions and an increasing influence of sediments originating from northern Baffin Bay, probably related to the deglaciation of Lancaster Sound.

5.1 Introduction

The mass balance of ice sheets is highly influenced by the behavior and stability of outlet glaciers and ice streams, as they are responsible for the main ice and sediment discharge (Bamber et al., 2000; Bennett, 2003). Therefore, understanding the temporal and spatial dynamics of ice streams

and their driving mechanism is crucial to estimating the future ice sheets stability and the linked consequences of ice mass loss. Besides the observation of today's ice sheet behavior and their variability, past ice stream and ice sheet reconstructions are a helpful tool to understand better their long-term response to a changing climate (e.g., Briner et al., 2020; Kaufman et al., 2004). The Laurentide Ice Sheet (LIS) covered large parts of Canada during the last glacial period, with several ice streams draining into the Arctic Ocean, Baffin Bay, and the northwestern North Atlantic (Margold et al., 2015). The retreat of its marine-terminating margins during the last deglaciation shows similarities to the present-day retreat of Greenland and West Antarctica (Briner et al., 2009a). Therefore, the deglaciation history of LIS, particularly its outlet glaciers and ice streams, is of great interest.

One of the multiple outlet glaciers of the northeastern LIS occupied the Clyde Inlet, a 120 km long fjord on northestern Baffin Island (Fig. 5-1), during the Last Glacial Maximum (LGM) (Margold et al., 2015). Several studies are focusing on the deglaciation history of the Clyde Inlet area, reconstructing the northeastern LIS's decay. Couette et al. (2023) recently identified the maximum extent and the retreat chronology of the LIS in the Clyde Inlet fjord and trough system using detailed bathymetry, seismic stratigraphy, and marine sediment core data. Specific glaciomarine landforms close to the shelf edge revealed that the LIS extended onto the Baffin Shelf during the LGM, though it has not reached the shelf edge (Couette et al., 2023). The onset of deglaciation started between 16 and 14 ka BP (Briner et al., 2005; Briner et al., 2007) and was characterized by the collapse of the Clyde ice shelf and the subsequent rapid retreat of the LIS (Couette et al., 2023). Cosmogenic ages of a moraine from the coastal lowlands date its deglaciation to around 12.5 ka BP (Briner et al., 2007), and a moraine system at the Clyde Inlets mouth indicates that the ice has reached it at the onset of the Holocene (Couette et al., 2023). Several moraines in the Clyde trough middle section suggest that the first ice retreat was interrupted by readvances, which probably correspond in timing with the colder Younger Dryas (~12.9 to 11.7 ka BP) (Couette et al., 2023). The following retreat of the LIS from the Clyde Inlet was described to happen rapidly, starting at the outer fjord at ~ 10 ka BP and reaching the fjord head at ~ 9.3 to 9.1 ka BP (Briner et al., 2007). However, several moraine deposits in the middle sector and at the fjord head indicate that the deglaciation was interrupted and followed by several readvances related to cooler periods like the Cockburn Substage between 8.3 and 9.5 ka BP and the 8.2 ka cold event (Andrews and Ives, 1978; Couette et al., 2023). Additionally, Briner et al. (2007) identified some readvances of the LIS during the early Holocene, which seemed not to be correlated with specific cold events but could potentially be caused by increased winter precipitation related to the influence of warm waters in Baffin Bay. The rapid retreat of the LIS from the Clyde Inlet coincides in timing with the Holocene Thermal Maximum in Arctic Canada between ~ 10 and 7 ka BP, in a period with warmer-than-present temperatures

(Briner et al., 2006; Fisher et al., 1995). The strong connection between climate variability and ice sheet dynamics reveals the regional climate as the main driver of the Clyde Inlet deglaciation, even if the specific deglaciation pattern also seemed to be influenced by the local topography (Couette et al., 2023). After its retreat from the multiple fjords on central to northeastern Baffin Island, the remnant of the LIS over the Foxe basin collapsed, and the remaining Foxe Dome became isolated as the early Barnes Ice Cap (Fig. 5-1) (Briner et al., 2009b). The Barnes Ice Cap steadily shrank throughout the mid to late Holocene, reaching its current size at about ~2 to 1 ka BP (Briner et al., 2009b). As inferred from proglacial lake studies, alpine glaciers on northeastern Baffin Island likely survived the Holocene Thermal Maximum (HTM) and had their minimum extent between ~6 to 3 ka BP (Thomas et al., 2010). Thomas et al. (2010) explained that the survival of the alpine glaciers during the early Holocene was likely caused by stronger seasonality and the presence of the LIS but also by increased precipitation associated with warmer surface ocean waters. Finally, lake sediment data, similar to other proxies, also reveal that the most pronounced advance of alpine glaciers on Baffin Island after 14 ka BP occurred during the Little Ice Age (LIA) between 1500 and 1900 AD (Andrews and Barnett, 1979) in response to cold temperatures and high precipitation (e.g., Briner et al., 2009b; Miller et al., 2005; Thomas et al., 2010).

The aim of this study is to improve our understanding of the deglaciation history of the LIS on Baffin Island. To achieve this, we reconstruct the retreat of the Clyde Inlet outlet glacier but also the shrinking ice dome on Baffin Island after the ice had left the fjord. Our approach involves analyzing radiogenic isotope (Sr, Pb, Nd) ratios in detrital material and mineral assemblages from two marine sediment cores. By identifying the sediment provenance of detrital material, Sr, Pb, and Nd isotope compositions can be used to trace the spatially focused addition of freshwater into the oceans, thereby providing valuable information about the chronology of spatial glacier dynamics. In this study, we present the radiogenic isotope data and mineralogical composition of the marine sediment core GeoB22346-3 from the head of the Clyde Inlet and GeoB22357-3, which were retrieved on the shelf in front of the fjord. The main objectives of the paper are [1] to reconstruct the sediment provenances in and outside of the Clyde Inlet by analyzing the radiogenic isotope mineralogical composition, [2] to reveal strengths and limitations of using radiogenic isotopes as sediment source tracer at such an ice-proximal core site, and [3] to observe glacial driven sedimentation and past ocean circulation processes on the Baffin Island margin.

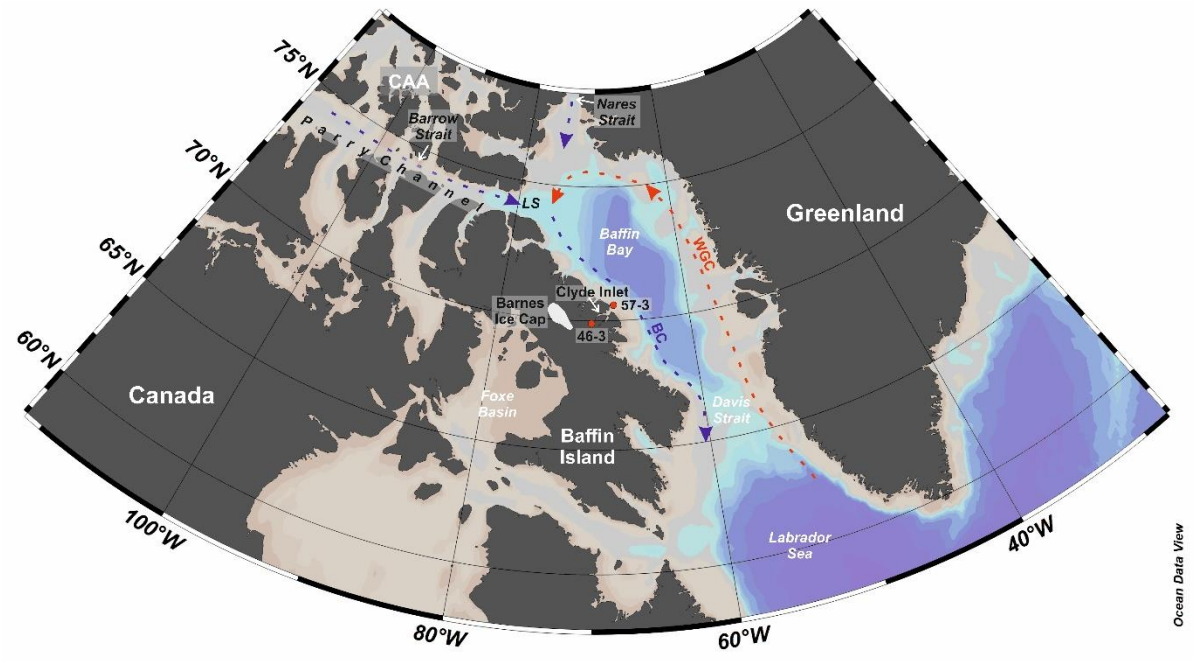

Figure 5-1: Overview map of the surrounding/research area showing the locations (red circles) of core GeoB22346-3 and GeoB22357-3 from the Clyde region/area and simplified present-day oceanography including the West Greenland Current (WGC) transporting relatively warm waters towards northern Baffin Bay and the Baffin Current (BC) that transports cold Arctic waters southwards towards Labrador Sea. LS: Lancaster Sound. Map created with Ocean Data View (Schlitzer, 2020).

5.2 Regional Setting

Baffin Bay is an oceanic basin between Greenland and the Canadian Arctic Archipelago (CAA), which connects the northwest Atlantic Ocean with the Arctic Ocean (Fig. 5-1). The basin is about 1300 km long and 450 km wide, with water depth reaching 2000 m to 2500 m in the deep central basin. In contrast to the broad western Greenland shelf (> 250 km), the continental shelf off Baffin Island is relatively narrow (50 to 60 km wide) (Bennett et al., 2013). The Baffin shelf is cut by several transverse troughs located offshore major fjord systems (Brouard and Lajeunesse, 2017) and which are the results of glacial erosion by outlet glaciers and sediment rework during Quaternary glaciations (Bennett et al., 2013; Brouard and Lajeunesse, 2017). Onshore, the study area is characterized by long fjords, which dissect the eastern coastal mountains of Baffin Island with gently descending forelands on the outer part of some inter-fjord peninsulas (Praeg et al., 2007). To the west of the eastern coastal mountains and the study area, the Barnes Ice Cap, a remnant of the LIS, lies on the interior uplands of Baffin Island (Praeg et al., 2007).

5.2.1 Oceanography and sea ice conditions

In the eastern part of the Baffin basin, the West Greenland Current (WGC) transports warm, relatively saline Atlantic waters northward along the western Greenland margin (Fig. 5-1) (Tang et al., 2004). Cold Arctic waters can enter the basin via Nares Strait, the Parry channel, and smaller gateways of the CAA and feed the Baffin Current (BC), which transports cold and relatively fresh water along the eastern Baffin Island coast through the Davis Strait into the North Atlantic (Fig. 5-1) (Tang et al., 2004). This counterclockwise pattern of circulation with warm northward flowing waters in the east and cold southward flowing waters in the west strongly influence the seasonal sea ice distribution in the basin. During most of the year, sea ice is present in Baffin Bay with minimum extent or complete disappearance in August and September (Tang et al., 2004). Full ice cover is typically reached during March, with exception of the eastern Davis Strait, where the relatively warm waters of the WGC inhibit sea ice formation. Icebergs transiting Baffin Bay are mainly provided by the Greenland Ice Sheet (GIS) or in smaller amounts by tidewater glaciers on the northern CAA.

5.2.2 Geology and related radiogenic isotope signatures

The northern part of Baffin Island mainly consists of the Committee belt, characterized by Archean to Paleoproterozoic crystalline shield rocks ascribed to the Rea craton (Harrison et al., 2011). The Committee belt extends from northern Baffin Island to northwestern Greenland. Thus, similar geological units and related radiogenic isotopic signatures occur on both sides of northern Baffin Bay. On northern Baffin Island, Mesoproterozoic siliciclastic rocks interbedded with some shales, limestones, and dolostones of the Borden Peninsula and Bylot Island overlie parts of the Rae Craton (Harrison et al., 2011). The CAA is dominated by large outcrops of Paleozoic dolostones and limestones, siliciclastic, and evaporites that cover the Precambrian basement (Harrison et al., 2011; Scott and de Kemp, 1998). In more detail, the geology around the outer Clyde Inlet and at the fjord head is dominated by Mesoarchean quartzo-feldspatic gneisses of the Rae craton, including undifferentiated deformed granitic intrusions (Fig. 5-2) (Harrison et al., 2011; Jackson and Berman, 2000). Around the middle part of the fjord and on the Clyde Inlet forelands, slightly younger Archean to Paleoproterozoic migmatites occur. Southwest of the Clyde Inlet head, between the southern Barnes ice cap and the fjord, there are again outcrops of Archean to Paleoproterozoic migmatites and small areas of Paleoproterozoic quartzite, marble, rusty schist iron formation (Harrison et al., 2011; Jackson and Berman, 2000).

A few studies have conducted radiogenic isotope analysis on bedrock samples from Baffin Island or even the Clyde Inlet area. McCulloch and Wasserburg (1978) measured the radiogenic Nd and Sr

isotope composition on a composite sample from Baffin Island, which showed unradiogenic ε_{Nd} values of -31.7 and relatively radiogenic $^{87}Sr/^{86}Sr$ values of 0.76. In general, the Pb isotope signatures of old crystalline rocks tend to be relatively radiogenic. However, while information on the radiogenic isotope signatures of bedrocks is scarce, there have been measurements conducted on marine sediments (including sediment cores) from northern Baffin Bay and the northwestern Greenland shelf that provide a range of Nd, Sr, and Pb isotope values that can be used for sediment provenance discussion. For instance, radiogenic isotope measurements on shelf sediments off northwest Greenland, close to Archean to Paleoproterozoic rocks, show ε_{Nd}, $^{87}Sr/^{86}Sr$, and $^{206}Pb/^{204}Pb$ values ranging from -36 to -21, 0.73 to 0.77, and 18 to 19, respectively (Madaj, 2021). In contrast to the old crystalline rocks found on Baffin Island and Greenland, younger rocks usually have higher ε_{Nd} and lower $^{87}Sr/^{86}Sr$ and $^{206}Pb/^{204}Pb$ values. For example, isotope analysis of a sediment surface sample from the Parry Channel, surrounded mainly by carbonate rocks, yielded higher ε_{Nd} (-19 to -12) and lower $^{87}Sr/^{86}Sr$ (0.72 to 0.74) (Maccali et al., 2018). Similarly, the Holocene radiogenic isotope composition from a sediment core from Barrow Strait range for Sr from 0.73 to 0.74, for ε_{Nd} around -17.6, and for $^{206}Pb/^{204}Pb$ around 19 (Table 9-4).

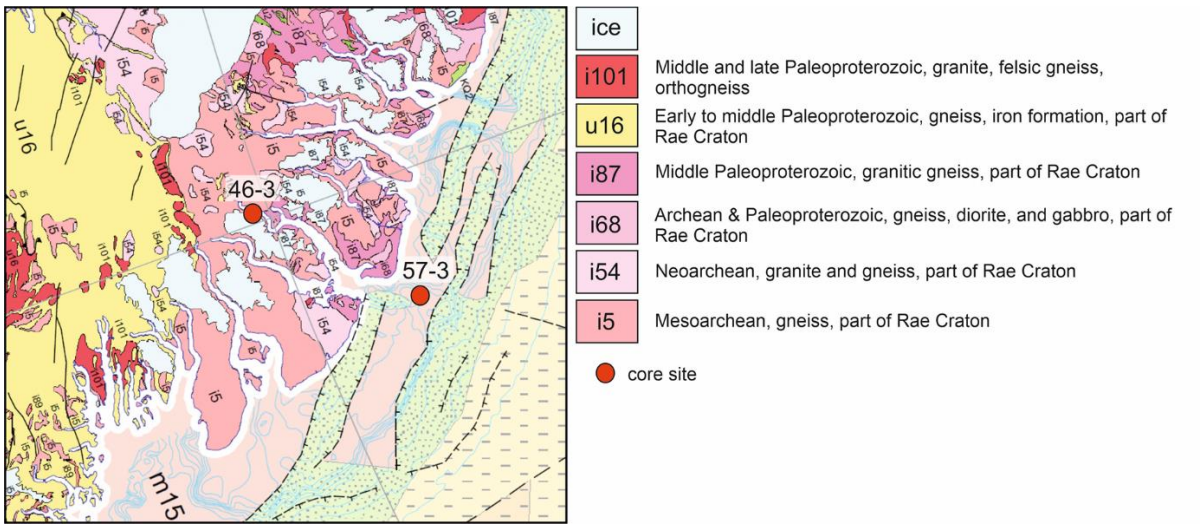

Figure 5-2: Detailed Geology of the Clyde Inlet area. Map modified after Harrison et al. (2011).

5.3 Materials and methods

In this study, two marine sediment cores from western Baffin Bay were selected to analyze their radiogenic isotope composition and mineral assemblages. Core GeoB22346-3 and GeoB22357-3, hereafter named 46-3 and 57-3, were collected with a gravity corer during the Maria S. Merian 66 (MSM66) cruise in 2017 within and off Clyde Inlet, northeastern Baffin Island (Dorschel et al., 2017). Sediment core 46-3 (69° 54.18'N/ 70° 13.54'W; 203 m water depth) has a recovery length of 783 cm, and core 57-3 (70° 36.28'N/ 67°53.63'W; 315 m water depth) has a total length of 902 cm.

For the isotope and mineral analyses here, twelve samples were collected from 46-3 and 24 samples from 57-3 with a sample weight of approximately 5 g for each sample. In addition to these data, magnetic susceptibility (MS) measurements on both cores were performed on board at 1 cm intervals and were calculated using MSCL software package (Dorschel et al., 2017) and are available at the PANGAEA online data repository (Lenz et al., dataset in review). Lithological descriptions of the two cores can be found in the cruise report (Dorschel et al., 2017) and are further discussed in Couette et al. (2023). Furthermore, bathymetric data and seismic and acoustic profiles of the research area, as well as elemental compositions of the two sediment cores, are presented in Couette et al. (2023).

5.3.1 Chronology

The preliminary age models of 46-3 and 57-3 are based on Acceleration Mass Spectrometry (AMS) ^{14}C dates measured on 7 and 6 samples (Figs. 5-3, 5-4; Tables 5-1, 5-2), respectively, measured at a MICADAS (MIni CArbon Dating System) ^{14}C laboratory of the Alfred Wegener Institute (AWI) in Bremerhaven, Germany. The age calibration and age-depth model were performed using the age-modeling UNDATABLE software (Lougheed and Obrochta, 2019) and the Marine20 dataset (Heaton et al., 2020). For the ^{14}C age calibration, a regional reservoir age correction (ΔR) for northeastern Baffin Island of 81 ± 18 years was applied (Pieńkowski et al., 2022). The age model was extended by linear extrapolation outside of the ^{14}C dating points.

Table 5-1. List of AMS ^{14}C dates from 46-3. Samples marked with a * are from Couette et al. (2023). Calibrated ages are the median probability ages and 95% confidence interval (minimum and maximum age) obtained with Calib 8.2 (Stuiver and Reimer, 1993).

Lab ID	Depth	Material	^{14}C Age		Reservoir	Calibrated Ages (yrs BP)		
AWI-	interval (cm)		yrs	±	Age (yrs)	Min.	Max.	Median
6223.1.1	152 - 155	Mixed Benthic Foraminifera	2442	71	81 ± 18	1586	2039	1812
6224.1.1	243 - 245	Mixed Benthic Foraminifera	3614	71	81 ± 18	3011	3459	3253
1726.1.1*	387	Mollusc shell fossils	5929	51	81 ± 18	5898	6252	6066
6225.1.1	483 - 485	Mixed Benthic Foraminifera	6833	85	81 ± 18	6805	7282	7057

6226.1.1	603 - 604	Mixed Benthic Foraminifera	8471	91	81 ± 18	8462	9027	8763
6227.1.1	723 - 724	Mixed Benthic Foraminifera	8421	102	81 ± 18	8408	8993	8701
1727.1.1*	767 - 768	Foraminifera	8902	193	81 ± 18	8769	9845	9303

Table 5-2. List of AMS ^{14}C dates from 57-3. Calibrated ages are the median probability ages and 95% confidence interval (minimum and maximum age) obtained with Calib 8.2 (Stuiver and Reimer, 1993).

Lab ID	**Depth**	**Material**	**^{14}C Age**		**Reservoir**	**Calibrated Ages (yrs BP)**		
AWI-	**interval (cm)**		**yrs**	**±**	**Age (yrs)**	**Min.**	**Max.**	**Median**
6229.1.1	128 - 129	Mixed Benthic Foraminifera	9044	99	81 ± 18	9191	9788	9475
6230.1.1	218 - 219	Mixed Benthic Foraminifera	9915	98	81 ± 18	10297	11009	10637
6231.1.1	248 - 249	Mixed Benthic Foraminifera	9894	38	81 ± 18	10383	10795	10598
6232.1.1	308 - 309	Mixed Benthic Foraminifera	10025	33	81 ± 18	10601	11043	10804
6233.1.1	368 - 369	Mixed Benthic Foraminifera	10442	95	81 ± 18	11101	11714	11374
6234.1.1	398 - 399	Mixed Benthic Foraminifera	10246	36	81 ± 18	10898	11255	11118

5.3.2 Computed tomography

Computed tomography (CT) scanning is a non-destructive method to gain detailed information on sedimentary facies and structures. CT scanning of the archive halves of both sediment cores was performed at the hospital Klinikum Bremen-Mitte, Bremen, Germany, using a Philips CT Brillance iCT Elite 256 equipped with a current of 300 mA and a 120 kV X-ray source voltage. The resolution used for core scanning was 0.293 mm in the x and y dimensions and 0.625 mm in the z-direction (0.3 mm reconstruction unit). The scans were rebuilt using a bone kernel (YB (Enhanced)) and the filtered Back Projection (fBP) mode before being exported as DICOM data. Processing of the CT data was performed using the Amira software (version 2021.08) (Stalling et al., 2005). By processing the

CT data, concentrations of ice rafted debris (IRD; lithic clasts with a grain size of >1 mm) in volume percentage were identified.

5.3.3 X-ray diffraction (XRD)

The bulk mineralogical assemblages of twelve samples of 46-3 and 17 samples of 57-3 were determined by X-ray diffraction (XRD). Therefore, the sediment fine fraction (< 63 µm) was ground manually with an agate mortar to reach an approximate grain size of < 2 µm. XRD measurements were performed by Christoph Vogt in the laboratory of the Crystallography Research Group, Faculty of Geosciences, University of Bremen on a Bruker D8 Discover diffractometer. Further details can be found in chapter 2 and in Okuma et al. (submitted).

5.3.4 Radiogenic isotope analysis

Sr, Nd, and Pb isotope compositions were analyzed in the laboratory of the Isotope Geochemistry Group at MARUM – Center for Marine Environmental Sciences, University of Bremen.
Approximately 2 g of wet sediment was filled into 15 ml centrifuge tubes and washed twice with Milli Q water (18.2 MΩ) to remove the soluble fraction and pore water from the sample. For further analysis, the < 63 µm grain size fraction was separated by wet sieving. After drying, samples were homogenized and ground with an agate mortar. The dry, coarse sediment fraction (>63 µm) was weighted to estimate the approximate grain size distribution within the sediment sample. To remove potential marine carbonates and authigenic Fe-Mn oxyhydroxide coatings, sediment samples were leached with acetic acid and/or a NaOH-buffered solution of hydroxylamine hydrochloride and 15 % acetic acid for 3 hours. The supernatants of each sample were saved in 40 ml PP containers. Leached samples were washed twice with Milli Q water and dried at 110°C in the oven.

For the dissolution of the siliciclastic sediment fraction (modified after Höppner et al., 2018), 100 mg of each decarbonated sample was transferred into 15 ml Teflon Savillex® beakers. In the first step, 3 ml of a concentrated HF-HNO_3 mixture was added to the samples (dissolution on the hotplate at 140°C for at least 48 hours). After drying, samples were redissolved in 3 ml aqua regia (3:1, 6 N HCl: concentrated HNO_3) for two days at 120°C. For the removal of organic matter, 100 µl H_2O_2 was added four to five times until the reaction stopped. After each repetition, samples were left on the hotplate for ~ 1 hour at 70°C. Afterward, 1 ml concentrated HNO_3 was added, and samples were placed on the hotplate at 70°C overnight for dissolution. In the last dissolution step, 3 ml HCl was added to the dry samples, which were then placed on the hotplate at 70°C overnight. Finally, the samples were dried again for chemical separation and redissolved in 1100 µl 2M HNO_3.

Sr and Pb were separated on the same column using 70 µl Sr.spec^{TM} resin following a modified method after Deniel and Pin (2001). Nd separation was performed in two steps using TRU.spec^{TM} for light rare earth elements and LN.spec^{TM} for Nd isolation (method after Pin et al., 1994).

Sr, Nd, and Pb isotope ratios were measured with a Thermo-Fisher Scientific TRITON Plus thermal ionization mass spectrometer (TIMS) at the Isotope Geochemistry Laboratory at MARUM. Sr and Pb were measured on a single filament, using a Ta and a Si activator, respectively, in the static multicollection mode. For Nd analyses, a double filament was used, and measurements were conducted in a static multicollection mode. For the correction of the instrumental mass fractionation during Sr and Nd isotope analysis, the stable isotope ratios $^{86}Sr/^{88}Sr$ (=0.1194) and $^{146}Nd/^{144}Nd$ (=0.7219) were used, respectively. During Pb isotope analysis, instrumental mass fractionation was corrected by applying a factor of 1.001 per atomic mass unit. To record the analytical accuracy and repeatability, reference material NIST SRM 987 was used for $^{87}Sr/^{86}Sr$, NIST SRM 981 for Pb isotope ratios, and JNdi-1 for $^{143}Nd/^{144}Nd$. The values analyzed during this PhD project are in the range of values analyzed by TIMS and published in the GeoReM database (http://georem.mpch-mainz.gwdg.de/, query November 2022, March 2023): NIST SRM987: 0.710242 ± 0.000032 ($2SD_{mean}$, n=15), 0.710250 ± 0.000040 (GeoReM; $2SD_{mean}$, n=1711, data <0.7102 and > 0.7103 are discarded); JNd-1: 0.512113 ± 0.000024 ($2SD_{mean}$, n=12), 0.512107±0.000024 (GeoReM; 2SDmean, n=414, data <0.51204 and >0.51217 are discarded); NIST SRM 981: 16.9004 ± 0.0133 ($^{206}Pb/^{204}Pb$; $2SD_{mean}$, n=12), 16.9211 ± 0.0423 ($^{206}Pb/^{204}Pb$; GeoReM; $2SD_{mean,}$ n=290, data >17 are discarded). Nd isotope ratios are presented in the ε_{Nd} notation using the Chondritic Uniform Reservoir (CHUR) value of $^{143}Nd/^{144}Nd$ = 0.512638 (Jacobsen and Wasserburg, 1980).

5.4 Results

The Sr, Nd, and Pb isotopic compositions of the silicate fraction of the two marine sediment cores 46-3 from the head of Clyde Inlet and 57-3 from the adjacent shelf are described in the following and are summarized in tables 9-2 and 9-3. Moreover, the relative mineralogical composition of the cores is listed in tables 9-5 and 9-6. Based on the lithological facies Couette et al. (2023) divided the 46-3 core into two and the 57-core into three depositional units. We used this main structure and further subdivided the core mainly based on major changes in the high-resolution MS and CT data. The downcore results of both cores are described using the following subdivision (Figs. 5-3, 5-4; the same numbers of the main units indicate the same depositional conditions as identified by Couette et al. (2023) and described in the brackets): 46-3: Unit 2 (ice-proximal glaciomarine sediment deposit) = core bottom to ~ 585 cm, unit 3 (ice-distal hemipelagic sedimentation) with unit 3a = ~ 585 to 490 cm, 3b = ~ 490 to 180 cm, and 3c = ~ 180 cm to the core top; 57-3: Unit 1 (diamicton) =

core bottom to ~ 840 cm and ~ 795 to 720 cm, unit 2 (ice-proximal glaciomarine sediment deposit) = ~ 840 to 795 cm and ~ 720 to 410 cm, unit 3 (ice-distal hemipelagic sedimentation) with unit 3a = ~ 410 to 75 cm, unit 3b = ~ 75 cm to core top.

5.4.1 Age model and sedimentation rates

The age model of 46-3, which is based on six calibrated ^{14}C dates (outlier at 603 cm is excluded), indicates that the sediment core from the Clyde Inlet head covers the last ~ 9.4 ka BP, capturing most of the Holocene period. Calculated sedimentation rates range from ~ 51 to a maximal 145 cm ka^{-1}, with the highest values in the lower part of the core in units 2 and 3a. Moderate sedimentation rates (~ 73 to 98 cm ka^{-1}) occur before the peak in the lowermost ~ 50 cm and after it with some variations in the lower part of unit 3b. The lowest sedimentation rates (~ 51 cm ka^{-1}) occur in the middle part of unit 3b before values slightly increase in the upper part (~ 63 to 84 cm ka^{-1}).

The final age model of core 57-3 is based on four calibrated ^{14}C dates (two outliers at 218 and 368 cm are excluded) taken within the upper four meters of the core. The model suggests that the core covers the time interval between 8.1 ka BP and 13 ka BP and allows an estimation of sedimentation rates on the shelf offshore the Clyde Inlet within this period. Calculated sedimentation rates in the core range between 107 and 291 cm ka^{-1}. Between the core bottom and ~ 250 cm, sedimentation rates are high (~ 275 to 291 cm ka^{-1}) before they drop and stay on a lower level in the upper part of the core (~ 93 to 107 cm ka^{-1}).

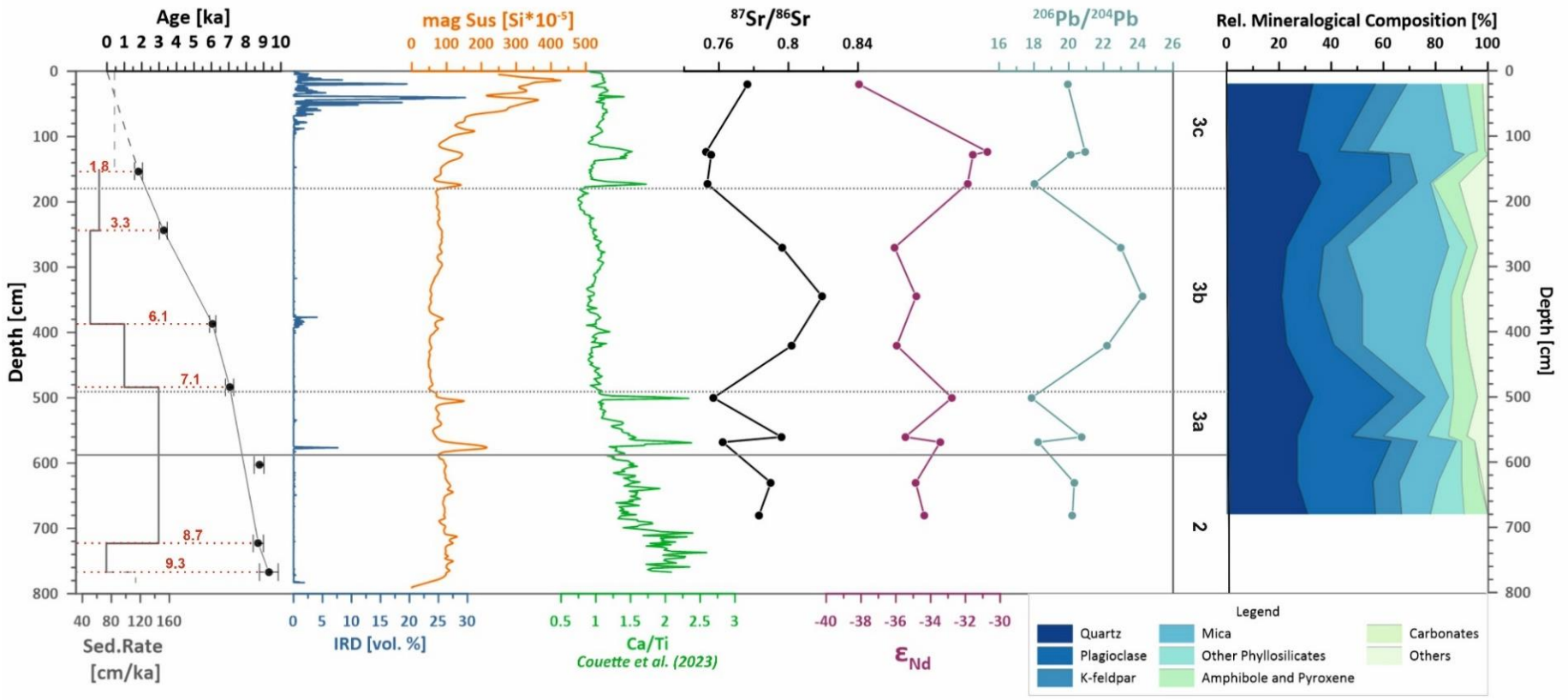

Figure 5-3: Different downcore records of GeoB22346-3, including calibrated median ages and related calculated sedimentation rate, IRD content, magnetic susceptibility (Lenz et al., dataset in review), Ca/Ti ratio (Couette et al., 2023), Sr, Nd, and Pb isotope compositions and mineralogical assemblages. Dating points with corresponding radiocarbon ages are shown as red dot.

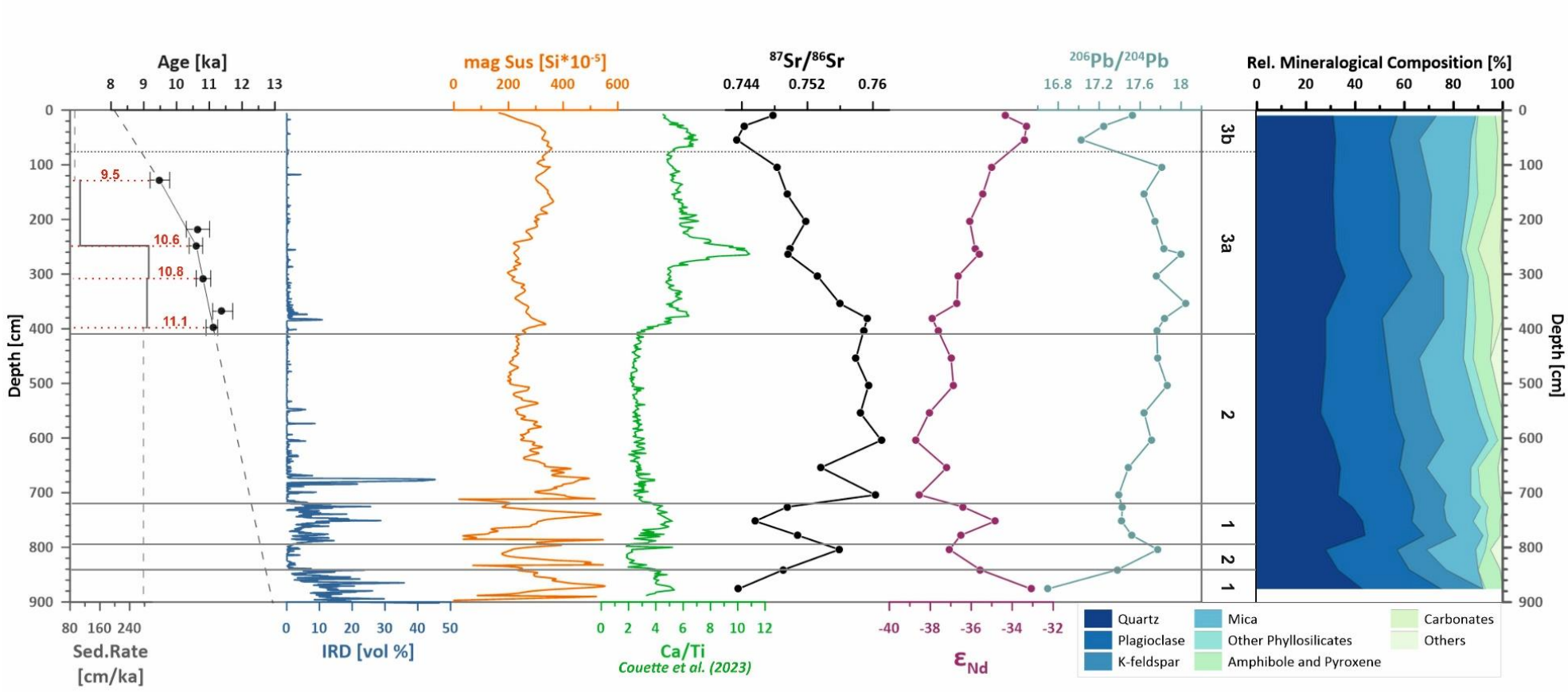

Figure 5-4: Different downcore records of GeoB22357-3, including calibrated median ages and related calculated sedimentation rate, IRD content, magnetic susceptibility (Lenz et al., dataset in review) Ca/Ti ratio (Couette et al., 2023), Sr, Nd, and Pb isotope compositions and mineralogical assemblages. Dating points with corresponding radiocarbon ages are shown as red dot.

5.4.2 Magnetic susceptibility (MS) and computed tomography (CT)

For core 46-3 (Fig. 5-3), the lowermost unit 2 is characterized by little to no occurrence of IRD content and, except to the lowermost few centimeters, by a uniform MS that measures between ~ 60 x 10^{-5} SI and 130 x 10^{-5} SI. Unit 3a is characterized by two distinct peaks in the MS (216 x 10^{-5} SI at 576 cm and 150 x 10^{-5} SI at 505 cm), which coincide with the lower peak with a short-term high concentration of IRD. In unit 3b, the MS is very constant, measuring between 50 x 10^{-5} SI and 80 x 10^{-5} SI. Parallel to that, there is almost no IRD content, except between 370 and 400 cm, where IRD concentrations slightly increase. The MS is increasing and more variable in the uppermost unit 3c, reaching values up to ~ 430 at 14 cm. Similarly, IRD concentrations increase significantly in this unit, especially in the upper 1 m of this section.

MS and IRD records of 57-3 (Fig. 5-4) are highly variable in unit 1, reaching high IRD concentrations of ~ 46 vol. % (901 cm) and maximum MS values of ~ 550 x 10^{-5} SI (867 cm), and minimum values of 85 x 10^{-5} SI (884 cm). Unit 1 is interrupted by a small and overlain by a thicker unit 2, characterized by generally lower IRD concentrations. MS values are less variable in the overlaying unit 2 and decrease continuously towards the unit 3 transition. In unit 3a, MS values first slightly increase before they decrease again in the middle part and reach some higher values at the end of the unit. IRD concentrations are predominantly low in this interval, with slightly enriched values between ~ 360 to 390 cm. The core top, unit 3b, starts with relatively high MS values (~ 360 x 10^{-5} SI), which decrease towards the core top (~ 165 x 10^{-5} SI). There are no to minor IRD concentrations in unit 3b.

5.4.3 Relative mineralogical composition (XRD)

The XRD analysis of core 46-3 shows significant variations in the mineralogical composition down-core (Fig. 5-3). The mineralogy is mainly dominated by quartz, which relative contribution varies between 21 % and 36 %, with mainly low values observed in unit 3b, between 270 cm and 420 cm, and two peaks at 172 cm and 500 cm. In addition, 46-3 is rich in mica and plagioclase, with values up to 39 % and 36 %, respectively. However, relative mica concentrations are highly variable, with the highest concentrations in unit 3b and two minima parallel to the high quartz values at 172 cm and 500 cm. Other clay minerals like chlorite and kaolinite play a minor role in the down-core mineralogy with maximum relative concentrations of 8 %. Relative K-feldspar concentrations are, on average, 11 %, with the highest value of 17 % at 345 cm. There are almost no carbonates detected by the XRD measurements (1 % at 630 cm).

The mineralogical composition of core 57-3 (Fig. 5-4) can be divided into two different sections. The lower section of the core, from the core bottom to a depth of about 550 cm, is characterized by

varying relative mineral abundances. Even if the quartz (on average ~34 %) and plagioclase (on average ~26 %) dominate over the entire core, the lower section exhibits the highest and lowest relative concentrations of these minerals. In contrast, the upper section, 550 cm to the core top, shows a more uniform relative mineralogy, only interrupted by a small layer at 304 to 381 cm with enhanced quartz or K-feldspar concentrations but depleted relative abundances of mica. Within the upper section (10 - 380 cm), a relative abundance of 3 - 9 % of dolomite can be detected. Relative amphibole and pyroxene abundances vary in both sections between 2 % and 9 %.

5.4.4 Sr, Nd, and Pb isotope composition

In the following, downcore changes in radiogenic isotope data (Sr, Nd, Pb) of 46-3 and 57-3 are described (Figs. 5-3 and 5-4). To observe potential changes in sediment provenance, $^{87}Sr/^{86}Sr$ and ε_{Nd} values (Sr-Nd plot), as well as $^{206}Pb/^{204}Pb$ and $^{207}Pb/^{204}Pb$ values are plotted against each other (Figs. 5-5, 5-6).

The Sr isotope composition of the detrital sediment fraction measured on 46-3 is highly variable, ranging from 0.75 to 0.82. In units 1 and 3a, $^{87}Sr/^{86}Sr$ values fluctuate between 0.76 and 0.8. The highest $^{87}Sr/^{86}Sr$ values are reached in unit 3b before Sr isotope values decrease again towards unit 3c (0.75 and 0.78). ε_{Nd} values of the detrital material are more uniform with just small variations in unit 2 to unit 3b. In unit 3c, ε_{Nd} values initially rise to values of up to -31 before the most unradiogenic ε_{Nd} value of about -38 is reached at the core top. The pattern of ε_{Nd} variations in the lower part of the core is in negative correlation with the Sr isotope composition within the same sediment section. The $^{206}Pb/^{204}Pb$ and $^{207}Pb/^{204}Pb$ measured on the detrital sediment fraction are highly variable, showing a similar pattern as the Sr isotope record, except in unit 3c, where $^{206}Pb/^{204}Pb$ slightly increase again. $^{206}Pb/^{204}Pb$ values range from 17.9 to 24.2, $^{207}Pb/^{204}Pb$ values from 15.4 to 16.2.

The isotope data of 46-3 do not show a specific cluster in the Sr-Nd isotope plot. However, two groups of data points can be distinguished. Data points between 7.9 and 7.1 ka BP and 2.1 and 1.5 ka BP show rather unradiogenic Sr isotope values and more radiogenic Nd isotope compositions, while the group of data points from 9 to 7.8 ka BP and 6.2 to 3.6 ka PB, as well as the from 0.5 ka BP are characterized by more radiogenic $^{87}Sr/^{86}Sr$ values and less radiogenic ε_{Nd} values. The data points of the first group are closest to the bedrock reference data from Baffin Island (McCulloch and Wasserburg, 1978) and overlap with available isotope signatures measured close to the Rea Craton (Paleoproterozoic) in NW Greenland (Madaj et al., 2021). The isotope signatures of the second group are not close to any known reference isotope signatures from the Baffin Bay area. The $^{206}Pb/^{204}Pb$ vs. $^{207}Pb/^{204}Pb$ plot reveals the high variability of the Pb isotope signatures of the

46-3 core. However, due to the large range of Pb isotope signatures, the data overlap with nearly all reference data sets suggesting that the data are not suitable for provenance discussion.

In general, the range of radiogenic isotope values in core 57-3 is smaller than in the core from the fjord head, with the Sr isotope composition ranging between 0.74 and 0.76. In the lower part of the core (bottom to 600cm), the fluctuation of Sr isotope values is strongest. Starting from the highest Sr isotope value at 600 cm in unit 2, the Sr isotope composition is initially just slightly decreasing before values drop more rapidly in unit 3a towards 0.74 in unit 3b. In unit 3b, $^{87}Sr/^{86}Sr$ values are slightly increasing again. Variations in the Nd isotope records occur parallel to the fluctuations in the Sr isotope composition but anticorrelate. The highest variability occurs between the core bottom and 600 cm, with ε_{Nd} values ranging between -38.7 and -33.1. After 600 cm, Nd isotope values increase in units 2 and 3a with smaller variations towards -33.4 at ~30 cm. Towards the core top, in unit 3b, ε_{Nd} values slightly drop again. $^{206}Pb/^{204}Pb$ and $^{207}Pb/^{204}Pb$ vary between 16.7 and 18 and between 15.3 and 15.4, respectively. The Pb isotope records show a steep increase between the core bottom and ~ 800 cm and afterward an overall increasing trend towards ~260 cm. Between 260 cm and unit 3b, values drop before increasing again towards the core top.

In the Sr-Nd isotope plot, the data of 57-3 tend to form a distinct cluster, which does not overlap with the data from the Clyde Inlet head. Specifically, the radiogenic isotope data for units 1, 3a, and 3b are generally less radiogenic in the Sr isotope composition and more radiogenic in the Nd isotope composition. Conversely, the isotope data for unit 2 have predominantly more radiogenic Sr isotope values and less radiogenic Nd isotope values. Data with higher Nd isotope compositions overlap with reference isotope signatures measures close to the Rea Craton (Paleoproterozoic) in NW Greenland, similar to some data points of the core 46-3. The $^{206}Pb/^{204}Pb$ vs. $^{207}Pb/^{204}Pb$ plot shows a narrow cluster of the 57-3 data. The cluster overlaps with reference signatures of the Rae Craton (Archean), data from central Baffin Bay, and central-west and southwest Greenland, which also consist mainly of Archean to Paleoproterozoic granites and gneiss.

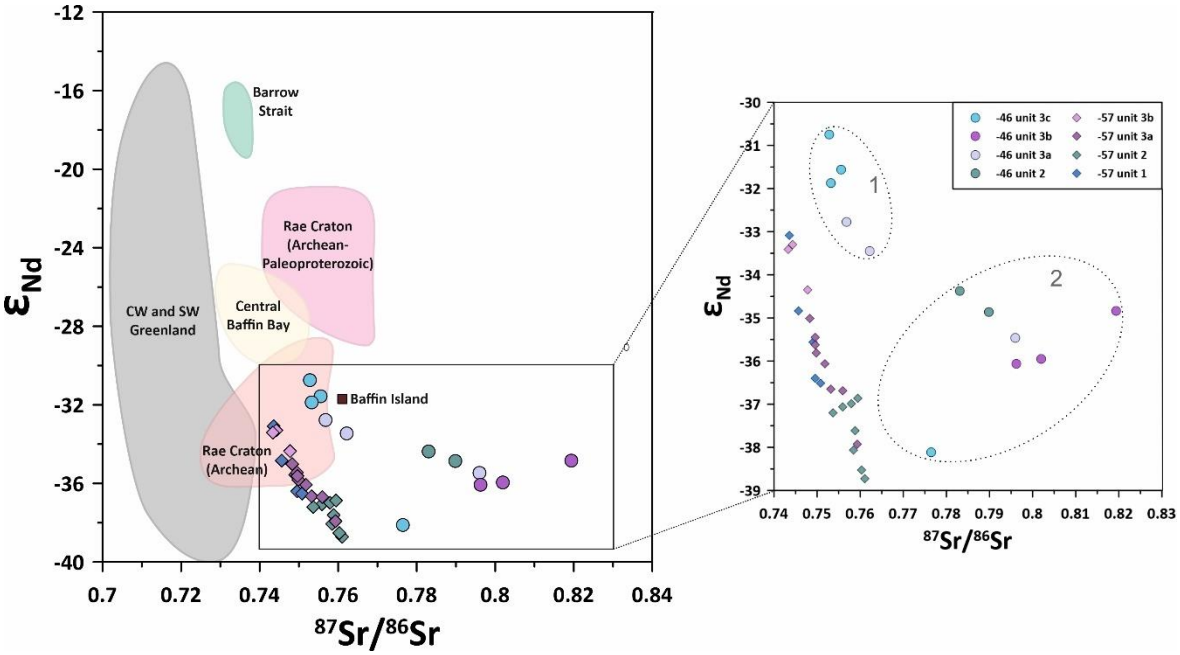

Figure 5-5: $^{87}Sr/^{86}Sr$ vs. ε_{Nd} plot of GeoB22346-3 and GeoB22357-3. Additionally, reference isotope signatures from different geological regions in Baffin Bay are included for provenance discussion. The colors of the background data are adapted to the colors used in Fig. 5-2. Areas not displayed in Fig. 5-2 are marked in grey. Background data are from marine sediment analyses of different studies: Rae Craton (Archean – Paleoproterozoic; light pink): sediment core (GeoB19927-3) from the western Greenland shelf (Madaj, 2021), Rae Craton (Archean; dark pink): sediment core (GeoB19946-4) from the northwestern Greenland shelf (Madaj, 2021), Barrow Strait (light green): Holocene isotope signatures of core PS72/287-3 (Table 9-4), and southwest (SW) and central west (CW) Greenland (grey): stream sediment data (Colville et al., 2011; Reyes et al., 2014), central Baffin Bay (yellow): isotope signatures of core PC16 (Kirillova, 2017).

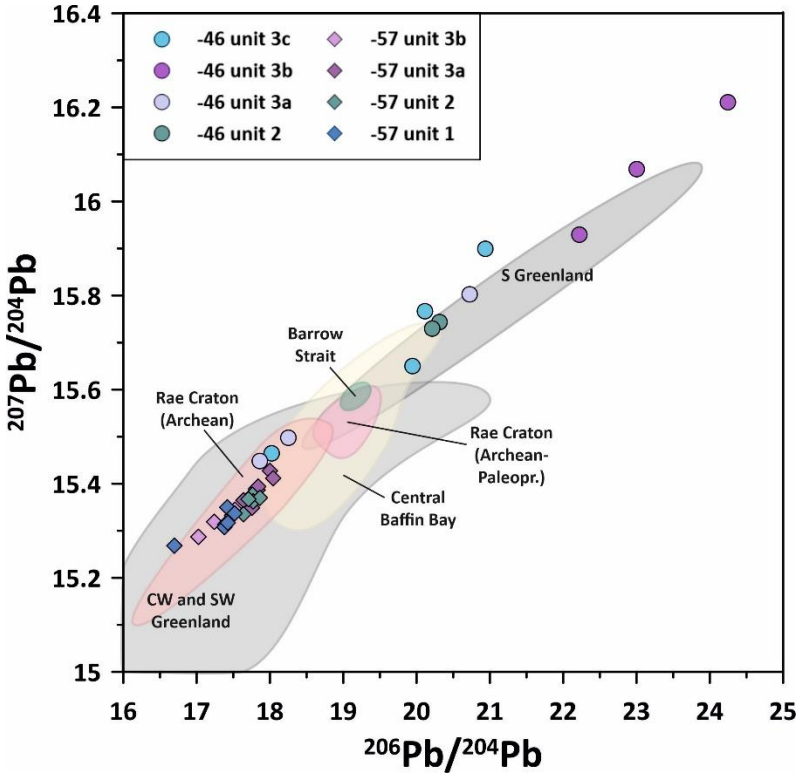

Figure 5-6: $^{206}Pb/^{204}Pb$ vs. $^{207}Pb/^{204}Pb$ plot of GeoB22346-3 and GeoB22357-3. Additionally, reference isotope signatures from different geological regions in Baffin Bay are included for provenance discussion. Background data are from marine sediment analyses of different studies: Rae Craton (Archean – Paleoproterozoic; light pink): sediment core (GeoB19927-3) from the western Greenland shelf (Madaj, 2021), Rae Craton (Archean; dark pink): sediment core (GeoB19946-4) from the northwestern Greenland shelf (Madaj, 2021), Barrow Strait (light green): Holocene isotope signatures of core PS72/287-3 (Table 9-4), and south(S), southwest (SW), and central west (CW) Greenland (grey): stream sediment data (Colville et al., 2011; Reyes et al., 2014), central Baffin Bay (yellow): isotope signatures of core PC16 (Kirillova, 2017).

5.5 Discussion

5.5.1 Processes influencing the radiogenic Sr, Nd, and Pb isotope composition in marine sediments at ice-proximal core sites

Before radiogenic isotopes can be used for provenance discussion, it is necessary to verify whether the data reliably reflect the sediment provenance or are influenced by additional processes. Indeed, studies showed that Sr isotope variations could result from grain-size effects (Eisenhauer et al., 1999; Tütken et al., 2002). In contrast, ε_{Nd} values appeared to be unaffected by particle grain size because Sm-Nd isotopes are potentially not fractionated between different-sized mineral fractions (Tütken et al., 2002). Moreover, radiogenic isotope studies on river sediments have shown that changing abundances of specific mineral species caused by mineral sorting processes during sediment transport can control the bulk Sr and Pb isotopic budget of river sediments without having

an effect on the Nd isotope composition (Garçon et al., 2014). Mineral species that affect the Sr isotope composition depend on their crystalline structure and their ability to incorporate rubidium, which is mainly carried by micas and K-feldspars in igneous and metamorphic rocks (Faure and Powell, 2012). Thus, the enrichment of micas in the sediment could lead to high $^{87}Sr/^{86}Sr$ values. The $^{206}Pb/^{204}Pb$ isotope composition is mainly influenced by Pb-rich clay minerals and K-feldspar, but also muscovite, and plagioclase can affect the isotopic budget (Garçon et al., 2014). Garçon et al. (2014) also showed that extremely radiogenic heavy minerals like zircon, monazite, and allanite have a crucial impact on the $^{206}Pb/^{204}Pb$ isotope composition and are responsible for the highest $^{206}Pb/^{204}Pb$ values. Because micas can also include minerals like zircon, a high amount of micas could potentially lead to higher radiogenic Pb isotope compositions, as well. This positive correlation between high mica concentrations and a radiogenic Sr and Pb isotope composition proposed by the literature can also be observed in the isotope and mineral data of 46-3. Especially in unit 3b of 46-3, where just minor variations in the IRD, MS, and Ca/Ti data suggest stable environmental conditions, the strongest rise in the $^{87}Sr/^{86}Sr$ and $^{206}Pb/^{204}Pb$ data occur parallel to increasing mica concentrations. Changes in the ε_{Nd} record occur in parts parallel to the Sr and Pb isotope records but are generally less variable, especially in the middle part of the core. Since many studies have shown that ε_{Nd} signatures are a highly reliable tracer for the provenance reconstruction of continental detritus (e.g., Garçon et al., 2014; Tütken et al., 2002) and Sr and Pb isotopic records show in parts a different evolution than the ε_{Nd} record, we suggest that Sr and Pb isotope composition in the 46-3 core are not only driven by the sediment source signature but are influenced by mineral abundances- mainly changing mica concentrations- at the 46-3 core site. It is likely that the variable mineral assemblage at the core 46-3 is caused by hydrodynamic mineral sorting caused by changing meltwater flux intensities and/ or varying transport distances, as it has been previously observed at fluvial settings (Garçon et al., 2014). Correlations of radiogenic Sr and Pb isotope composition and meltwater conditions may thus be useful for reconstructing past glacial conditions in the Clyde Inlet region. In contrast, the isotopic and mineralogical composition of the 57-3 core from the shelf is less variable, with lower $^{87}Sr/^{86}Sr$ and $^{206}Pb/^{204}Pb$ values. Even if mineralogical changes occur, the mineral composition does not seem to be the controlling factor of the radiogenic Sr and Pb isotope composition from the Clyde Inlet shelf.

In summary, these data provide insights into the mechanisms that drive changes in radiogenic Sr and Pb isotope compositions in marine sediment records, which are close to river or meltwater systems in polar regions. Specifically, they allow the differentiation and identification of changing sediment sources and variations in meltwater fluxes.

5.5.2 Monitoring early to late Holocene glacier variability on NE Baffin Island on radiogenic isotope composition from the Clyde Inlet head (GeoB22346-3)

According to the age model, the core 46-3 covers the last ~9.5 ka BP. Thus, the core data covers the final period of rapid deglaciation of NE Baffin Island fjords and the breakup of the Barnes Ice Cap during the middle Holocene (Briner et al., 2009b). Even if the radiogenic isotope compositions at the Clyde Inlet head can hardly be used for sediment provenance reconstruction, they do provide valuable insights into sediment transport processes and information regarding meltwater intensities and ice margin conditions.

Based on the deglaciation chronology of the Clyde Inlet by Briner et al. (2007), the ice margin retreated from the outer fjord to the fjord head between ~10 ka BP and ~7.9 ka BP. This rapid melting occurred during a period of warmer-than-present temperatures, the HTM between ~ 10 to 7 ka BP as a result of a foregone high boreal summer insolation (Fig. 5-7) (Axford et al., 2009; Briner et al., 2006). This warm period was interrupted by periods of pronounced cooling between 9.5 and 8 ka BP (Axford et al., 2009; Briner et al., 2006). In response to these cold events, the ice margin advanced or stopped several times in the fjord, as inferred from multiple moraines deposited between 9.4 and 8.8 ka BP (Briner et al., 2007; Couette et al., 2023). The radiogenic isotope records of all three systems from the core 46-3 reveal some variability between ~ 9 and 7 ka BP, which could be related to ice sheet dynamics and associated sediment deposition during that time. Distinct peaks in the Ca/Ti ratio at 569 cm and 501 cm are associated with sandy layers, thus, coarser material (Couette et al., 2023) and could be evidence for an ice readvance. Even though a changing grain size distribution in these layers could possibly explain changes in the Sr isotope compositions (cf. 5.5.1), variations in the Nd isotope signature rather suggest a change in sediment provenance probably related to a changing ice margin position. The peak at 569 cm occurs parallel to a small peak in IRD content and the MS (Fig. 5-3) and is dated to ~7.8 ka BP. The peak at 501 cm corresponds to a maximum in the MS at ~ 7.1 ka BP. These time intervals do not coincide with the known ice advance around the 8.2 cold event (Young et al., 2012). However, the significant age gap between 7.1 and 8.7 ka BP causes a high inaccuracy of the age model in this period (Fig. 5-3). Thus, it would be very vague to discuss precise timings of ice margin dynamics during the early to mid-Holocene based on the available data and core chronology. Besides these short-term variations during the early Holocene, the Sr and Pb isotope records show an overall increasing trend until ~ 5 ka BP, while the Nd isotope signatures stay relatively constant until ~ 3.8 ka BP (Fig. 5-7). In summary, these patterns potentially suggest an overall retreat of the ice margin until ~ 5 to 3.8 ka BP. Since the highly radiogenic Sr and Pb isotope compositions during unit 3b (maximum between 6.2 and 3.8 ka BP) seem to reflect the enhanced accumulation of clay minerals (cf. 5.5.1) associated with either

weak meltwater intensities or a long sediment transport, it is likely that the ice margin already retreated into the hinterland before ~ 6.2 ka BP. This roughly agrees with the reported complete retreat of the ice stream from the Clyde Inlet at around 7 ka BP (Briner et al., 2007). A constant meltwater supply towards the fjord head during ice margin retreat during the mid-Holocene, probably resulted in uniform sedimentation patterns, as indicated by a uniform MS in unit 3b in the 46-3 core. Similar constant MS values were measured in lacustrine sediments on northeastern Baffin Island (Big Round Lake), which were (besides other proxies) related to a minimum alpine glacier extent on northeastern Baffin Island between ~ 6 to 3 ka BP (Thomas et al., 2010).

5.5.2.1 Ice advance during Neoglaciation

Multiple studies report about a readvance of alpine glaciers on Baffin Island during the late Holocene due to the Neoglacial cooling (Briner et al., 2009b). As some studies indicate that a Neoglaciation already started at some sites around 6 ka BP, most alpine glaciers on Baffin Island began to expand after ~ 3.5 ka BP and reached their maximum Holocene extent during the Little Ice Age (LIA; ~ 1400 AD to 1900 AD) (Briner et al., 2009b; Moore et al., 2001; Thomas et al., 2010).

Thomas et al. (2010) used proglacial lake sediments to observe changes in the alpine glacier extent on northeastern Baffin Island. Similar to one of their lake MS records, the high-resolution MS and Ca/Ti data of the 46-3 core start to increase and become more variable after ~ 2.2 ka BP (Fig. 5-7). A pronounced increase in IRD concentrations in 46-3 occurs later at ~ 1.2 ka BP. Therefore, high-resolution data of 46-3 potentially reflect glacier readvance in the Clyde Inlet region starting at ~2.2 ka BP, and that becomes more intense after ~ 1.2 ka BP. Also, the radiogenic isotope records seem to reveal a change in the prevailing sedimentation processes. Following the radiogenic Sr and Pb isotope compositions during the mid-Holocene, Sr and Pb isotope ratios significantly decrease after ~ 3.8 ka BP. Parallel to it, Nd isotope composition shows the most prominent changes after ~ 3.8 ka BP with values of ~ -30 to -40. The most radiogenic ε_{Nd} values between -30.7 and -31.9 occur between about 1.6 and 2.2 ka BP, in sediment layers between 123 cm and 172 cm. Due to the pronounced change in ε_{Nd} values, changes in the radiogenic isotope composition during the late Holocene are likely related to a change in sediment provenance. Since reference isotope signatures from Baffin Island are scarce and the geology shows, in general, just small variation, it is challenging to differentiate between the potential sediment sources in the Clyde region. However, we can at least speculate about a variation in the sediment source occurring after the mid-Holocene, which is most likely related to the advance of multiple glaciers around the Clyde Inlet starting after ~ 3.8 ka BP.

All in all, radiogenic Sr, Nd, and Pb isotope compositions in a glacially influenced fjord system seem to be strongly affected by ice sheet dynamics. In detail, the radiogenic isotope composition can be either controlled by changing sediment sources (Sr, Nd, and Pb), which can differ due to the retreat/advance of the ice margin, or by changing transport processes and energies that affect the mineralogical composition of the bulk sediment (Sr and Pb). These relationships allow us to speculate about the timing of ice retreat and advance in the Clyde Inlet area.

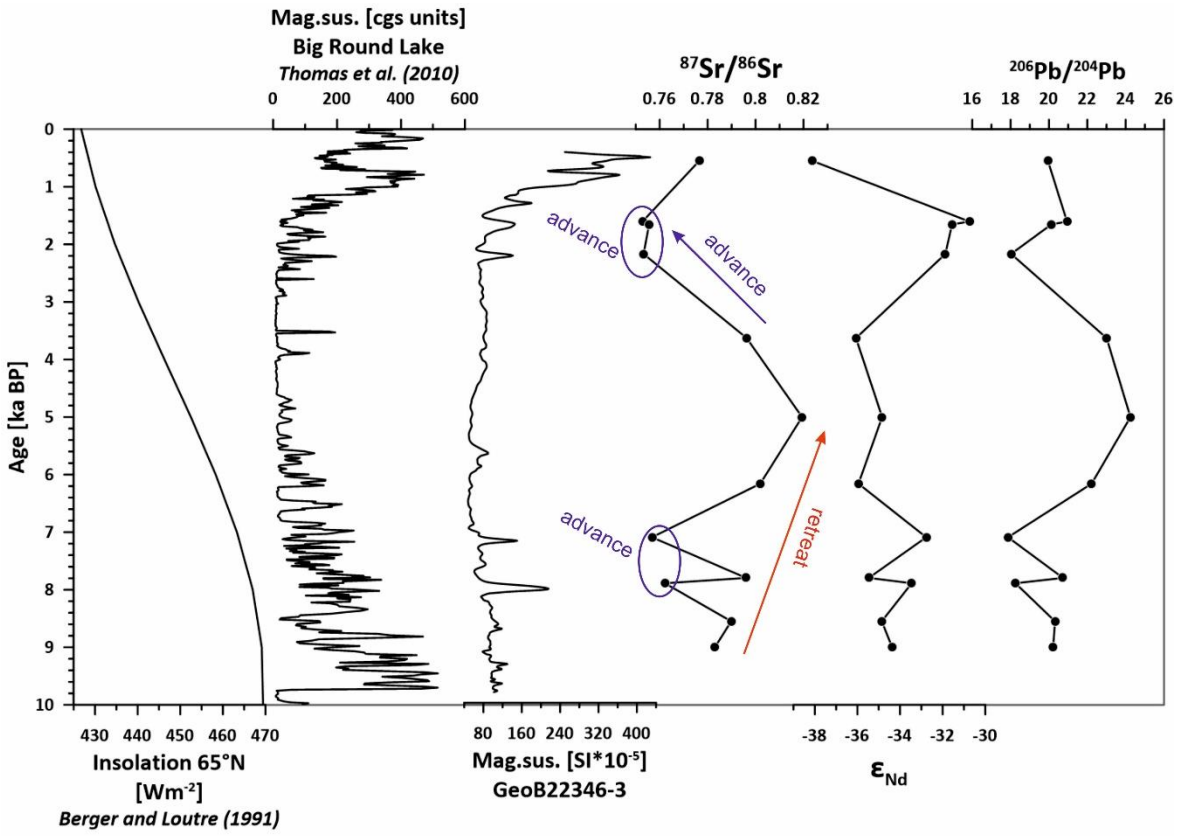

Figure 5-7: Summer Insolation at 65°N (Berger and Loutre, 1991) and magnetic susceptibility measured on lacustrine sediments of the Big Round Lake (Thomas et al., 2010) in comparison with magnetic susceptibility (Lenz et al., dataset in review) and radiogenic isotope compositions measured on GeoB22346-3. Red and blue arrows indicate time periods of ice retreat and advance, respectively. Additionally, the timings of short-term ice advances are marked with blue circles.

5.5.3 Monitoring outlet glacier retreat from the NE Baffin Island shelf behind the Clyde fjord head during the Late Pleistocene to Mid Holocene

The location of the proximal sediment core 57-3 on the continental shelf allows us to detect the sediment input from Baffin Island and related meltwater and transport processes. Moreover, radiogenic isotope composition and mineral assemblages could identify material from other source regions in Baffin Bay transported to the core site by ocean currents. Even if the age model of the

core is limited, it suggests that the sediment record covers approximately the last 8.9 to 13.5 ka BP. That time interval covers parts of the initial Clyde shelf deglaciation between 16 and 11.7 ka BP and the early Holocene step-wise retreat of the ice margin in the fjord (Couette et al., 2023). Thus, the 57-3 core very likely includes valuable information about the early LIS deglaciation processes that are not covered by the core from the Clyde Inlet head.

Couette et al. (2023) already presented the lithology and element ratios of the 57-3. However, they do not include dates for the core as they did for the 46-3 core. Thus, the collected dates in this study are a valuable addition to their study. According to their research, the base of the 57-3 core is characterized by two diamicton layers (unit 1), identified as glaciogenic debris-flows deposited during ice stillstands. These layers are interrupted and overlain by ice-proximal glaciomarine deposits (unit 2). The uppermost, about 4 meters, consist of ice-distal hemipelagic sediments, which can also be found at the top of most other cores in the Clyde Inlet region (Couette et al., 2023). That seems to be contradictory to the age model, suggesting that there is a sediment gap at the top of the core. There are three radiocarbon ages, ranging between 9.5 and 10.6 ka BP dated at 130 cm to 250 cm sediment depth (Fig. 5-4), which are situated within the upper layer of sediment identified by Couette et al. (2023). This could mean that the sediment of the uppermost 1.3 m was either deposited steadily after 9 ka BP but, at some point, with a meager sedimentation rate or that some sediment was eroded during this time interval due to ocean bottom currents. The analysis of multiple sediment cores from the northeast Baffin margin show similar depositional patterns (Jenner et al., 2018). For example, radiocarbon analysis from sediments of 64PC from the upper continental slope of Baffin Island north of the Buchan Trough suggests ages at 138 cm of 9.46 ka BP and 111 cm of 8.72 ka BP (Campbell et al., 2017; Kelleher et al., 2022). In general, Jenner et al. (2018) conclude that the lithological features of the different cores suggest that in Baffin Bay, the direct glacial supply is more significant for sedimentation than the effect of glacial meltwater. Therefore, we assume that the sediment top (~1 m) was deposited during the interval when the ice stream finally retreated behind the Clyde Inlet head after its last readvance at ~7.9 ka BP (Briner et al., 2007) and meltwater runoff predominantly delivered sediment to the Clyde Inlet fjord and just minor amounts to the shelf.

Radiogenic isotope data of the 57-3 core show minor variations in sediment provenance on the Baffin Island shelf during the last deglaciation and the Holocene. The slight differences in continental bedrock geology may have caused the small changes in the isotope signatures. While the Clyde foreland and some areas close to the fjord head are predominantly characterized by the occurrence of the slightly younger Paleoproterozoic igneous and metamorphic rocks, the hinterland and more distal regions mainly compose of the Archean rocks (Fig. 5-2). The range of Sr and Nd

isotope signatures of the core generally fit with the expected values for the nearby Rea Craton, the main sediment source area. The radiogenic isotope data in the lower part of the core (bottom to ~ 600 cm) was likely caused by the retreating ice shelf, while the second part of unit 2 shows fewer variable values due to less iceberg discharge and/or a stillstand of the ice margin during that time. After this interval, radiogenic Sr and Nd isotope data decrease and increase, respectively, within unit 3a. According to the age model, which seems to be, due to the abundance of dating points, robust in unit 3, this gradual change occurred between 11.1 and 8.9 ka BP. The interval fits with the rapid retreat of the ice margin into the fjord and the subsequent deglaciation of the Clyde Inlet (Couette et al., 2023). Hence, the gradually decreasing $^{87}Sr/^{86}Sr$ and increasing ε_{Nd} values likely reflect the increasing distance of the ice margin to the core site and the decreasing influence of sediment originating from the Clyde Inlet area on the shelf. In addition to the sediment from the nearby land, material transported by ocean currents could be deposited on the shelf during post-glacial periods.

Couette et al. (2023) argue that the elevated Ca/Ti ratios in the lower part of core 57-3 are probably related to the increased accumulation of detrital carbonates originating from northern Baffin Bay. The Baffin Bay detrital carbonate events (BBDC) are carbonate-rich layers, which can be found in multiple sediment cores from Baffin Bay and which are associated with the iceberg and meltwater discharge from Lancaster Sound, northern Baffin Bay (Aksu and Piper, 1987; Andrews et al., 1998; Hiscott et al., 1989). The timing of the last event, BBDC 0, is around 12.7 to 11 ka BP (Jackson et al., 2017). While the high Ca/Ti ratios in the upper part of the core occurred after ~ 11.1 ka BP (with a maximum at ~ 10.6), which is slightly after the BBDC 0, they are likely related to the final decay of the Lancaster Sound ice stream during the early Holocene, which resulted in the opening of the Parry Channel and the onset of the Arctic-Atlantic throughflow at between 11 and 10 ka BP (Kelleher et al., 2022; Pieńkowski et al., 2014). In addition, reference isotope signatures from Barrow Strait (in the central part of the Parry Channel) show significantly higher ε_{Nd} values in an area surrounded by detrital carbonates than what we observed in the 57-3 core. Even if the ε_{Nd} values slightly increase after ~11 ka BP, they do not show maxima that could be related to distinct peaks of carbonate layers and are probably related to an enhanced input of sediment originating from northern Baffin Bay after the deglaciation of the Parry Channel.

5.6 Conclusion

Based on two radiocarbon-dated sediment cores from the head of the Clyde Inlet (GeoB2234-3) and from the shelf in front of it (GeoB22357-3), we reconstructed changing sedimentation processes and sediment provenances during the last deglaciation of the fjord. We focused on the Sr, Nd, and Pb isotope composition of the two cores to investigate glacial dynamics and used the

mineralogical assemblages to assess the different factors that control the radiogenic isotope composition in such a fjord system. Moreover, high-resolution MS and CT data were used to identify the timing of main sedimentological changes at both sites. Our data allow the following conclusions:

- Highly variable Sr and Pb isotope data at the fjord head (46-3) indicate a strong mineralogical control. The variable radiogenic isotope and mineralogical compositions reflect changing meltwater fluxes related to fluctuations of the ice margin during the last deglaciation after the ice retreated out of the Clyde Inlet. Similar effects cannot be observed on the shelf, were radiogenic isotope compositions are mainly controlled by sediment provenance.
- 46-3 data reveal high-frequency ice margin fluctuations during the early Holocene, a weakening meltwater discharge associated with a minimum ice extent during the mid-Holocene, and a readvance of alpine glaciers staring at 2.2 ka BP due to the Neoglacial cooling.
- 57-3 data show variable radiogenic isotope compositions in layers previously identified as diamiction and which were formed during the late Pleistocene when the LIS extended onto the Baffin shelf. The data suggest a transition from ice-proximal to ice-distal conditions at around 11 ka BP. After this transition, higher carbonate contents and gradually increasing ε_{Nd} values likely reflect the stronger influence of sediments originating from northern Baffin Bay after the deglaciation of Lancaster Sound and the opening of the Parry Channel.

Acknowledgements

We would like to thank the master and crew of the R/V Maria S. Merian for their work during expedition MSM66. Sample material has been provided by the GeoB Core Repository at the MARUM – Center for Marine Environmental Sciences, University of Bremen, Germany. We further gratefully acknowledge Klinikum Bremen-Mitte and Christian Timann and Arne-Jörn Lemke for supporting the CT measurements in their facilities. Additionally, we want to thank Catalina Gebhardt for providing the magnetic susceptibility data of the cores. This project was supported by the Deutsche Forschungsgemeinschaft (DFG) through the International Research Training Group “Processes and impacts of climate change in the North Atlantic Ocean and the Canadian Arctic” (IRTG 1904 ArcTrain).

References

Aksu, A.E., Piper, D.J.W., 1987. Late Quaternary sedimentation in Baffin Bay. Canadian Journal of Earth Sciences 24.

Andrews, J.T., Barnett, D.M., 1979. Holocene (Neoglacial) moraine and proglacial lake chronology, Barnes Ice Cap, Canada. Boreas 8, 341-358.

Andrews, J.T., Ives, J.D., 1978. "Cockburn" Nomenclature and the Late Quaternary History of the Eastern Canadian Arctic. Arctic and Alpine Research 10, 617-633.

Andrews, J.T., Kirby, M.E., Aksu, A.E., Barber, D.C., Meese, D., 1998. Late Quaternary Detrital Carbonate (DC-) Layers in Baffin Bay marine sediments (67°-74°N): Correlation with Heinrich Events in the north Atlantic? Quaternary Science Reviews 17, 1125-1137.

Axford, Y., Briner, J.P., Miller, G.H., Francis, D.R., 2009. Paleoecological evidence for abrupt cold reversals during peak Holocene warmth on Baffin Island, Arctic Canada. Quaternary Research 71, 142-149.

Bamber, J.L., Vaughan, D.G., Joughin, I., 2000. Widespread complex flow in the interior of the antarctic ice sheet. Science 287, 1248-1250.

Bennett, M.R., 2003. Ice streams as the arteries of an ice sheet: their mechanics, stability and significance. Earth-Science Reviews 61, 309-339.

Bennett, R., Campbell, D.C., Furze, M.F.A., 2013. The shallow stratigraphy and geohazards of the Northeast Baffin Shelf and Lancaster Sound. Geological Survey of Canada Open File 7355.

Berger, A., Loutre, M.F., 1991. Insolation values for the climate of the last 10 million of years. Quaternary Science Reviews 10, 297-317.

Briner, J.P., Bini, A.C., Anderson, R.S., 2009a. Rapid early Holocene retreat of a Laurentide outlet glacier through an Arctic fjord. Nature Geoscience 2, 496-499.

Briner, J.P., Cuzzone, J.K., Badgeley, J.A., Young, N.E., Steig, E.J., Morlighem, M., Schlegel, N.J., Hakim, G.J., Schaefer, J.M., Johnson, J.V., Lesnek, A.J., Thomas, E.K., Allan, E., Bennike, O., Cluett, A.A., Csatho, B., de Vernal, A., Downs, J., Larour, E., Nowicki, S., 2020. Rate of mass loss from the Greenland Ice Sheet will exceed Holocene values this century. Nature 586, 70-74.

Briner, J.P., Davis, P.T., Miller, G.H., 2009b. Latest Pleistocene and Holocene glaciation of Baffin Island, Arctic Canada: key patterns and chronologies. Quaternary Science Reviews 28, 2075-2087.

Briner, J.P., Michelutti, N., Francis, D.R., Miller, G.H., Axford, Y., Wooller, M.J., Wolfe, A.P., 2006. A multi-proxy lacustrine record of Holocene climate change on northeastern Baffin Island, Arctic Canada. Quaternary Research 65, 431-442.

Briner, J.P., Miller, G.H., Davis, P.T., Finkel, R.C., 2005. Cosmogenic exposure dating in arctic glacial landscapes: implications for the glacial history of northeastern Baffin Island, Arctic Canada. Canadian Journal of Earth Sciences 42, 67-84.

Briner, J.P., Overeem, I., Miller, G., Finkel, R., 2007. The deglaciation of Clyde Inlet, northeastern Baffin Island, Arctic Canada. Journal of Quaternary Science 22, 223-232.

Brouard, E., Lajeunesse, P., 2017. Maximum extent and decay of the Laurentide Ice Sheet in Western Baffin Bay during the Last glacial episode. Sci Rep 7, 10711.

Campbell, D.C., Jenner, K.A., Higgins, J., Piper, D.J.W., 2017. Analysis of piston cores and high-resolution sub-bottom profiler data, Baffin Bay slope, Nunavut. Geological Survey of Canada Open File 8135.

Colville, E.J., Carlson, A.E., Beard, B.L., Hatfield, R.G., Stoner, J.S., Reyes, A.V., Ullman, D.J., 2011. Sr-Nd-Pb isotope evidence for ice-sheet presence on southern Greenland during the Last Interglacial. Science 333, 620-623.

Couette, P.-O., Lajeunesse, P., Ghienne, J.-F., Dorschel, B., Gebhardt, C., Hebbeln, D., Brouard, E., 2023. Retreat and stabilization of a marine-based ice margin along a high arctic fjord-cross-shelf trough system. Quaternary Science Reviews 302, 107949.

Deniel, C., Pin, C., 2001. Single-stage method for the simultaneous isolation of lead and strontium from silicate samples for isotopic measurements. Analytica Chimica Acta 426, 95-103.

Dorschel, B., Allan, E., Bartels, M., Campbell, C., Couette, P.-O., Diekamp, V., Dreutter, S., Duboc, Q., Geils, J., Greco, M., Lenz, K.-F., Lübben, B., Lütjens, M., Madaj, L., Perez, L., Recinos, B., Saini, J., Schade, T., Täuber, F., Ulner, L.-C., Warnke, F., Weiser, J., 2017. WESTBAFF - Reconstruction of the Laurentide Ice sheet drainage into the northwest Baffin Bay and the palaoceanography of the west Baffin Bay, Cruise No. MSM66, 22nd of July 2017 - 28th of August 2017, Nuuk (Greenland) - Reykjavik (Iceland). MARIA S. MERIAN-Berichte, Gutachterpanel Forschungsschiffe MSM66.

Eisenhauer, A., Meyer, H., Rachold, V., Tütken, T., Wiegand, B., Hansen, B.T., Spielhagen, R.F., Lindemann, F., Kassens, H., 1999. Grain size separation and sediment mixing in Arctic Ocean sediments: evidence from the strontium isotope systematic. Chemical Geology 158, 173-188.

Faure, G., Powell, J.L., 2012. Strontium Isotope Geology. Springer Science & Buisness Media.

Fisher, D.A., Koerner, R.M., Reeh, N., 1995. Holocene climatic records from the Agassiz Ice Cap, Ellesmere Island, NWT, Canada. The Holocene 5, 19-24.

Garçon, M., Chauvel, C., France-Lanord, C., Limonta, M., Garzanti, E., 2014. Which minerals control the Nd–Hf–Sr–Pb isotopic compositions of river sediments? Chemical Geology 364, 42-55.

Harrison, J.C., St-Onge, M.R., Petrov, O.V., Strelnikov, S.I., Lopatin, B.G., Wilson, F.H., Tella, S., Paul, D., Lynds, T., Shokalsky, S.P., Hults, C.K., Bergman, S., Jepsen, H.H., Solli, A., 2011. Geological Map of the Arctic. Geological Survey of Canada, p. Map 2159A.

Heaton, T.J., Köhler, P., Butzin, M., Bard, E., Reimer, R.W., Austin, W.E.N., Bronk Ramsey, C., Grootes, P.M., Hughen, K.A., Kromer, B., Reimer, P.J., Adkins, J., Burke, A., Cook, M.S., Olsen, J., Skinner, L.C., 2020. Marine20—The Marine Radiocarbon Age Calibration Curve (0–55,000 cal BP). Radiocarbon 62, 779-820.

Hiscott, R.N., Aksu, A.E., Nielsen, O.B., 1989. Provenance and dispersal pattern, Pliocene-Pleistocene section at site 645, Baffin Bay. Proceedings of Ocean Drilling Program, Scientific Results 105.

Höppner, N., Lucassen, F., Chiessi, C.M., Sawakuchi, A.O., Kasemann, S.A., 2018. Holocene provenance shift of suspended particulate matter in the Amazon River basin. Quaternary Science Reviews 190, 66-80.

Jackson, G.D., Berman, R.G., 2000. Precambrian metamorphic and tectonic evolution of northerrn Baffin Island, Nunavut, Canada. The Canadian Mineralogist 38, 399-421.

Jackson, R., Carlson, A.E., Hillaire-Marcel, C., Wacker, L., Vogt, C., Kucera, M., 2017. Asynchronous instability of the North American-Arctic and Greenland ice sheets during the last deglaciation. Quaternary Science Reviews 164, 140-153.

Jacobsen, S.B., Wasserburg, G.J., 1980. Sm-Nd Isotopic Evolution of Chondrites. Earth and Planetary Science Letters 50, 139-155.

Jenner, K.A., Campbell, D.C., Piper, D.J.W., 2018. Along-slope variations in sediment lithofacies and depositional processes since the Last Glacial Maximum on the northeast Baffin margin, Canada. Marine Geology 405, 92-107.

Kaufman, D.S., Ager, T.A., Anderson, N.J., Anderson, P.M., Andrews, J.T., Bartlein, P.J., Brubaker, L.B., Coats, L.L., Cwynar, L.C., Duvall, M.L., Dyke, A.S., Edwards, M.E., Eisner, W.R., Gajewski, K.,

Geirsdóttir, A., Hu, F.S., Jennings, A.E., Kaplan, M.R., Kerwin, M.W., Lozhkin, A.V., MacDonald, G.M., Miller, G.H., Mock, C.J., Oswald, W.W., Otto-Bliesner, B.L., Porinchu, D.F., Rühland, K., Smol, J.P., Steig, E.J., Wolfe, B.B., 2004. Holocene thermal maximum in the western Arctic (0–180°W). Quaternary Science Reviews 23, 529-560.

Kelleher, R., Jennings, A., Andrews, J., Brooks, N.K.S., Marchitto, T., Feng, S., Woelders, L., Normandeau, A., Jenner, K., Bennett, R., Brookins, S., 2022. Late glacial retreat of the Lancaster Sound Ice Stream and early Holocene onset of Arctic/Atlantic throughflow in the Arctic Island channels. Arctic, Antarctic, and Alpine Research 54, 395-427.

Kirillova, V., 2017. Radiogenic isotopes on marine sediments from the Baffin Bay: implications for the sediment supply during the last deglaciation. Dissertation, Faculty of Geosciences, University Bremen, Bremen, Germany.

Lenz, K.-F., Campbell, C., Gebhardt, C., in review. Processed physical properties measured on core GeoB22357-3 [dataset]. https://doi.pangaea.de/10.1594/PANGAEA.959766.

Lougheed, B.C., Obrochta, S.P., 2019. A Rapid, Deterministic Age-Depth Modeling Routine for Geological Sequences With Inherent Depth Uncertainty. Paleoceanography and Paleoclimatology 34, 122-133.

Maccali, J., Hillaire-Marcel, C., Not, C., 2018. Radiogenic isotope (Nd, Pb, Sr) signatures of surface and sea ice-transported sediments from the Arctic Ocean under the present interglacial conditions. Polar Research 37, 1442982.

Madaj, L., 2021. Holocene Ice Sheet Dynamics and Detriral Provenance Shifts Along the West Greenland Margin Recorded by Radiogenic Isotopes. Dissertation, Faculty of Geosciences, University Bremen, Bremen, Germany.

Margold, M., Stokes, C.R., Clark, C.D., 2015. Ice streams in the Laurentide Ice Sheet: Identification, characteristics and comparison to modern ice sheets. Earth-Science Reviews 143, 117-146.

McCulloch, M.T., Wasserburg, G.J., 1978. Sm-Nd and Rb-Sr Chronology of Continental Crust Formation. Science 200, 1003-1011.

Miller, G.H., Wolfe, A.P., Briner, J.P., Sauer, P.E., Nesje, A., 2005. Holocene glaciation and climate evolution of Baffin Island, Arctic Canada. Quaternary Science Reviews 24, 1703-1721.

Moore, J.J., Hughen, K.A., Miller, G.H., Overpeck, J.T., 2001. Little Ice Age recorded in summer temperature reconstructions from varved sediments of Donard Lake, Baffin Island, Canada. Journal of Paleolimnology 25, 503-517.

Okuma E., Hingst, J., Weiser, J., Madaj, L., Titschack, J., Vogt, C., Kienast, M., Hillaire-Marcel, C., Hebbeln, D., Kasemann, S.A. (submitted). Deglacial and Holocene sediment dynamics and provenances off Lancaster Sound: implications for paleoenvironmental conditions in northern Baffin Bay. Submitted to Quaternary Science Reviews.

Pieńkowski, A.J., Coulthard, R.D., Furze, M.F.A., 2022. Revised marine reservoir offset (ΔR) values for molluscs and marine mammals from Arctic North America. Boreas.

Pieńkowski, A.J., England, J.H., Furze, M.F.A., MacLean, B., Blasco, S., 2014. The late Quaternary environmental evolution of marine Arctic Canada: Barrow Strait to Lancaster Sound. Quaternary Science Reviews 91, 184-203.

Pin, C., Briot, D., Bassin, C., Poitrasson, F., 1994. Concomitant separation of strontium and samarium-neodymium for isotopic analysis in silicate samples, based on specific extraction chromatography. Analytica Chimica Acta 298, 209-217.

Praeg, D., Maclean, B., Sonnichsen, G., 2007. Quaternary Geology of the Northeast Baffin Island Continental Shelf, Cape Aston to Buchan Gulf (70° to 72°N). Geological Survey of Canada Open File 5409.

Reyes, A.V., Carlson, A.E., Beard, B.L., Hatfield, R.G., Stoner, J.S., Winsor, K., Welke, B., Ullman, D.J., 2014. South Greenland ice-sheet collapse during Marine Isotope Stage 11. Nature 510, 525-528.

Schlitzer, R., 2020. Ocean Data View, https://odv.awi.de.

Scott, D.J., de Kemp, E.A., 1998. Bedrock geology compilation, northern Baffin Island and northern Melville Peninsula, Northwest Territories. Geological Survey of Canada Open File 3633.

Stalling, D., Westerhoff, M., Hege, H.-C., 2005. Amira: A Highly Interactive System for Visual Data Analysis. Visualization Handbook, 749-767.

Stuiver, M., Reimer, P.J., 1993. Extended ^{14}C Data Base and Revised CALIB 3.0 ^{14}C Age Calibration Program. Radiocarbon 35, 215-230.

Tang, C.C.L., Ross, C.K., Yao, T., Petrie, B., DeTracey, B.M., Dunlap, E., 2004. The circulation, water masses and sea-ice of Baffin Bay. Progress in Oceanography 63, 183-228.

Thomas, E.K., Szymanski, J., Briner, J.P., 2010. Holocene alpine glaciation inferred from lacustrine sediments on northeastern Baffin Island, Arctic Canada. Journal of Quaternary Science 25, 146-161.

Tütken, T., Eisenhauer, A., Wiegand, B., Hansen, B.T., 2002. Glacial-interglacial cycles in Sr and Nd isotopic composition of Arctic marine sediments triggered by the Svalbard/Barents Sea ice sheet. Marine Geology 182, 351-372.

Young, N.E., Briner, J.P., Rood, D.H., Finkel, R.C., 2012. Glacier extent during the Younger Dryas and 8.2-ka event on Baffin Island, Arctic Canada. Science 337, 1330-1333.

6. Marine radiogenic isotope record from Barrow Strait reveals late Pleistocene to early Holocene ice sheet dynamics in the Canadian Arctic Archipelago

Johanna Hingst[a], Claude Hillaire-Marcel[b], Friedrich Lucassen[a], Rüdiger Stein[a], and Simone A. Kasemann[a]

[a]MARUM – Center for Marine Environmental Science and Faculty of Geosciences, University of Bremen, Germany
[b]Geotop – Centre de recherche sur la dynamique du système Terre, Université du Québec à Montréal, Canada

Manuscript in preparation

Abstract

During the last glacial maximum, the Parry Channel, a marine channel in the Canadian Arctic Archipelago (CAA), which connects northern Baffin Bay with the Arctic Ocean, was blocked by the confluent Laurentide and Innuitian ice sheets. The deglaciation of the two ice sheets and the related opening of the Parry Channel resulted in changing oceanographic and sedimentological processes in Baffin Bay and the deposition of specific carbonate-rich sediment layers in the Arctic Ocean, Baffin Bay, and the North Atlantic. While the latest deglaciation history of Barrow Strait and Lancaster Sound, two passages at the eastern part of the Parry Channel, is well documented, there is little knowledge about the spatial and temporal variability of glacial and meltwater-related sediment input into Barrow Strait during that period. In this study, we use the Sr, Nd, and Pb isotope composition of the siliciclastic sediment fraction of the marine sediment core PS72/287-3 from Barrow Strait as sediment provenance proxies to reconstruct sedimentation patterns and associated ice sheet dynamics during the last deglaciation and the Holocene. Variable radiogenic isotope data during the deglacial period suggest fluctuating ice margin positions and the input of old igneous and metamorphic rocks originating from the south of the CAA. Uniform data during the early Holocene indicate the landward ice margin retreat after 10 ka BP and a constant sediment supply from proximal islands by mainly river discharge. Additionally, measurements on the leachate fraction show highly radiogenic Pb isotope signatures, which seem to be characteristic of the detrital carbonates in the CAA.

6.1 Introduction

Marine sediments are recorders of past environmental changes. In the Arctic realm, sedimentary records can contain information about, e.g., past ocean circulation and terrestrial runoff, and they also hold information on past sea ice conditions and surrounding continental ice sheet dynamics (e.g., Stein, 2008). Provenance studies using mineral assemblages and radiogenic isotopes can help

resolve past ice sheet configurations, iceberg calving patterns, and ocean circulation (Fagel et al., 2014). The radiogenic Sr, Nd, and Pb isotope signatures of marine sediments from Baffin Bay and Labrador Sea have successfully been used to reconstruct the deglaciation history of the Laurentide Ice Sheet (LIS) and Greenland Ice Sheet (GIS), which bordered Baffin Bay to the west and east, respectively (Colville et al., 2011; Farmer et al., 2003; Reyes et al., 2014). In contrast to Baffin Bay and Labrador Sea, provenance studies using radiogenic isotopes are still rare in the Canadian Arctic Archipelago (CAA), even if the region is of special importance. The CAA was covered during the Last Glacial Maximum (LGM) by the Innuitian Ice Sheet (IIS), which blocked the Parry Channel and Nares Strait by conferencing with the LIS and the GIS, preventing the inflow of Arctic waters into Baffin Bay (Fig. 6-1 A) (Dyke et al., 2002; Jennings et al., 2019; Jennings et al., 2011; Pieńkowski et al., 2014; Pieńkowski et al., 2012). Nowadays, these gateways account for an important part of the exchange of sea ice and Arctic waters, which does influence not only Baffin Bay but also Labrador Sea circulation (Holland et al., 2001; Jones et al., 2003; Tang et al., 2004). The deglaciation history of the Parry Channel, especially of its central and eastern parts, is well documented. Several studies on marine sediment cores from Barrow Strait, in the central Parry Channel, prove the presence of glacial grounded ice and the subsequent lift-off between 11.5 and 11 ka BP (Pieńkowski et al., 2013; Pieńkowski et al., 2012). The following period was characterized by the transition of ice-proximal to ice-distal conditions and the separation of the LIS and IIS at ~ 11 ka BP (Pieńkowski et al., 2014). Additionally, an increase in foraminiferal abundances indicates the establishment of a deep Arctic throughflow by 10.3 ka BP (Pieńkowski et al., 2013). Early Holocene environmental conditions were marked by increased biological activity and reduced seasonal sea ice cover that were probably caused by warmer temperatures during the Holocene Thermal Maximum (HTM) (Pieńkowski et al., 2013; Pieńkowski et al., 2014). According to Pieńkowski et al. (2014), present-day like environmental conditions in the central CAA were established by ~ 5.6 ka BP. While the main focus of these studies was to reconstruct deglaciation-related changes in sea ice and ocean circulation, we will concentrate on the changing sediment processes in Barrow Strait during and after its deglaciation.

Additionally, the core site allows us to investigate the specific radiogenic isotope signature of sediments deposited proximal to the carbonate outcrops on land of the CAA. Carbonate-enriched layers are a popular feature of sedimentary records from the Arctic Ocean, Baffin Bay, and the North Atlantic (Stein, 2008). Detrital carbonates occurring in the coarse fraction of marine sediments, including dropstones, are often attributed to iceberg rafted material discharged by the LIS and IIS (e.g., Andrews et al., 1998; Andrews and Tedesco, 1992; Dong et al., 2017) due to the high abundance of Paleozoic carbonates in northeastern Canada and the Canadian Arctic Archipelago (CAA). Dolomite-enriched layers are not only composed of coarse sediments but also consist of a

high proportion of dolomite in the fine fraction (<63 µm). Swärd et al. (2022) studied the fine fraction of a sediment core from the Mackenzie Trough offshore the Mackenzie river, draining a large area of the Canadian Arctic. They used radiogenic isotopes (Sr and Nd) as well as the mineralogical composition to fingerprint the sediment source, which would have the potential to better distinguish between sources of dolomite in the Arctic Ocean. However, they concluded that more detailed radiogenic isotope studies of carbonate-enriched sediments proximal to the source area, e.g., in the CAA, are necessary to determine the source of carbonate-enriched units in marine sediments from the central Arctic Ocean (Swärd et al., 2022).

The main objectives of this study are (1) to relate variations in radiogenic isotope compositions to changing sediment provenance associated with past ice sheet dynamics in the CAA and (2) to specify the radiogenic isotope signature of detrital carbonates from the CAA.

6.2 Regional Setting

The Parry Channel, which is part of the Northwest passage, is one of the major channels connecting Baffin Bay and the Arctic Ocean (Fig. 6-1 A). The channel is situated in the CAA, a complex environment composed of multiple islands, narrow channels, and larger basins. Barrow Strait is situated in the central part of the Parry channel, connecting the Lancaster Sound to the east with the Viscount Melville Sound to the west. Due to differences in sea level, modern circulation is dominated by a southeastward flow of Arctic waters through the channels of the CAA into Baffin Bay and finally into the north Atlantic Ocean (Michel et al., 2006; Prinsenberg and Bennett, 1987). However, also warmer Atlantic-derived waters can penetrate from northern Baffin Bay into Lancaster Sound, where they mix with the eastward-flowing Arctic waters (e.g., Tang et al., 2004). Like many other channels of the CAA, Barrow Strait is not deep, just about 300 m. Water depth increase westwards towards Lancaster Sound (~ 750 m) and finally even more towards Baffin Bay. Annual sea ice cover and land-fast sea ice in the CAA persist approximately from November to June; therefore, the ice-free season is relatively short (Vare et al., 2009).

Barrow Strait is bordered to the north by Bathurst, Cornwallis, and Devon Islands and to the south by Prince of Wales and Somerset Islands. Geologically these islands are characterized by Paleozoic carbonates and clastic sediment (Fig. 6-1 B). Additionally, east of the Peel Sound, west and south Somerset Island compose of Archean to Paleoproterozoic granites and gneiss. Similar old igneous and metamorphic rocks can be found on Bylot, eastern Devon, and northern Baffin Island, as well as in northeastern Canada. Slightly younger Paleo- to Mesoproterozoic sediments and volcanic rocks occur on the Borden Peninsula. Younger Devonian carbonates and clastic sediments, as well

as Paleozoic to Cenozoic sediments, can be found on western Bathurst and Melville Island (Harrison et al., 2011; Okulitch, 1991).

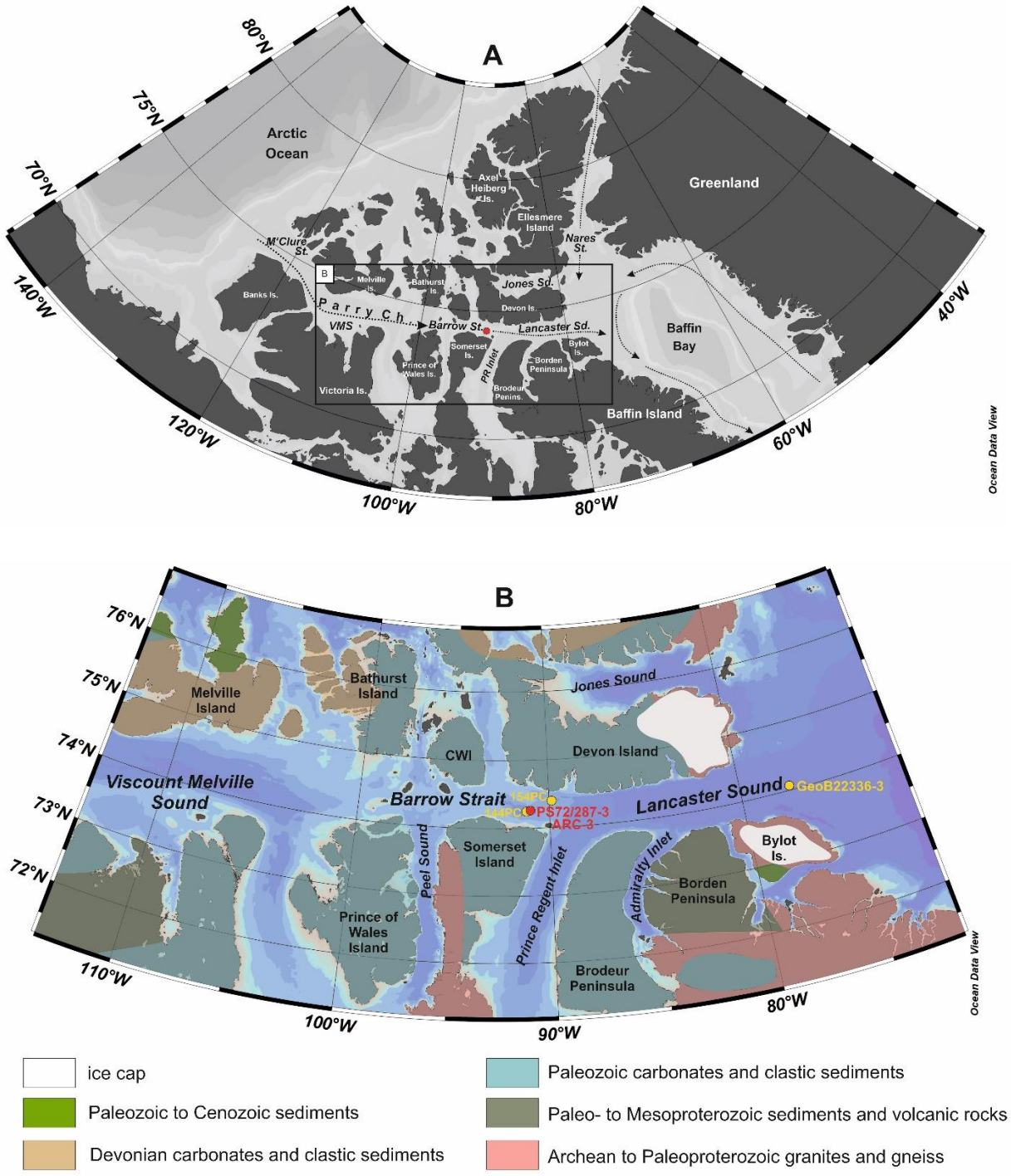

Figure 6-1: A: Overview map of the research area. Dotted lines and arrows indicate modern ocean circulation patterns (adopted after Michel et al., 2006). B: Detailed map of the research area. Core site locations of PS72/287-3 and ARC-3 are indicated by a single red dot due to the small distance between the two sites. Other core sites discussed in this manuscript are indicated as yellow dots. Simplified bedrock geology from (Harrison et al., 2011; Okulitch, 1991).

6.3 Materials and Methods

In this study, we choose the marine gravity core PS72/287-3 from Barrow Strait (74°15.95'N, 90°59.09'W; water depth: 337 m; core length: 463 cm), Canadian Arctic Archipelago, which was retrieved during cruise ARK-XXIII/3 in 2008 (Jokat, 2009), to measure the radiogenic Sr, Nd, and Pb isotope composition of the sediment. The coring location was selected based on parasound images to penetrate through the Holocene unit into the well-stratified layer below, which was not sampled before (Fig. 6-2) (Stein et al., 2009). Physical properties, including magnetic susceptibility data and X-ray images of the core, later used to calculate the concentration of ice-rafted debris (IRD), are published on the PANGAEA online data repository (Nissen, 2010; Matthiessen and Stein, 2008). An approximate chronology of the core was inferred from comparing the parasound profile at the core location with the profile from the close, dated core ARC-3 retrieved during the ArcticNet cruise in 2005 (Nissen et al., 2010; Rochon and *participants*, 2005; Stein et al., 2009). ARC-3 comprises the upper sediment unit 1, which is visible on the parasound and has a maximum age of ~ 10 ka BP (Vare et al., 2009). Since PS72/287-3 contains 3.1 m sediment of the same upper unit and additionally ~1.5 m of the unit below, PS72/287-3 likely covers the post-glacial Holocene period (unit 1) and parts of the last glacial/deglacial period (unit 2) (Stein et al., 2009). Additional information on the sediment age was obtained by the correlation of the increase in dry bulk density at 9.7 ka BP in ARC-3 with the peak in wet bulk density at the reflector R2 in PS72/287-3 (Nissen et al., 2010). Magnetic susceptibility (MS) measurements were performed on board at 1 cm intervals using a Multi Sensor Core Logger (MSCL, GEOTEK Ltd., UK) (Stein et al., 2009).

For radiogenic isotope analysis, 16 sediment samples were taken between 10 cm and 450 cm core depth. Sampling depths were chosen based on the MS record and aimed to cover major changes in the sediment composition.

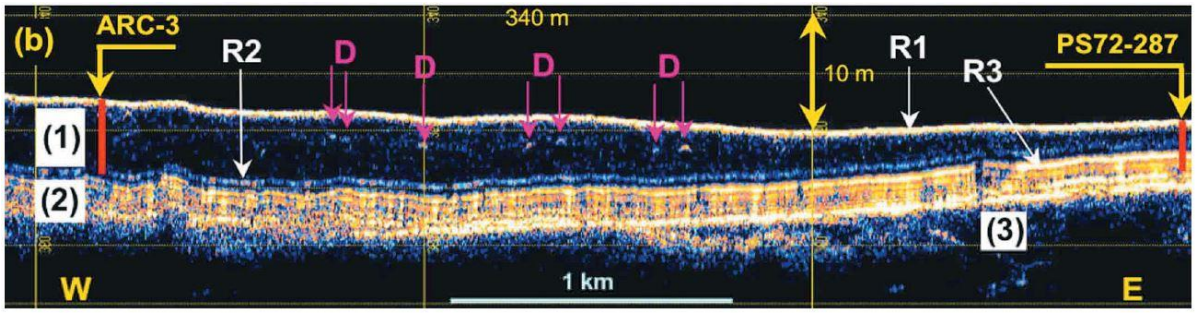

Figure 6-2: Parasound sub-bottom image from Barrow Strait showing the core locations of PS72/287-3 and ARC-3. Key reflectors R1 to R3 are marked. The Holocene unit 1 and the underlying unit 2 are indicated. From (Nissen et al., 2010).

6.3.1 Radiogenic Isotope Analysis

The radiogenic isotope compositions of Sr, Nd, and Pb were prepared and measured in the laboratories of the Isotope Geochemistry Group at MARUM – Center for Marine Environmental Sciences, University of Bremen. Initially, about 2 g of wet sediment samples were washed twice with Milli Q water (18.2 MΩ) to remove the soluble fraction and residual pore water before the <63 µm grain-size fraction was separated by wet sieving for further analysis. To separate the carbonate from the silicate fraction and dissolve potential authigenic Fe-Mn oxyhydroxide coatings on the sediment, samples were leached with a solution of hydroxylamine hydrochloride and 15 % acetic acid, buffered with NaOH (for 3 hours; adapted from Gutjahr et al., 2007). The leachate fraction was stored in PP containers after this step, while the remaining detrital samples were washed with Milli Q water (twice) and dried. Afterward, 100 mg of the siliciclastic fraction was transferred into 15 ml Teflon Savillex® beakers for the sample digestion process, which includes several steps (modified after Höppner et al., 2018). For sample dissolution, we added 3 ml of a concentrated HF:HNO_3 (5:1) mixture at 140 °C (at least 48 hours). After drying, we re-dissolved the samples with 3 ml of aqua regia (3:1, 6 N HCl: concentrated HNO_3) at 120 °C for two days. In order to remove potential contents of organic matter, we added 100 µl of H_2O_2 to the samples (4 to 5 times) until the reaction stopped. Following the addition of 1 ml of concentrated HNO_3, each sample was set on the hotplate (70 °C) overnight to dissolve again, dried, and then re-dissolved in 3 ml 6 N HCl. For chemical separation, we dried and re-dissolved the samples in 1100 µl 2N HNO_3. For the dissolution of the leachates, samples were transferred into 15 ml Teflon Savillex® beakers and were dried at 85°C on the hotplate. For redissolution, we added three times 2 ml of concentrated HNO_3 and 6 M HCl, respectively, and placed the closed samples on the hotplate at 85°C overnight. After each step, samples were dried at 85°C on the hotplate. Finally, samples were redissolved in 1100 µl 2M HNO_3 for the column chemistry.

To separate Nd, Sr, and Pb from the sample matrix, we performed column chemistry. Sr and Pb were separated on the same column using 70 µl of Sr.spec™ resin, following a modified method after Deniel and Pin (2001). The isolation of Nd was performed in two steps using TRU.spec™ for light rare earth elements and LN.spec™ for Nd separation (Eichrom®) (method after Pin et al., 1994).

Isotope ratios were measured with a Thermo-Fisher Scientific TRITON Plus thermal ionization mass spectrometer (TIMS). Sr and Pb isotope compositions were measured using a single filament, a Ta and a Si activator, respectively, and the static multicollection mode, whereas Nd isotope composition was analyzed on double filaments in a static multicollection mode. The stable ratio of $^{86}Sr/^{88}Sr$ (= 0.1194) was used to correct the instrumental mass fractionation that occurs during Sr isotope analysis. To assess the analytical accuracy and repeatability of the $^{87}Sr/^{86}Sr$ data, the

reference material NIST SRM 987 was used and yielded a mean value of 0.710246 ± 0.000018 ($2SD_{mean}$, n = 5), which is within the range of values analyzed by TIMS and published in the GeoRem database of 0.710250±0.000034 ($2SD_{mean}$, n= 1711, data <0.7102 and >0.7103 are discarded) (http://georem.mpch-mainz.gwdg.de/, query November 2022). During Pb isotope analysis, instrumental mass fractionation was corrected by applying a factor of 1.001 per atomic mass unit. Reference material NIST SRM 981 yielded a mean value of 16.9004 ± 0.0133 ($^{206}Pb/^{204}Pb$; $2SD_{mean}$, n=12), which agrees with the published mean value of 16.9211 ± 0.0423 ($^{206}Pb/^{204}Pb$; GeoReM; $2SD_{mean,}$ n=290, data >17 are discarded) During Nd analysis, instrumental mass fractionation was corrected to $^{146}Nd/^{144}Nd$ (= 0.7219). The analytical accuracy and repeatability for $^{143}Nd/^{144}Nd$ were monitored by the reference material JNdi-1, which yielded a value of 0.512111 ± 0.000022 ($2SD_{mean}$, n = 3) that agrees with the published values of 0.512107±0.000024 ($2SD_{mean}$, n= 414, data <0.51204 and >0.51217 are discarded) analyzed by TIMS (GeoRem database, http://georem.mpch-mainz.gwdg.de/, query November 2022). The $^{143}Nd/^{144}Nd$ ratio is reported in the ε_{Nd} notation relative to the Chondritic Uniform Reservoir (CHUR) value ($^{143}Nd/^{144}Nd$ = 0.512638; Jacobsen and Wasserburg, 1980) to emphasize changes in radiogenic Nd isotope composition.

6.3.2 Approximate carbonate content

Dry sediment samples have been weighted before and after the leaching process. Assuming that most of the leached material is composed of carbonate, we were able to calculate the approximate carbonate content in the sediment samples (Fig. 6-3).

6.4 Results

The marine downcore radiogenic isotope records are subdivided into two units, as proposed by Stein et al. (2009). Thus, unit 1, containing Holocene sediments, ranges from 0 to 312 cm, and unit 2, with glacial/deglacial sediments, reaches from 312 to 463 cm.

6.4.1 Radiogenic Isotope compositions

In the following, downcore changes in radiogenic isotope data (Sr, Nd, Pb) of PS72/287-3 are presented (Fig. 6-3, Table 9-4). To investigate potential differences in sediment provenance, $^{87}Sr/^{86}Sr$ and ε_{Nd} values of the siliciclastic sediment fraction (Sr-Nd plot), and $^{206}Pb/^{204}Pb$ and $^{207}Pb/^{204}Pb$ values are plotted against each other (Figs. 6-4, 6-5).

6.4.1.1 Siliciclastic sediment fraction

$^{87}Sr/^{86}Sr$ values are the highest, with some variability in the lower part of unit 2 between the core bottom and ~ 380 cm, reaching 0.753. Upward, $^{87}Sr/^{86}Sr$ values decrease towards 0.735 at 350 cm, staying more constant in the rest of unit 2. In unit 1, $^{87}Sr/^{86}Sr$ values slightly drop between 250 and

150 cm to values around 0.733 before they increase again towards the core top (~0.736). Between 350 cm and the core top, variations in the Sr isotope composition are very small. Like the Sr isotope record, $^{206}Pb/^{204}Pb$ values are the highest and most variable in the lower part of unit 2, ranging between 21 and 19.9. Between 350 cm and the core top, $^{206}Pb/^{204}Pb$ values are uniform, with a mean value of 19.2. ε_{Nd} values in unit 2 show short-term variations but generally increase in the section from -28 (core bottom) to -18 (350 cm) before values drop again at the end of the section towards -24. In unit 1, ε_{Nd} values show an increasing trend between 312 cm and 150 cm, reaching a maximum value of -16 (150 cm). Upward, ε_{Nd} values slightly decrease towards -19 (103 cm) before values increase again in the upper part of the section and stay constant around -18.

The Sr-Nd isotope plot shows that Sr and Nd isotope signatures of unit 2 have a considerable scatter, though partly overlapping with reference data of the Archean to Paleoproterozoic granites and gneiss, obtained at the northwestern Greenland margin (Madaj, 2021) and at the northeastern Baffin Island margin (GeoB22357-3; Table 9-3). Sr and Nd isotope values of unit 1 form a more distinct cluster, except for one data point from the transition of the two sections. The cluster does not overlap with any of the reference data. However, it is close to the radiogenic isotope composition measured on a surface sediment sample taken east of our core site (Maccali et al., 2018).

The $^{206}Pb/^{204}Pb$ vs. $^{207}Pb/^{204}Pb$ also show a large scatter of the data from unit 2 and a more distinct cluster of unit 1 data points. Unit 2 data points do not overlap and are not even close to reference data of Archean to Paleoproterozoic granites and gneiss. However, the Pb isotope values range is similar to those measured on Mesoproterozoic carbonates from the Borden Peninsula (Kirillova, 2017). The unit 1 cluster plots again close to the reference signature taken at the western Parry Channel.

6.4.1.2 Leachate fraction

$^{87}Sr/^{86}Sr$ values of the leachate fraction are uniform in the core, ranging around 0.709. In contrast, ε_{Nd} and $^{206}Pb/^{204}Pb$ records show more variability. The ε_{Nd} values follow a similar pattern as described for the ε_{Nd} record of the siliciclastic sediment fraction. However, there is a considerable offset between these two records in unit 2, with constantly lower ε_{Nd} values (between -20 and -32) in the leachate fraction. $^{206}Pb/^{204}Pb$ values of the leachate fraction in unit 2 are much higher than those of the siliciclastic fraction and range between 19.7 and 25.4. However, the two records show the same variability patterns in unit 2. In unit 1, $^{206}Pb/^{204}Pb$ values range between 19.2 and 20.2, thus, are close to the values measured in the siliciclastic fraction.

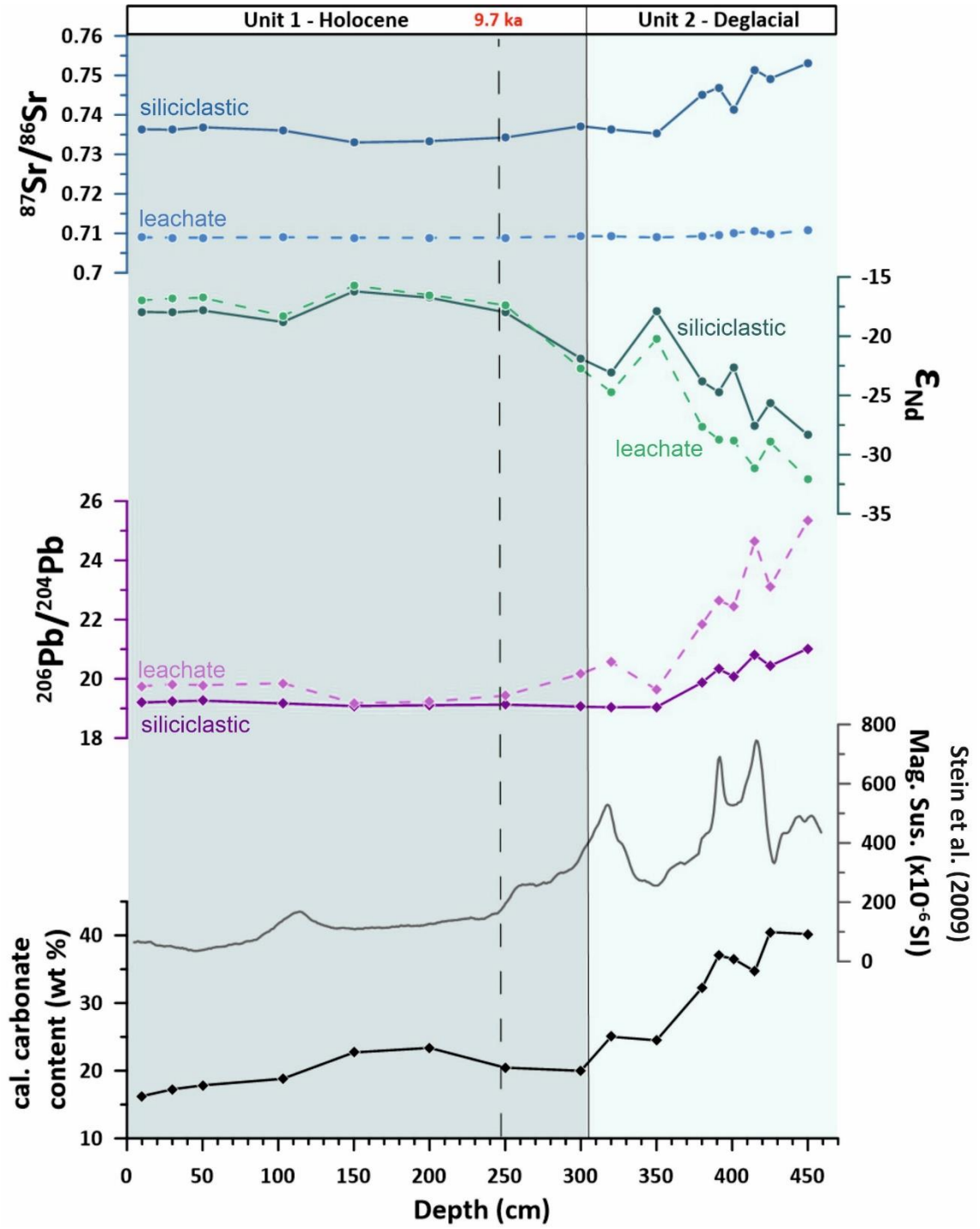

Figure 6-3: Radiogenic Sr, Nd, and Pb isotope downcore records of the siliciclastic (solid line) and leachate fraction (dashed line), respectively. Additionally, high-resolution magnetic susceptibility (Stein et al., 2009) and the approximate, calculated carbonate content in wt.% are displayed. Light and dark green bars indicate the identified units 1 and 2. The 9.7 ka age point developed by Nissen et al. (2010) is indicated by a dashed line and a red number.

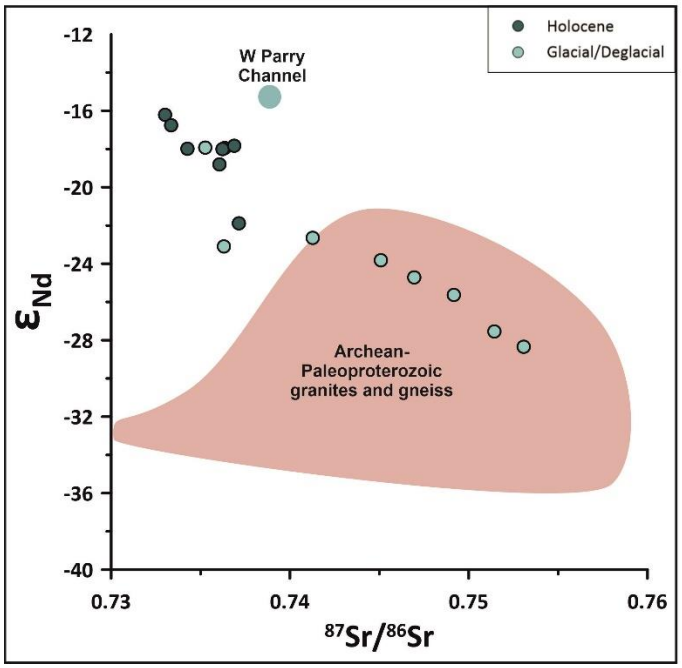

Figure 6-4: $^{87}Sr/^{86}Sr$ versus ε_{Nd} isotope plot for the marine sediment core PS72/287-3 from Barrow Strait. The colors of the data points indicate the corresponding unit: light green dots = Unit 2, Glacial/Deglacial; dark green dots = Unit 1, Holocene. Reference isotope signatures from different geological terrains are shown for provenance discussion. Their colors are adapted to the colors in Fig. 6-1 B. Reference isotope data are from different marine sediment studies: Archean to Paleoproterozoic granites and gneiss: sediment cores from the western Greenland shelf (Madaj, 2021) and the northeastern Baffin Island shelf (GeoB22357-3; Table 9-3); Western Parry Channel: surface sediment data from Maccali et al. (2018).

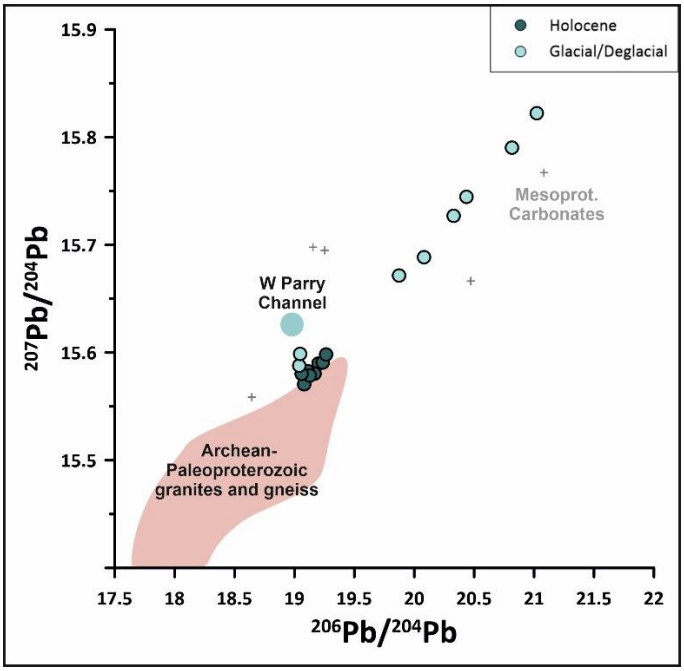

Figure 6-5: $^{206}Pb/^{204}Pb$ versus $^{207}Pb/^{204}Pb$ isotope plot for the marine sediment core PS72/287-3 from Barrow Strait. The colors of the data points indicate the corresponding unit: light green dots = Unit 2,

Glacial/Deglacial; dark green dots = Unit 1, Holocene. Reference isotope signatures from different geological terrains are shown for provenance discussion. Their colors are adapted to the colors in Fig. 6-1 B. Reference isotope data are from different marine sediment studies: Archean to Paleoproterozoic granites and gneiss: sediment cores from the western Greenland shelf (Madaj, 2021) and the northeastern Baffin Island shelf (GeoB22357-3; Table 9-3); Western Parry Channel: surface sediment data from Maccali et al. (2018); Mesoproterozoic Carbonates from Borden Peninsula from Kirillova (2017).

6.4.2 Carbonate Content

The estimated carbonate content in the samples ranges between ~ 16 and 41 wt %. The highest values occur at the core bottom with 40.5 wt %. After that, the carbonate content decreased in unit 2, reaching a value of 24.5. In unit 1, values are generally lower and slightly increase in the lower section from about 20 to 23.4. In the upper section, values gradually decrease towards the core top reaching minimum values.

6.5 Discussion

Changes in the radiogenic Sr, Nd, and Pb isotope composition in the marine sediment record PS72/287-3 give evidence about the provenance of the siliciclastic sediment transported towards Barrow Strait during the last deglaciation and the Holocene. Additionally, leachate radiogenic isotope signatures are used to identify the specific isotope signatures of detrital carbonates from the CAA. Both of these issues are addressed in the following sections.

6.5.1 Potential sources of the siliciclastic sediment fraction

The provenance discussion is mainly based on the Sr and Nd isotope composition and, to a lesser extent, on the Pb isotope signatures. As described in the following section, we cannot exclude that residual detrital carbonate contents in the siliciclastic sediment fraction control the Pb isotope composition. Furthermore, reference Pb isotope signatures are less abundant than Sr and Nd values in the research area.

The geology of the proximal surrounding land areas of Barrow Strait is dominated by Paleozoic carbonates and siliciclastic (Fig. 6-1 B). Reference bedrock radiogenic isotope data from this remote area are scarce. However, Nd, Sr, and Pb isotope data of marine surface sediment of Maccali et al. (2018) from the western Parry Channel and Nd isotope data of CAA rivers of Grenier et al. (2022) provide a range of values for the proximal source areas. According to these studies, Sr, Nd, and Pb isotope signatures of surface sediments in western Parry Channel range around 0.74, -15.2, and 19, respectively (Figs. 6-4, 6-5) (Maccali et al., 2018). Assuming that surface sediment composition is mainly controlled by river discharge of near land areas, these isotope signatures are probably characteristic of a mixture of Paleozoic carbonates and siliciclastic and Devonian sediments that

border the eastern Parry Channel (Fig. 6-1 B). Grenier et al. (2022) analyzed the river Nd isotope signatures of 13 rivers, draining different geological terrains of the CAA (Fig. 6-6). Since the river Nd isotope composition is controlled by the bedrock geology, this data set provides a detailed reference data set for Nd isotope signatures in the CAA. Thereafter, the areas around Barrow Strait, composed of mainly Paleozoic carbonates and siliciclastics, show typical ε_{Nd} isotope values between -15.1 to -16.1. Geological terrains with a mixture of these sedimentary rocks and older Archean to Paleoproterozoic granites and gneiss, as they occur, e.g., on southwestern Somerset Island, have lower (less radiogenic) ε_{Nd} values around -23. The lowest ε_{Nd} values can be found in areas dominated by the Archean to Paleoproterozoic granites and gneiss, e.g., on Bylot Island and south of the CAA in northeastern Canada. Archean to Paleoproterozoic granites and gneiss are also characteristic of northern Baffin Island and northwestern Greenland. Marine radiogenic isotope records proximal to these areas provide additional Sr, Nd, and Pb isotope compositions (Figs. 6-4, 6-5). Reference $^{87}Sr/^{86}Sr$ values range between 0.73 and 0.76. ε_{Nd} values are usually low and can range from ~ -22 to -36.

As described in section 6.4.1.1, unit 2 data points in the Sr-Nd plot show a large scatter and partly overlap with reference data obtained close to geological terrains dominated by Archean to Paleozoic granites and gneiss. The isotope values of unit 2 also plot on a mixing line between highly radiogenic Sr and unradiogenic Nd isotope compositions and the unit 1 cluster, characterized by less radiogenic Sr and more radiogenic Nd isotope values. This could indicate the mixing of two main sediment sources at Barrow Strait during the last deglaciation and a constant sediment source during the Holocene. Since the isotope values in unit 2 gradually approximate the unit 1 cluster, the influence of the end member with more radiogenic Sr and less radiogenic Nd isotope signatures seems to become less important as a sediment source with retreating ice during the deglaciation. Due to the local geology, it is likely that the one sediment source with the radiogenic Sr and unradiogenic Nd isotope signature is the Archean to Paleoproterozoic rocks occurring on western Somerset Island and south of it. The other sediment source is probably indicated by the radiogenic isotope values of unit 1 and dominated the Holocene sediment input to Barrow Strait. Since the cluster is close to the reference value taken east of Barrow Strait, Sr and Nd isotope values suggest a source area composed of younger, probably sedimentary rocks as they also occur east of Barrow Strait. However, especially the good agreement of the Nd isotope values with the river Nd isotope data from northern Somerset and Cornwallis Island (Fig. 6-6) suggests that the main sediment source areas during the Holocene are these proximal islands and the Paleozoic carbonates and clastic sediments there.

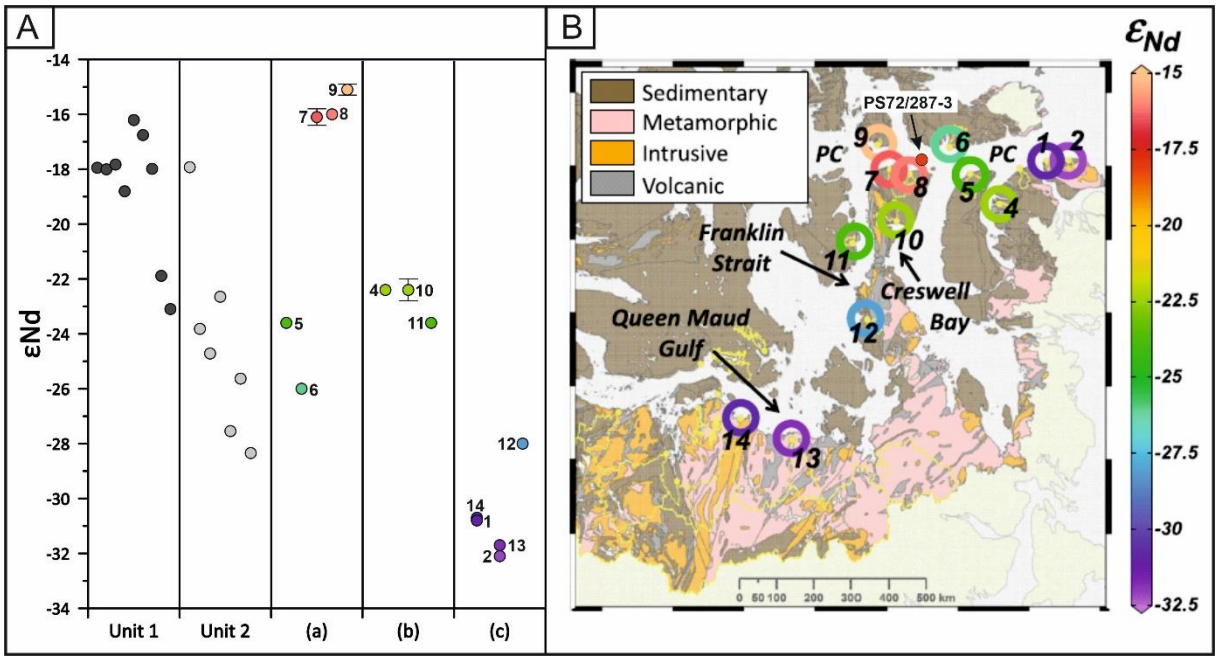

Figure 6-6: Panel A: ε_{Nd} values of units 1 and 2 of PS72/287-3 and the river samples shown in Panel B published by Grenier et al. (2022). Errors are just shown for values with an error bigger than the size of the symbols. Small numbers refer to the river number in Panel B. Rivers are subdivided into four different groups according to the main geology in the river drainage area: (a) mainly Paleozoic carbonates and siliciclastic (sedimentary); (b) a mix of Mesoproterozoic to Paleozoic carbonates and Archean to Paleoproterozoic granites and gneiss (sedimentary + metamorphic + volcanic + intrusive); (c) mainly Archean to Paleoproterozoic granites and gneiss, Mesoproterozoic and Paleozoic carbonates, siliciclastics, and carbonates, Mesozoic to Cenozoic siliciclastic (sedimentary + metamorphic + volcanic + intrusive). Panel B: modified after Grenier et al. (2022).

6.5.2 Implications for the ice margin retreat

According to the rough age core chronology, PS72/287-3 extends to the last glacial to deglacial period. Thus, it probably includes information about the time of ice sheet retreat from the Parry Channel after the extensive glaciation during the LGM. As described by Stein et al. (2009) and (Nissen et al., 2010), there are two prominent layers between 378 and 399 cm and 412 and 428 cm, which show the highest IRD contents, are unsorted and have high wet bulk density, that were identified as diamicton. These subglacial deposits support the presence of a thick ice sheet in the area (Nissen et al., 2010). These intervals, which also occur parallel to the peaks in the MS (Nissen et al., 2010), are marked by peaks in the Sr, Nd, and Pb isotope composition (Fig. 6-3). The peaks have higher $^{87}Sr/^{86}Sr$ and lower ε_{Nd} values, thus, would suggest an enhanced input of Archean to Paleoproterozoic igneous and metamorphic rocks by ice eroding western Somerset Island or areas even more to the south on northeastern Canada. Since ice streams of the LIS existed in the Peel Sound and the Prince Regent Inlet during the LGM and the late Pleistocene (e.g., Margold et al., 2015), significant amounts of glacially eroded terrestrial material from northeastern Canada were

probably transported toward Barrow Strait and Lancaster Sound. Since the peaks in these layers seem to interrupt a general decreasing and increasing trend in the Sr and Nd isotope composition, respectively, they probably correspond to a short-term glacial advance during a deglacial period. Such a cold period could be the Younger Dryas, an interval of colder conditions between ~ 12.9 and 11.7 ka BP (Rasmussen et al., 2006). As observed in the easternmost Lancaster Sound, the generally retreating ice shelf in the sound stabilized during the Younger Dryas cold period until 12.5 ka BP (Furze et al., 2018). By analyzing the IRD source of sub-ice shelf deposits, Furze et al. (2018) reconstructed the input of material from northern Baffin Island through the Admiralty Inlet towards Lancaster Sound (Fig. 6-1 B). Even if a better age model would be necessary to make reliable assumptions, it is possible that the enriched Sr and depleted Nd isotope compositions in the diamicton layers reflect an ice advance/stabilization during the Younger Dryas and an enhanced input of sediment transported through Prince Regent Inlet and/or Peel Sound. However, the overall decreasing Sr and increasing Nd isotope values in unit 2 probably indicate the gradually changing sediment supply by a retreating ice stream during the last deglaciation.

While in the lower part of unit 1, Sr, Nd, and Pb isotope signatures are partly still variable, they become more uniform slightly before 9.7 ka BP (Fig. 6-3). This probably suggests the establishment of a constant sediment supply after ~ 10 ka BP at Barrow Strait. This coincides in timing with the deglaciation history of Lancaster Sound and Barrow Strait reconstructed by Pieńkowski et al. (2012, 2014) on two sedimentary records from east and east-central Barrow Strait (154PC and 144PC; Fig. 6-1 B). Their finding suggests the deglaciation at 154PC by ~ 11.5 ka BP and at 144PC by ~ 10.8 BP and, with that, the transition from ice-proximal to -distal sedimentation after ~ 11.5 ka in Barrow Strait. Increased biological productivity and foraminiferal diversity in 154PC set the beginning of post-glacial sedimentation to ~9.7 ka BP (Pieńkowski et al., 2014). By that time also, the Prince Regent Inlet was probably fully deglaciated after the ice stream retreated rapidly from this area between ~ 10.8 and 10.2 ka BP (Dyke et al., 2002). The cluster of radiogenic isotope data after ~ 10 ka BP in the Sr-Nd plot of our core would support constant sediment supply and one major source region during the post-glacial period. The landward retreat of ice margins and ice streams during the early Holocene could have led to predominant sediment input by river discharge from the proximal island after ~10 ka BP, which agrees with the Nd isotope signature measured in the river water of these islands.

A slight increase in Sr and a decrease in Nd isotope ratios in the lower part of unit 1 correspond to a small rise in IRD content (Nissen et al., 2010). Higher IRD contents during the late Holocene were previously related to the advance of tidewater glaciers due to cooler conditions during the Neoglacial cooling (Miller et al., 2005; Okuma et al., submitted). Studies on terrestrial moraines on

northern Baffin Island have shown that the alpine glacier readvance in this area was most pronounced after ~ 3.5 ka BP (Briner et al., 2009). Slight changes in the radiogenic isotope compositions, including lower ε_{Nd} values, at Lancaster Sound (GeoB22336-3; Fig. 6-1 B) were previously related to the advance of tidewater glaciers on eastern Devon Island and the greater supply of material with relatively lower ε_{Nd} values from this region (Okuma et al., submitted). Even though most icebergs discharged by tidewater glaciers on Devon Island probably travelled towards Baffin Bay with the prevailing ocean currents, an occasional occurrence at Barrow Strait can also not be excluded.

6.5.3 Radiogenic isotope composition of detrital dolomites in the CAA

In the following, the radiogenic isotope compositions of the leachate fraction will be discussed. Since we applied just one leaching step to dissolve carbonates and potential authigenic minerals, the isotope signatures of the leachates could show a mixed signal of these components. However, due to the high abundance of detrital carbonates in the research area, we assume that our data mainly reflect the radiogenic isotope composition of the detrital carbonate.

$^{87}Sr/^{86}Sr$ values of the leachates are constantly low and range around 0.709 to 0.711. These values are in the range of modern seawater Sr isotope signature of ~ 0.70917 (Paytan et al., 2021). Thus, the dissolved carbonates, which reflect the seawater Sr isotope composition during their precipitation, seem to control the Sr isotope composition in the leachate fraction. While ε_{Nd} values in unit 1 are close to the values of the siliciclastic fraction, ε_{Nd} values of the leachate fraction in unit 2 are constantly lower than the siliciclastic signature. Due to the significant enrichment of Nd, minerals with the strongest influence on the Nd isotope composition of sediment are monazite/ allanite and, to a lesser degree, clay minerals. In contrast, carbonates are usually not enriched in Nd and contribute just in minor amounts to the isotopic budget (Garçon et al., 2014). Thus, the leached carbonates are unlikely to control the offset between the leachate and siliciclastic sediment fraction in unit 2. A potential reason for the general lower Nd isotope values in the leachates could be the partial dissolution of clay minerals during the leaching processes. $^{206}Pb/^{204}Pb$ values in the leachate fraction are highly radiogenic in unit 2, significantly exceeding the Pb isotope composition of the siliciclastic sediment fraction. Radiogenic Pb isotope values of the authigenic mineral phase have often been discussed to reflect not only the source rock signature but also chemical weathering intensities because of the preferential release uranium- and thorium-bearing minerals during chemical weathering, yielding more radiogenic Pb isotope ratios (Süfke et al., 2022; von Blanckenburg and Nägler, 2001). However, Kirillova (2017) also found highly radiogenic $^{206}Pb/^{204}Pb$ values of up to ~ 24 in Baffin Bay sediments, which lack Fe-Mn coatings as an authigenic mineral phase. She concluded that leached detrital dolomites are responsible for the radiogenic Pb isotope

composition. HH-leaching of Mesoproterozoic dolomites from the Borden Basin yield even more radiogenic Pb isotope compositions and support the assumption that dissolved dolomites are responsible for the high $^{206}Pb/^{204}Pb$ values observed in the HH-leachates (Kirillova, 2017). Therefore, we assume that the highly radiogenic $^{206}Pb/^{204}Pb$ values in the leachate fraction in unit 2 reflect the high content of detrital carbonates and that decreasing values towards unit 1 indicate the reduced influence and lower concentrations of the detrital carbonates during the deglaciation. Moreover, possible residual detrital carbonate in the siliciclastic sediment fraction is likely responsible for the elevated $^{206}Pb/^{204}Pb$ values in this sediment fraction in unit 2, where carbonate concentrations are higher than in unit 1 (Fig. 6-3). The parallel evolution of the leachate and silicate Pb isotope records supports the idea of one factor controlling both isotopic compositions – the detrital carbonates.

Finally, radiogenic isotope data of both sediment fractions of PS72/287-3 help gain better insight into the radiogenic isotope composition of detrital dolomites from the CAA. Especially, highly radiogenic Pb isotope values seem to be a good indicator for the high content of detrital dolomites in marine sediments. Nd isotope composition in the different fractions was ambiguous during the glacial/deglacial period. However, similar ε_{Nd} values in both fractions during post-glacial times suggest that areas composed of Paleozoic carbonates and clastic sediments in the CAA have specific ε_{Nd} values between -15 to -18.

6.6 Conclusions

Based on the radiogenic Sr, Nd, and Pb isotope compositions of the silicate fraction of PS72/287-3 from Barrow Strait, we gain insights into changing sediment supply and related deglaciation of the eastern Parry Channel during the late Pleistocene and Holocene. Due to a restricted age model, a precise deglaciation history cannot be constrained. However, variable radiogenic Sr and Nd isotope values in unit 2, deposited during the last deglaciation, reflect the strong influence of older igneous and metamorphic rocks as they occur on western Somerset Island and further south of the CAA, especially during intervals of ice sheet advance/stabilization. With the proceeding deglaciation of the CAA, sediment supply from such areas becomes less important. Moreover, constant radiogenic isotope values in all three systems after ~ 10 ka BP indicate the landward ice margin retreat and constant sediment supply by river discharge from the proximal island during the Holocene.

Additional isotope signatures measured on the leachate fraction support the hypothesis that high amounts of detrital carbonates can lead to highly radiogenic $^{206}Pb/^{204}Pb$ values in marine sediments. Therefore, the influence of detrital carbonates should be considered in interpreting radiogenic isotope compositions in different sediment fractions of marine sediments.

Acknowledgements

We gratefully acknowledge the master and crew of the Polarstern for their work during the ARK-XXIII/3 expedition. This project was supported by the Deutsche Forschungsgemeinschaft (DFG) through the International Research Training Group “Processes and impacts of climate change in the North Atlantic Ocean and the Canadian Arctic” (IRTG 1904 ArcTrain).

References

Andrews, J.T., Kirby, M.E., Aksu, A.E., Barber, D.C., Meese, D., 1998. Late Quaternary Detrital Carbonate (DC-) Layers in Baffin Bay marine sediments (67°-74°N): Correlation with Heinrich Events in the north Atlantic? Quaternary Science Reviews 17, 1125-1137.

Andrews, J.T., Tedesco, K., 1992. Detrital carbonate-rich sediments, northwestern Labrador Sea: Implications for ice-sheet dynamics and iceberg rafting (Heinrich) events in the North Atlantic. Geology 20, 1087-1090.

Briner, J.P., Davis, P.T., Miller, G.H., 2009. Latest Pleistocene and Holocene glaciation of Baffin Island, Arctic Canada: key patterns and chronologies. Quaternary Science Reviews 28, 2075-2087.

Colville, E.J., Carlson, A.E., Beard, B.L., Hatfield, R.G., Stoner, J.S., Reyes, A.V., Ullman, D.J., 2011. Sr-Nd-Pb isotope evidence for ice-sheet presence on southern Greenland during the Last Interglacial. Science 333, 620-623.

Dong, L., Liu, Y., Shi, X., Polyak, L., Huang, Y., Fang, X., Liu, J., Zou, J., Wang, K., Sun, F., Wang, X., 2017. Sedimentary record from the Canada Basin, Arctic Ocean: implications for late to middle Pleistocene glacial history. Climate of the Past 13, 511-531.

Dyke, A.S., Andrews, J.T., Clark, P.U., England, J.H., Miller, G.H., Shaw, J., Veillette, J.J., 2002. The Laurentide and Innuitian ice sheets during the Last Glacial Maximum.

Fagel, N., Not, C., Gueibe, J., Mattielli, N., Bazhenova, E., 2014. Late Quaternary evolution of sediment provenances in the Central Arctic Ocean: mineral assemblage, trace element composition and Nd and Pb isotope fingerprints of detrital fraction from the Northern Mendeleev Ridge. Quaternary Science Reviews 92, 140-154.

Farmer, G.L., Barber, D., Andrews, J., 2003. Provenance of Late Quaternary ice-proximal sediments in the North Atlantic: Nd, Sr and Pb isotopic evidence. Earth and Planetary Science Letters 209, 227-243.

Furze, M.F.A., Pieńkowski, A.J., McNeely, M.A., Bennett, R., Cage, A.G., 2018. Deglaciation and ice shelf development at the northeast margin of the Laurentide Ice Sheet during the Younger Dryas chronozone. Boreas 47, 271-296.

Garçon, M., Chauvel, C., France-Lanord, C., Limonta, M., Garzanti, E., 2014. Which minerals control the Nd–Hf–Sr–Pb isotopic compositions of river sediments? Chemical Geology 364, 42-55.

Grenier, M., Brown, K.A., Colombo, M., Belhadj, M., Baconnais, I., Pham, V., Soon, M., Myers, P.G., Jeandel, C., François, R., 2022. Controlling factors and impacts of river-borne neodymium isotope signatures and rare earth element concentrations supplied to the Canadian Arctic Archipelago. Earth and Planetary Science Letters 578, 117341.

Harrison, J.C., St-Onge, M.R., Petrov, O.V., Strelnikov, S.I., Lopatin, B.G., Wilson, F.H., Tella, S., Paul, D., Lynds, T., Shokalsky, S.P., Hults, C.K., Bergman, S., Jepsen, H.H., Solli, A., 2011. Geological Map of the Arctic. Geological Survey of Canada, p. Map 2159A.

Holland, M.M., Bitz, C.M., Eby, M., Weaver, A.J., 2001. The Role of Ice–Ocean Interactions in the Variability of the North Atlantic Thermohaline Circulation Journal of Climate 14, 656-675.

Jennings, A.E., Andrews, J.T., Oliver, B., Walczak, M., Mix, A., 2019. Retreat of the Smith Sound Ice Stream in the Early Holocene. Boreas 48, 825-840.

Jennings, A.E., Sheldon, C., Cronin, T.M., Francus, P., Stoner, J.S., Andrews, J.T., 2011. The Holocene History of Nares Strait. Focus on Geology Special Issue on Arctic Oceanography.

Jokat, W., 2009. The Expedition of Research Vessel "Polarstern" to the Arctic in 2008 (ARK-XXIII/3), in: Jokat, W. (Ed.), Reports of Polar and Marine Research. Alfred-Wegener-Institute für Polar- und Meeresforschung, Bremerhaven, Germany.

Jones, E.P., Swift, J.H., Anderson, L.G., Lipizer, M., Civitarese, G., Falkner, K.K., Kattner, G., McLaughlin, F., 2003. Tracing Pacific water in the North Atlantic Ocean. Journal of Geophysical Research 108.

Kirillova, V., 2017. Radiogenic isotopes on marine sediments from the Baffin Bay: implications for the sediment supply during the last deglaciation. Dissertation, Faculty of Geosciences, University Bremen, Bremen, Germany.

Maccali, J., Hillaire-Marcel, C., Not, C., 2018. Radiogenic isotope (Nd, Pb, Sr) signatures of surface and sea ice-transported sediments from the Arctic Ocean under the present interglacial conditions. Polar Research 37, 1442982.

Madaj, L., 2021. Holocene Ice Sheet Dynamics and Detriral Provenance Shifts Along the West Greenland Margin Recorded by Radiogenic Isotopes. Dissertation, Faculty of Geosciences, University Bremen, Bremen, Germany.

Margold, M., Stokes, C.R., Clark, C.D., 2015. Ice streams in the Laurentide Ice Sheet: Identification, characteristics and comparison to modern ice sheets. Earth-Science Reviews 143, 117-146.

Matthiessen, J., Stein, R. 2008: Documentation of sediment core PS72/287-3 [dataset]. Alfred Wegener Institute - Polarstern core repository, PANGAEA, https://doi.org/10.1594/PANGAEA.707970

Michel, C., Ingram, R.G., Harris, L.R., 2006. Variability in oceanographic and ecological processes in the Canadian Arctic Archipelago. Progress in Oceanography 71, 379-401.

Miller, G.H., Wolfe, A.P., Briner, J.P., Sauer, P.E., Nesje, A., 2005. Holocene glaciation and climate evolution of Baffin Island, Arctic Canada. Quaternary Science Reviews 24, 1703-1721.

Niessen, F., 2010: Physical properties of sediment core PS72/287-3 [dataset]. Alfred Wegener Institute, Helmholtz Centre for Polar and Marine Research, Bremerhaven, PANGAEA, https://doi.org/10.1594/PANGAEA.737858

Nissen, F., Matthiessen, J., Stein, R., 2010. Sedimentary Environment and Glacial History of the Northwest Passage (Canadian Arctic Archipelago) Reconstructed from High-Resolution Acoustic Data. Polarforschung 79, 16.

Okulitch, A.V., 1991. Geology of the Canadian Arctic Archipelago, Northwest Territories and North Greenland. Geological Survey of Canada, p. Map 1715A.

Okuma E., Hingst, J., Weiser, J., Madaj, L., Titschack, J., Vogt, C., Kienast, M., Hillaire-Marcel, C., Hebbeln, D., Kasemann, S.A. (submitted). Deglacial and Holocene sediment dynamics and provenances off Lancaster Sound: implications for paleoenvironmental conditions in northern Baffin Bay. Submitted to Quaternary Science Reviews.

Paytan, A., Griffith, E.M., Eisenhauer, A., Hain, M.P., Wallmann, K., Ridgwell, A., 2021. A 35-million-year record of seawater stable Sr isotopes reveals a fluctuating global carbon cycle. Science 371, 1346-1350.

Pieńkowski, A.J., England, J.H., Furze, M.F.A., Blasco, S., Mudie, P.J., MacLean, B., 2013. 11,000 yrs of environmental change in the Northwest Passage: A multiproxy core record from central Parry Channel, Canadian High Arctic. Marine Geology 341, 68-85.

Pieńkowski, A.J., England, J.H., Furze, M.F.A., MacLean, B., Blasco, S., 2014. The late Quaternary environmental evolution of marine Arctic Canada: Barrow Strait to Lancaster Sound. Quaternary Science Reviews 91, 184-203.

Pieńkowski, A.J., England, J.H., Furze, M.F.A., Marret, F., Eynaud, F., Vilks, G., Maclean, B., Blasco, S., Scourse, J.D., 2012. The deglacial to postglacial marine environments of SE Barrow Strait, Canadian Arctic Archipelago. Boreas 41, 141-179.

Prinsenberg, S.J., Bennett, E.B., 1987. Mixing and transports in Barrow Strait, the central part of the Northwest Passage. Continental Shelf Research 7, 913-935.

Rasmussen, S.O., Andersen, K.K., Svensson, A.M., Steffensen, J.P., Vinther, B.M., Clausen, H.B., Siggaard-Andersen, M.L., Johnsen, S.J., Larsen, L.B., Dahl-Jensen, D., Bigler, M., Röthlisberger, R., Fischer, H., Goto-Azuma, K., Hansson, M.E., Ruth, U., 2006. A new Greenland ice core chronology for the last glacial termination. Journal of Geophysical Research 111.

Reyes, A.V., Carlson, A.E., Beard, B.L., Hatfield, R.G., Stoner, J.S., Winsor, K., Welke, B., Ullman, D.J., 2014. South Greenland ice-sheet collapse during Marine Isotope Stage 11. Nature 510, 525-528.

Rochon, A., *participants, o.*, 2005. ArcticNet 2005, Leg 1 Cruise Report CCGS Amundsen, 05 August to 15 September, 2005. 1-220.

Stein, R., 2008. Arctic Ocean Sediments: Processes, Proxies, and Paleoenvironment. Elsevier.

Stein, R., Nissen, F., Matthiessen, J., 2009. Marine Geology.- In: W.Jokat (ed), The Expedition of the Research Vessel "Polarstern" to the Artic in 2008 (ARK-XXIII/3), Reports of Polar and Marine Research. Alfred-Wegener Institut für Polar- und Meeresforschung, Bremerhaven, Germany, pp. 12-15.

Süfke, F., Gutjahr, M., Keigwin, L.D., Reilly, B., Giosan, L., Lippold, J., 2022. Arctic drainage of Laurentide Ice Sheet meltwater throughout the past 14,700 years. Communications Earth & Environment 3.

Swärd, H., Andersson, P., Hilton, R., Vogt, C., O'Regan, M., 2022. Mineral and isotopic (Nd, Sr) signature of fine-grained deglacial and Holocene sediments from the Mackenzie Trough, Arctic Canada. Arctic, Antarctic, and Alpine Research 54, 346-367.

Tang, C.C.L., Ross, C.K., Yao, T., Petrie, B., DeTracey, B.M., Dunlap, E., 2004. The circulation, water masses and sea-ice of Baffin Bay. Progress in Oceanography 63, 183-228.

Vare, L.L., Massé, G., Gregory, T.R., Smart, C.W., Belt, S.T., 2009. Sea ice variations in the central Canadian Arctic Archipelago during the Holocene. Quaternary Science Reviews 28, 1354-1366.

von Blanckenburg, F., Nägler, T.F., 2001. Weathering versus circulation-controlled changes in radiogenic isotope tracer composition of the Labrador Sea and North Atlantic Deep Water. Paleoceanography 16, 424-434.

7. Conclusions and Outlook

The aim of this study was to identify changes in detrital sediment provenances in western Baffin Bay to reconstruct spatial and temporal variations in meltwater discharge and material transport related to the retreating ice sheets bordering Baffin Bay during the last deglaciation. In marine sediments, radiogenic Sr, Nd, and Pb isotope compositions are reliable tracers for the provenance of detrital material (e.g., Banner, 2004). The investigation of radiogenic isotope ratios in marine sediments from the Arctic realm has been previously used to identify changes in detrital provenance (Colville et al., 2011; Fagel et al., 2004; Fagel et al., 2014; Kirillova, 2017; Madaj, 2021; Reyes et al., 2014; Tütken et al., 2002). The four sedimentary records from western Baffin Bay and the Canadian Arctic Archipelago (CAA) analyzed in this study and presented in chapters 4 to 6 focus on three research areas characterized by individual environmental settings and different glacial histories. The data reveal variations in the detrital sediment provenance that are related to the proximity to ice sheets, glacial erosion, spatially induced meltwater input, and changes in ocean circulation closely linked to regional ice sheet retreat during the last deglaciation period. Moreover, the here presented data show that there are additional parameters that can influence the radiogenic isotope composition, especially in land-proximal sediments. Thus, combining all three isotope systems and incorporating other sediment proxies provided the most reliable information about the sedimentary and environmental history of the research area.

At the mouth of Lancaster Sound in northwestern Baffin Bay, variations in the radiogenic isotope composition in sediment core GeoB22336-4 during the early Holocene revealed an enhanced sediment supply from Barrow Strait. Thus, the radiogenic isotope data provided valuable information about the opening of the Barrow Strait-Lancaster Sound gateway and the establishment of an oceanic connection from the Arctic Ocean to the Atlantic through Baffin Bay during the early Holocene. Additionally, changing radiogenic isotope values at the core top suggest a stronger input of sediments from older igneous and metamorphic rocks with lower ε_{Nd} values as they occur on Devon Island. Together with increasing IRD concentrations, these data were interpreted as an indication of regional glacier readvances on Devon Island during the late Holocene.

Radiogenic isotope data of the continental detritus obtained from sediment cores from the Clyde Inlet fjord on northeastern Baffin Island (GeoB22346-3) and from the shelf offshore (GeoB22357-3) provided valuable insights into the deglaciation history of an outlet glacier draining the northeastern Laurentide Ice Sheet (LIS) during the last glacial period. At the fjord head, variable Sr and Pb isotope ratios seem to be controlled by changing mineralogical compositions, probably related to changing meltwater fluxes during the Holocene. Even if these data cannot be used to

reliably reconstruct changes in the detrital sediment provenance at the core site, they provide information about the ice margin retreat and glacier extent. Similar to the Lancaster Sound data, changing radiogenic isotope compositions in the Baffin Island fjord during the late Holocene are associated with the readvance of local glaciers due to the Neoglacial cooling. On the Baffin Island shelf, variations in the radiogenic isotope data indicate a transition from ice-proximal to ice-distal conditions at around 11 ka BP and an increasing influence of sediments originating from northern Baffin Bay, probably related to changing ocean circulation after the opening of Lancaster Sound during the early Holocene.

Sr, Nd, and Pb isotope compositions of the silicate fraction of sediment core PS72/287-3 from Barrow Strait are variable during the deglacial period. They suggest variable sediment provenances related to a dynamic retreat of the regional ice sheets. Uniform values after ~ 10 ka BP indicate the landward ice margin retreat and constant sediment supply by river discharge from the proximal island during the Holocene. Moreover, radiogenic isotope values in the leachates seem to be strongly influenced by leached detrital carbonates from the sediment.

Besides the valuable information about past ice sheets and glacier dynamics on Baffin Island in the Canadian Arctic Archipelago, our study also highlighted limitations in the sensitivity of radiogenic isotopes from Baffin Bay marine sediments as tracers. First, the restricted availability of a sufficiently dense cover of reference isotope signatures from around Baffin Bay partly limited the interpretation of potential sediment sources. Available bedrock isotope signatures were often measured with different intentions and, thus, are not always useful for sediment provenance discussion of marine sediments. Reliable reference data for this purpose are obtained on stream sediment samples, which should reflect a composite reference isotope signature for the proximal geological terrains (Colville et al., 2011). However, the availability of such data is restricted. Moreover, it has been observed that intense meltwater discharge can lead to grain size and mineral sorting, which could bias the radiogenic isotope composition of the sediment. Similar effects have been observed in river sediments (Garçon et al., 2014) but should also be considered in meltwater-influenced fjord systems. Therefore, additional information about the mineralogical composition of the sediment is needed for an accurate interpretation of the radiogenic isotope data. Our data also support the observation that Pb isotope values in sediment leachates reflect the signal of detrital dolomites (Kirillova, 2017). Pb isotope values in similar leachates have been previously interpreted to show changing continental weathering conditions (Süfke et al., 2022; von Blanckenburg and Nägler, 2001). This illustrates that radiogenic isotope signatures in different sediment fractions should be interpreted with caution.

In summary, the isotope data analyzed in marine sediment cores from western Baffin Bay and the Canadian Arctic Archipelago (CAA) reveal variations during the late Pleistocene and the Holocene that are related to the deglaciation of the Laurentide and Innuitian ice sheets, which bordered western and northern Baffin Bay during the last glacial period. Holocene radiogenic isotope data of the sediment detritus in a fjord on northeastern Baffin Island reveal the Holocene retreat of an outlet glacier of the northeastern LIS interrupted by short-term ice margin fluctuations. Provenance changes in the detrital material on the Baffin Island shelf are related to changing ocean circulation in Baffin Bay after the deglaciation of the Parry Channel. Deglaciation patterns of Lancaster Sound and Barrow Strait, eastern Parry Channel, are recorded in sedimentary records from Barrow Strait and northern Baffin Bay. Changing isotope compositions at both core sites are used to determine the timing of ice sheet retreat and the onset of an Arctic-Atlantic throughflow. Moreover, radiogenic isotope data revealed changes in sediment provenances, also in cases when mineralogical evidence was ambiguous. Thus, they are a valuable addition to other sediment proxies.

Through the intensive investigation of several sediment cores from central Baffin Bay (Kirillova, 2017), the western Greenland shelf (Colville et al., 2011; Reyes et al., 2014; Madaj, 2021), and northern and western Baffin Bay (Madaj, 2021; this study), a complex data set of reference radiogenic isotope signatures can be used for future studies. Future studies should focus on land-distal research areas to exclude, e.g., mineralogical effects on the radiogenic isotope composition. The Labrador Sea would be an interesting study area for further provenance studies using radiogenic isotope compositions. Previous provenance studies in the Labrador Sea, which were based on the sediment's mineralogical composition, observed the input of material from western Greenland and outcrops north of Baffin Bay during different periods of ice sheet deglaciation (Andrews et al., 2014; Andrews and Piper, 2022). With the grown data set of radiogenic isotope signatures from marine sediments from Baffin Bay, further radiogenic isotope analysis could provide additional details on sediment provenances and related past ice sheet deglaciation patterns on Greenland and in the Canadian Arctic.

Additionally, it would be interesting to conduct further research on the radiogenic isotope compositions of different fractions from Baffin Bay marine sediments. Trace element analysis on the sediment leachates would be necessary to prove the presence or absence of Fe-Mn coatings and detrital carbonates. If the radiogenic isotope composition of detrital carbonates from the CAA could be further specified by measurements on bedrock samples from the area, this information could be used to trace the input of CAA sediments into Baffin Bay, the Labrador Sea, and the Arctic Ocean during the last deglaciation.

References

Andrews, J.T., Gibb, O.T., Jennings, A.E., Simon, Q., 2014. Variations in the provenance of sediment from ice sheets surrounding Baffin Bay during MIS 2 and 3 and export to the Labrador Shelf Sea: site HU2008029-0008 Davis Strait. Journal of Quaternary Science 29, 3-13.

Andrews, J.T., Piper, D.J., 2022. Late Quaternary changes in sediment sources in the Labrador Sea. Canadian Journal of Earth Sciences.

Banner, J.L., 2004. Radiogenic isotopes: systematics and applications to earth surface processes and chemical stratigraphy. Earth-Science Reviews 65, 141-194.

Colville, E.J., Carlson, A.E., Beard, B.L., Hatfield, R.G., Stoner, J.S., Reyes, A.V., Ullman, D.J., 2011. Sr-Nd-Pb isotope evidence for ice-sheet presence on southern Greenland during the Last Interglacial. Science 333, 620-623.

Fagel, N., Hillaire-Marcel, C., Humblet, M., Brasseur, R., Weis, D., Stevenson, R., 2004. Nd and Pb isotope signatures of the clay-size fraction of Labrador Sea sediments during the Holocene: Implications for the inception of the modern deep circulation pattern. Paleoceanography 19, n/a-n/a.

Fagel, N., Not, C., Gueibe, J., Mattielli, N., Bazhenova, E., 2014. Late Quaternary evolution of sediment provenances in the Central Arctic Ocean: mineral assemblage, trace element composition and Nd and Pb isotope fingerprints of detrital fraction from the Northern Mendeleev Ridge. Quaternary Science Reviews 92, 140-154.

Garçon, M., Chauvel, C., France-Lanord, C., Limonta, M., Garzanti, E., 2014. Which minerals control the Nd–Hf–Sr–Pb isotopic compositions of river sediments? Chemical Geology 364, 42-55.

Kirillova, V., 2017. Radiogenic isotopes on marine sediments from the Baffin Bay: implications for the sediment supply during the last deglaciation. Dissertation, Faculty of Geosciences, University Bremen, Bremen, Germany.

Madaj, L., 2021. Holocene Ice Sheet Dynamics and Detriral Provenance Shifts Along the West Greenland Margin Recorded by Radiogenic Isotopes. Dissertation, Faculty of Geosciences, University Bremen, Bremen Germany.

Reyes, A.V., Carlson, A.E., Beard, B.L., Hatfield, R.G., Stoner, J.S., Winsor, K., Welke, B., Ullman, D.J., 2014. South Greenland ice-sheet collapse during Marine Isotope Stage 11. Nature 510, 525-528.

Süfke, F., Gutjahr, M., Keigwin, L.D., Reilly, B., Giosan, L., Lippold, J., 2022. Arctic drainage of Laurentide Ice Sheet meltwater throughout the past 14,700 years. Communications Earth & Environment 3.

Tütken, T., Eisenhauer, A., Wiegand, B., Hansen, B.T., 2002. Glacial-interglacial cycles in Sr and Nd isotopic composition of Arctic marine sediments triggered by the Svalbard/Barents Sea ice sheet. Marine Geology 182, 351-372.

von Blanckenburg, F., Nägler, T.F., 2001. Weathering versus circulation-controlled changes in radiogenic isotope tracer composition of the Labrador Sea and North Atlantic Deep Water. Paleoceanography 16, 424-434.

8. Acknowledgements

Writing this thesis was just possible with the support and help of many people, for which I would like to express my sincere gratitude. First of all, I would like to thank my supervisor Simone Kasemann for giving me the opportunity to conduct this PhD project and for the guidance and support during the last three and a half years. I am very grateful for our scientific discussions, all her comments and ideas on my data and text drafts, and, finally, for advising and pushing me during the final phase of my PhD.

Further, I want to thank my co-supervisor and Canadian partner from ArcTrain, Claude Hillaire-Marcel, for sharing his expertise about radiogenic isotopes and especially his immense knowledge about the past climate and environmental history of my research area, for interesting and constructive data discussions, comments on abstracts and posters and for discussing my opportunities for a research stay in Canada.

Special thanks go to Friedrich Lucassen, Rüdiger Stein, and Dierk Hebbeln for being part of my thesis committee and for giving me a lot of advice and scientific input during our meetings and whenever needed. Thanks to Rüdiger Stein also for providing me with sediment samples from the Barrow Strait core during a time when access to the laboratories was very limited. I also want to thank Friedrich Lucassen for introducing me to the lab work, teaching me all the methods I needed for radiogenic isotope analysis, telling me a lot about mineralogy and geology in general, and commenting on and improving my text drafts.

Special thanks go to the entire working group of Isotope Geochemistry at MARUM, to fantastic former and present colleagues, for welcoming me to the group, creating a pleasant working environment, having lunch, coffee, and cake breaks, nice chats, productive discussions, and always supporting me. I also would like to thank Anette Meixner for her support in the lab, for coming up with new ideas for sample preparation, and for always helping me with analytical problems. I am also very grateful for the help of Lina Madaj, who showed me everything I needed to know about the lab work and shared many of her experiences, making the start of my PhD a lot easier. In addition, I want to thank Barbara Muntz for her administrative support and for always asking me how I am doing. I am most grateful for the support of Frederike Wilckens, Gustavo Macedo de Paula Santos, and Johanna Menges, who helped me improve my thesis and always encouraged me to finish it in time. I also would like to thank my office colleagues Juan Camilo Gómez Gutiérrez and Eric Elias for keeping me in a relaxed company, providing me with excellent coffee, and smiling at me whenever I looked too stressed. I am happy that I met all of you!

I would like to thank Emmanuel Okuma for the joint work on our first manuscript, for many hours of discussion, and for sharing this experience with me.

I am also immensely grateful that my PhD project was part of the International Research Training Group ArcTrain. Thanks to ArcTrain for the excellent research network, the financial support, the training, our different meetings, and the chance to visit Canada for the first time during one of our Annual Meetings. I would like to thank Michal Kucera, Anne de Vernal, Jade Falardeau, and Kelsey Koerner for putting so much effort into ArcTrain. Thanks also to Sicca for organizing the monthly ArcTrain seminar that brought us all together for nice and productive discussions. Special thanks also go to our PhD representatives Linda, Jennifer, and Kevin for their energy in taking care of everything relevant for the ArcTrain students for three and a half years. Thanks to Franziska for reading and commenting on my thesis and for answering all my questions about the PhD submission. And thanks to all the other ArcTrain students for our weekly lunch meetings, our great times together at meetings and conferences, for sharing experiences and worries of the PhD life, coming together for dinner, bowling, drinks, and a lot of fun!

I also would like to thank my old and new friends from Bremen and Oldenburg for supporting me, offering distraction from work life, and sharing much fun and joy. Special thanks go to my family for giving me the opportunity to start my academic journey, supporting and believing in me, and always offering a place to come back to. Huge thanks and my deepest gratitude go to Henning for the enormous support during the last years, for the last-minute comments on my thesis, and for always being there for me.

9. Appendices

9.1 Radiogenic Isotope Data

Table 9-1: Sr and Nd isotope compositions of core GeoB22336-4 from the mouth of Lancaster Sound in northern Baffin Bay. Pb (corr.) isotope values were corrected by a bulk uncertainty of 0.1 % per atomic mass unit. ε_{Nd} values were calculated using the CHUR value of 0.512638 (Jacobsen and Wasserburg, 1980). Uncertainties ($2SD_{mean}$) are given for the last digit.

Sample ID	Depth [cm]		Age	Radiogenic isotope data (dt fraction)						
	Top	Bottom	[ka BP]	$^{87}Sr/^{86}Sr$	$^{206}Pb/^{204}Pb$	$^{206}Pb/^{204}Pb$ corr.	$^{207}Pb/^{204}Pb$	$^{207}Pb/^{204}Pb$ corr.	$^{143}Nd/^{144}Nd$	εNd
JH38	20	21	0.554	0.737083±10	18.8039±11	18.82	15.5344±9	15.55	0.511384±6	-24.46
JH39	60	61	1.554	0.738320±8	18.9796±13	19.00	15.5524±11	15.57	0.511336±7	-25.40
JH74	80	81	2.163	0.739444±11	18.7236±11	18.74	15.5578±7	15.57	0.511486±4	-22.47
JH40	100	101	2.813	0.740838±8	19.1302±12	19.15	15.5692±9	15.58	0.511467±6	-22.84
JH75	120	121	3.466	0.740862±11	18.8668±10	18.89	15.5546±8	15.57	0.511495±6	-22.30
JH76	140	141	4.069	0.741112±10	18.8052±11	18.82	15.5571±10	15.57	0.511488±5	-22.43
JH41	160	161	4.687	0.741854±8	19.1480±13	19.17	15.5693±10	15.58	0.511283±8	-26.43
JH42	200	201	5.987	0.742466±9	19.2493±11	19.27	15.5796±9	15.60	0.511472±5	-22.75
JH77	230	231	6.580	0.741940±9	18.9636±9	18.98	15.5616±9	15.58	0.511492±6	-22.35
JH43	260	261	7.239	0.742783±7	19.3097±12	19.33	15.5880±10	15.60	0.511472±7	-22.75
JH78	280	281	7.659	0.742551±7	19.0578±10	19.08	15.5644±8	15.58	0.511488±5	-22.43
JH44	300	301	8.148	0.742471±8	19.3906±14	19.41	15.6016±12	15.62	0.511482±5	-22.55
JH79	310	311	8.454	0.740623±9	19.0446±10	19.06	15.5849±9	15.60	0.511547±6	-21.28
JH80	320	321	8.765	0.738791±9	19.1166±11	19.14	15.5846±9	15.60	0.511591±4	-20.42
JH81	330	331	9.100	0.739496±9	19.0891±12	19.11	15.5894±9	15.60	0.511567±5	-20.89
JH82	340	341	9.451	0.739833±11	19.0241±14	19.04	15.5978±8	15.61	0.511553±4	-21.17
JH83	350	351	9.864	0.740025±8	19.0852±12	19.10	15.5867±10	15.60	0.511575±6	-20.74
JH45	360	361	10.084	0.742119±8	19.5176±11	19.54	15.6319±10	15.65	0.511488±5	-22.43
JH46	380	381	10.319	0.741508±8	19.5720±13	19.59	15.6519±9	15.67	0.511286±6	-26.37
JH47	400	401	10.533	0.743261±9	19.6741±10	19.69	15.6602±8	15.68	0.511429±4	-23.58

JH48	420	421	10.769	0.745302±8	19.7983±15	19.82	15.6595±9	15.68	0.511321±4	-25.69
JH49	440	441	11.025	0.746470±8	20.5316±13	20.55	15.7530±10	15.77	0.511279±5	-26.51
JH84	450	451	11.133	0.746333±8	20.0124±12	20.03	15.6869±8	15.70	0.511342±4	-25.28
JH50	470	471	11.322	0.733335±9	19.7478±14	19.77	15.6520±12	15.67	0.511676±5	-18.77
JH51	490	491	12.143	0.736263±8	19.9637±12	19.98	15.6921±9	15.71	0.511174±8	-28.56
JH52	500	501	12.589	0.745270±7	20.3660±13	20.39	15.7300±9	15.75	0.511301±4	-26.08
JH53	520	521	12.931	0.741352±9	20.0784±11	20.10	15.7033±9	15.72	0.511282±6	-26.45
JH85	530	531	13.092	0.741204±9	19.5804±13	19.60	15.6559±11	15.67	0.511331±4	-25.50
JH54	540	541	13.249	0.746604±8	19.3225±10	19.34	15.5871±7	15.60	0.511560±5	-21.03
JH55	550	551	13.415	0.742983±7	19.7796±9	19.80	15.6544±7	15.67	0.511298±5	-26.14
JH56	580	581	13.950	0.738149±9	19.7220±13	19.74	15.6680±11	15.68	0.511285±6	-26.39
JH57	600	601	14.312	0.738269±9	20.3375±11	20.36	15.7366±9	15.75	0.511262±5	-26.84

Sample ID	**Depth [cm]**		**Age**	**Radiogenic isotope data (HH-leachates)**						
	Top	**Bottom**	**[ka BP]**	**$^{87}Sr/^{86}Sr$**	**$^{206}Pb/^{204}Pb$**	**$^{206}Pb/^{204}Pb$ corr.**	**$^{207}Pb/^{204}Pb$**	**$^{207}Pb/^{204}Pb$ corr.**	**$^{143}Nd/^{144}Nd$**	**εNd**
JH38	20	21	0.554	0.709290±8	20.1064±13	20.13	15.6789±10	15.69	0.511665±5	-18.98
JH39	60	61	1.554	0.709209±7	20.1987±12	20.22	15.6922±9	15.71	0.511700±6	-18.30
JH40	100	101	2.813	0.709260±9	20.2046±13	20.22	15.6186±17	15.63	0.511726±6	-17.79
JH41	160	161	4.687	0.709213±7	20.0673±37	20.09	15.3668±83	15.38	0.511691±6	-18.47
JH42	200	201	5.987	0.709366±7	20.2378±16	20.26	15.6305±19	15.65	0.511654±6	-19.19
JH43	260	261	7.239	0.709521±9	20.3106±14	20.33	15.6646±18	15.68	0.511633±6	-19.60
JH44	300	301	8.148	0.709538±7	20.3329±18	20.35	15.4967±31	15.51	0.511616±5	-19.94
JH45	360	361	10.084	0.709191±8	20.4892±19	20.51	15.6376±47	15.65	0.511486±6	-22.47
JH46	380	381	10.319	0.709154±8	21.2527±17	21.27	15.6346±20	15.65	0.511279±6	-26.51
JH47	400	401	10.533	0.709097±7	20.7701±11	20.79	15.6701±17	15.69	0.511396±6	-24.23
JH48	420	421	10.769	0.709316±8	21.7124±19	21.73	15.7718±29	15.79	0.511201±6	-28.03
JH49	440	441	11.025	0.709343±7	22.8759±29	22.90	15.6118±43	15.63	0.511082±6	-30.35
JH50	470	471	11.322	0.709669±8	20.7692±19	20.79	15.5745±42	15.59	0.511354±6	-25.05
JH51	490	491	12.143	0.709938±7	22.4328±43	22.46	15.7229±73	15.74	0.511105±7	-29.90
JH52	500	501	12.589	0.709709±8	23.3336±34	23.36	15.9928±40	16.01	0.511091±6	-30.18

JH53	520	521	12.931	0.710256±8	22.9928±17	23.02	15.8901±23	15.91	0.511011±6	-31.74
JH54	540	541	13.249	0.709192±9	19.7162±21	19.74	15.4501±45	15.47	0.511514±6	-21.93
JH55	550	551	13.415	0.709549±7	21.8874±28	21.91	15.5083±52	15.52	0.511144±6	-29.14
JH56	580	581	13.950	0.709629±7	22.1696±26	22.19	15.8227±74	15.84	0.511139±5	-29.24
JH57	600	601	14.312	0.710078±8	22.3225±42	22.34	15.5773±78	15.59	0.511074±6	-30.51

Table 9-2: Sr, Pb and, Nd isotope compositions of core GeoB22346-3 from the Clyde Inlet head. Pb (corr.) isotope values were corrected by a bulk uncertainty of 0.1 % per atomic mass unit. ε_{Nd} values were calculated using the CHUR value of 0.512638 (Jacobsen and Wasserburg, 1980). Uncertainties ($2SD_{mean}$) are given for the last digit.

Sample ID	Depth [cm]		Age	Radiogenic isotope data (dt fraction)						
	Top	Bottom	[ka BP]	$^{87}Sr/^{86}Sr$	$^{206}Pb/^{204}Pb$	$^{206}Pb/^{204}Pb$ corr.	$^{207}Pb/^{204}Pb$	$^{207}Pb/^{204}Pb$ corr.	$^{143}Nd/^{144}Nd$	εNd
JH01	20	21	0.2	0.776481±8	19.9247±6	19.94	15.6344±5	15.65	0.510684±6	-38.12
JH02	123	124	1.5	0.752798±8	20.9174±9	20.94	15.8834±7	15.90	0.511062±6	-30.74
JH03	128	129	1.5	0.755534±8	20.0946±7	20.11	15.7509±6	15.77	0.511020±6	-31.56
JH04	172	173	2.1	0.753255±8	18.0059±5	18.02	15.4491±4	15.46	0.511004±6	-31.87
JH05	270	271	3.8	0.796260±9	22.9801±10	23.00	16.0527±7	16.07	0.510789±6	-36.07
JH06	345	346	5.1	0.819383±8	24.2218±9	24.25	16.1947±6	16.21	0.510852±5	-34.84
JH07	420	421	6.2	0.801938±9	22.1984±9	22.22	15.9134±7	15.93	0.510795±5	-35.95
JH08	500	501	7.1	0.756788±8	17.8445±7	17.86	15.4328±7	15.45	0.510958±5	-32.77
JH09	560	561	7.7	0.795990±9	20.7038±8	20.72	15.7868±6	15.80	0.510820±6	-35.46
JH10	568	569	7.8	0.762168±7	18.2336±6	18.25	15.4822±6	15.50	0.510923±5	-33.45
JH11	630	631	8.3	0.789833±8	20.2926±9	20.31	15.7279±7	15.74	0.510851±5	-34.86
JH12	680	681	8.6	0.783038±8	20.1933±5	20.21	15.7140±4	15.73	0.510876±6	-34.37
Sample ID	**Depth [cm]**		**Age**	**Radiogenic isotope data (HH-leachates)**						
	Top	**Bottom**	**[ka BP]**	$^{87}Sr/^{86}Sr$	$^{206}Pb/^{204}Pb$	$^{206}Pb/^{204}Pb$ corr.	$^{207}Pb/^{204}Pb$	$^{207}Pb/^{204}Pb$ corr.	$^{143}Nd/^{144}Nd$	εNd
JH02	123	124	1.5	0.791290±9	29.8780±66	29.91	16.8589±36	16.88	0.510778±38	-36.28
JH04	172	173	2.1	0.802511±10	31.2066±24	31.24	16.9904±15	17.01	0.510742±8	-36.99
JH06	345	346	5.1	0.783255±8	34.5750±30	34.61	17.3690±15	17.39	0.510736±9	-37.10
JH08	500	501	7.1	0.826657±9	30.8117±43	30.84	16.9617±22	16.98	0.510862±7	-34.64
JH10	568	569	7.8	0.827290±9	30.7989±30	30.83	16.9432±18	16.96	0.510862±6	-34.64
JH12	680	681	8.6	0.812719±12	32.0555±43	32.09	17.1069±24	17.12	0.510712±7	-37.57

Table 9-3: Sr, Pb and, Nd isotope compositions of the detrital sediment fraction of core GeoB22357-3 from the Clyde Inlet shelf. Pb (corr.) isotope values were corrected by a bulk uncertainty of 0.1 % per atomic mass unit. ε_{Nd} values were calculated using the CHUR value of 0.512638 (Jacobsen and Wasserburg, 1980). Uncertainties ($2SD_{mean}$) are given for the last digit.

Sample ID	Depth [cm]		Age	Radiogenic isotope data (dt fraction)						
	Top	Bottom	[ka BP]	$^{87}Sr/^{86}Sr$	$^{206}Pb/^{204}Pb$	$^{206}Pb/^{204}Pb$ corr.	$^{207}Pb/^{204}Pb$	$^{207}Pb/^{204}Pb$ corr.	$^{143}Nd/^{144}Nd$	εNd
JH14	10	11	8.2	0.747755±7	17.5049±10	17.52	15.3294±8	15.34	0.510877±5	-34.35
JH15	29	30	8.4	0.744270±8	17.2238±16	17.24	15.3037±14	15.32	0.510931±5	-33.30
JH16	54	55	8.7	0.743368±8	17.0084±5	17.03	15.2718±5	15.29	0.510925±6	-33.42
JH17	104	105	9.2	0.748314±9	17.7903±12	17.81	15.3731±11	15.39	0.510843±6	-35.01
JH18	154	155	9.7	0.749524±8	17.6228±11	17.64	15.3495±9	15.36	0.510821±6	-35.44
JH19	204	205	10.2	0.751774±8	17.7297±9	17.75	15.3568±8	15.37	0.510789±5	-36.07
JH20	254	255	10.6	0.749871±8	17.8141±12	17.83	15.3712±9	15.39	0.510802±6	-35.81
JH21	263	264	10.6	0.749620±8	17.9818±9	18.00	15.4120±8	15.43	0.510812±6	-35.62
JH22	304	305	10.8	0.753249±8	17.7375±10	17.76	15.3335±8	15.35	0.510759±5	-36.65
JH23	354	355	11	0.755961±9	18.0266±11	18.04	15.3962±9	15.41	0.510757±9	-36.69
JH24	381	382	11	0.759324±8	17.8214±14	17.84	15.3785±12	15.39	0.510694±5	-37.92
JH25	404	405	11.1	0.758853±9	17.7441±12	17.76	15.3613±11	15.38	0.510710±6	-37.61
JH26	454	455	11.3	0.757921±9	17.7531±16	17.77	15.3471±17	15.36	0.510742±5	-36.99
JH27	504	505	11.5	0.759452±8	17.8454±15	17.86	15.3547±9	15.37	0.510748±5	-36.87
JH28	554	555	11.7	0.758465±9	17.6219±9	17.64	15.3199±8	15.34	0.510687±5	-38.06
JH29	604	605	11.8	0.761015±8	17.6905±11	17.71	15.3517±10	15.37	0.510653±5	-38.72
JH30	654	655	12	0.753654±9	17.4680±11	17.49	15.3173±10	15.33	0.510731±6	-37.20
JH31	704	705	12.2	0.760297±8	17.3724±11	17.39	15.2982±10	15.31	0.510663±6	-38.53
JH32	726	727	12.3	0.749546±9	17.4082±11	17.43	15.3017±9	15.32	0.510772±5	-36.40
JH33	752	753	12.4	0.745626±8	17.4012±14	17.42	15.3344±13	15.35	0.510852±5	-34.84
JH34	778	779	12.5	0.750817±9	17.5013±11	17.52	15.3217±10	15.34	0.510766±5	-36.52
JH35	804	805	12.6	0.755883±9	17.7540±11	17.77	15.3589±9	15.37	0.510738±6	-37.06
JH36	841	842	12.7	0.749074±8	17.3620±7	17.38	15.2925±6	15.31	0.510815±5	-35.56

JH37	876	877	12.8	0.743568±8	16.6804±13	16.70	15.2531±11	15.27	0.510942±5	-33.08

Table 9-4: Sr, Pb, and Nd isotope data of core PS72/287-3 from Barrow Strait. Chronology estimation is based on Parasound data and correlation with the dated core ARC-3 (Nissen et al., 2010; Stein et al., 2009; Vare et al., 2009). Pb (corr.) isotope values were corrected by a bulk uncertainty of 0.1 % per atomic mass unit. ε_{Nd} values were calculated using the CHUR value of 0.512638 (Jacobsen and Wasserburg, 1980). Uncertainties ($2SD_{mean}$) are given for the last digit.

Sample ID	Depth [cm]		Time Interval	Radiogenic isotope data (dt fraction)						
	Top	Bottom		$^{87}Sr/^{86}Sr$	$^{206}Pb/^{204}Pb$	$^{206}Pb/^{204}Pb$ corr.	$^{207}Pb/^{204}Pb$	$^{207}Pb/^{204}Pb$ corr.	$^{143}Nd/^{144}Nd$	εNd
JH 58	10	11	Holocene	0.736352±8	19.2008±12	19.22	15.5898±9	15.61	0.511718±5	-17.95
JH 59	30	31	Holocene	0.736225±8	19.2358±12	19.26	15.5907±10	15.61	0.511715±6	-18.00
JH 60	50	51	Holocene	0.736881±8	19.2641±10	19.28	15.5982±7	15.61	0.511724±5	-17.83
JH 61	103	104	Holocene	0.736056±7	19.168±11	19.19	15.5804±10	15.60	0.511674±4	-18.80
JH 62	150	151	Holocene	0.733013±8	19.0812±13	19.10	15.5705±11	15.59	0.511807±5	-16.21
JH 63	200	201	Holocene	0.733351±8	19.1094±11	19.13	15.5828±9	15.60	0.511779±5	-16.76
JH 64	250	251	Holocene	0.734265±9	19.1282±10	19.15	15.5786±7	15.59	0.511716±5	-17.99
JH 65	300	301	Holocene	0.737142±8	19.0605±10	19.08	15.5802±9	15.60	0.511516±6	-21.89
JH 66	320	321	Glacial/ Deglacial	0.736304±8	19.0397±12	19.06	15.5878±10	15.60	0.511454±6	-23.10
JH 67	350	351	Glacial/ Deglacial	0.735260±7	19.0472±9	19.07	15.5987±8	15.61	0.511719±5	-17.93
JH 68	380	381	Glacial/ Deglacial	0.745085±7	19.8729±10	19.89	15.6715±7	15.69	0.511417±6	-23.82
JH 69	391	392	Glacial/ Deglacial	0.746950±8	20.3285±11	20.35	15.7269±8	15.74	0.511371±4	-24.72
JH 70	401	402	Glacial/ Deglacial	0.741271±8	20.0813±11	20.10	15.6885±9	15.70	0.511477±5	-22.65
JH 71	415	416	Glacial/ Deglacial	0.751435±8	20.8154±13	20.84	15.7902±10	15.81	0.511226±5	-27.54
JH 72	425	426	Glacial/ Deglacial	0.749166±8	20.4356±14	20.46	15.7445±11	15.76	0.511324±7	-25.63

JH 73	450	451	Glacial/ Deglacial	0.753075±10	21.0221±13	21.04	15.8222±9	15.84	0.511185±6	-28.34
Sample ID	**Depth [cm]**		**Time Interval**	**Radiogenic isotope data (HH-leachates)**						
	Top	**Bottom**		**$^{87}Sr/^{86}Sr$**	**$^{206}Pb/^{204}Pb$**	**$^{206}Pb/^{204}Pb$ corr.**	**$^{207}Pb/^{204}Pb$**	**$^{207}Pb/^{204}Pb$ corr.**	**$^{143}Nd/^{144}Nd$**	**εNd**
JH 58	10	11	Holocene	0.708961±8	19.7499±18	19.77	15.6442±15	15.66	0.511768±6	-16.97
JH 59	30	31	Holocene	0.708919±9	19.8207±34	19.84	15.6638±27	15.68	0.511776±4	-16.81
JH 60	50	51	Holocene	0.708906±8	19.7849±50	19.80	15.6480±40	15.66	0.511779±5	-16.76
JH 61	103	104	Holocene	0.708998±8	19.8519±16	19.87	15.6550±12	15.67	0.511701±5	-18.28
JH 62	150	151	Holocene	0.708891±7	19.1835±13	19.20	15.5796±12	15.60	0.511831±5	-15.74
JH 63	200	201	Holocene	0.708869±7	19.2295±16	19.25	15.5947±14	15.61	0.511791±5	-16.52
JH 64	250	251	Holocene	0.708913±7	19.4334±39	19.45	15.6142±32	15.63	0.511747±5	-17.38
JH 65	300	301	Holocene	0.709257±9	20.1693±34	20.19	15.7114±28	15.73	0.511472±5	-22.75
JH 66	320	321	Glacial/ Deglacial	0.709256±8	20.5716±24	20.59	15.7525±20	15.77	0.511371±5	-24.72
JH 67	350	351	Glacial/ Deglacial	0.708931±7	19.6395±22	19.66	15.6313±18	15.65	0.511600±5	-20.25
JH 68	380	381	Glacial/ Deglacial	0.709299±8	21.8362±23	21.86	15.8806±16	15.90	0.511222±6	-27.62
JH 69	391	392	Glacial/ Deglacial	0.709560±7	22.6510±20	22.67	15.9720±14	15.99	0.511166±5	-28.71
JH 70	401	402	Glacial/ Deglacial	0.710115±7	22.4289±37	22.45	15.9442±25	15.96	0.511159±4	-28.85
JH 71	415	416	Glacial/ Deglacial	0.710477±7	24.6347±37	24.66	16.2067±20	16.22	0.511042±5	-31.13
JH 72	425	426	Glacial/ Deglacial	0.709752±8	23.1072±21	23.13	16.0322±14	16.05	0.511155±5	-28.93
JH 73	450	451	Glacial/ Deglacial	0.710848±9	25.349±22	25.37	16.291±15	16.31	0.510995±6	-32.05

9.2 Mineralogical Data (XRD)

Table 9-5: Mineralogical composition of the < 63 µm sediment fraction of core GeoB22346-3 from the Clyde Inlet head.

Sample ID	Sediment Depth [cm]		Mineral Content [%]						
	Top	Bottom	Quartz	Albite	K-feldspar	Mica	Other Phyllosilicates	Amphibole + Pyroxene	Others
JH01	20	21	33	24	12	13	10	6	2
JH02	123	124	27	16	11	33	9	3	0
JH03	128	129	31	31	8	21	2	7	1
JH04	172	173	36	27	10	5	1	10	10
JH05	270	271	23	14	9	39	7	4	5
JH06	345	346	21	14	17	27	7	4	9
JH07	420	421	23	18	11	24	10	7	6
JH08	500	501	33	31	12	9	2	9	4
JH09	560	561	27	21	12	17	8	7	8
JH10	568	569	27	36	10	15	2	5	5
JH11	630	631	27	29	10	15	9	7	5
JH12	680	681	31	26	10	11	13	10	0

Table 9-6: Mineralogical composition of the < 63 µm sediment fraction of core GeoB22357-3 from the Baffin Island shelf.

Sample ID	Sediment Depth [cm]		Mineral Content [%]							
	Top	Bottom	Quartz	Albite	K-feldspar	Mica	Other Phyllosilicates	Amphibole + Pyroxene	Carbonates	Others
JH14	10	11	31	26	16	16	1	7	3	
JH16	54	55	32	22	12	21	2	9	3	
JH18	154	155	31	27	13	15	4	7	4	
JH20	254	255	32	26	12	13	2	5	9	
JH22	304	305	36	27	13	10	2	6	6	
JH24	381	382	28	23	25	9	4	7	4	
JH26	454	455	28	25	13	18	4	7		4
JH28	554	555	26	30	15	19	4	7		
JH29	604	605	31	29	16	18	4	2		
JH30	654	655	34	24	11	18	3	8		
JH31	704	705	33	30	14	10	4	8		
JH32	726	727	39	25	12	15	3	7		
JH33	752	753	43	20	14	11	5	6		
JH34	778	779	44	24	13	11	2	5		
JH35	804	805	28	29	12	20	4	2		6
JH36	841	842	33	29	15	13	0	9		1
JH37	876	877	43	32	17	0	1	7		

9.3 Radiogenic Isotope Data for Standard Reference Material

Table 9-7: Radiogenic isotope data of standard reference material measured with the thermal ionization mass spectrometer during the PhD project.

NIST SRM 987		JNdi-1		NIST SRM 981		
Date	**$^{87}Sr/^{86}Sr$**	**Date**	**$^{144}Nd/^{143}Nd$**	**Date**	**$^{206}Pb/^{204}Pb$**	**$^{207}Pb/^{204}Pb$**
06.10.20	0.710225±5	14.10.20	0.512092±6	14.10.20	16.9139±11	15.4611±10
14.10.20	0.710227±6	12.11.20	0.512123±5	19.10.20	16.8991±8	15.4414±8
10.06.20	0.710217±6	14.07.20	0.512098±6	02.03.20	16.8990±8	15.5441±10
25.06.20	0.710231±9	17.02.20	0.512131±5	02.03.20	16.8895±7	15.4286±7
28.01.20	0.710283±7	20.02.20	0.512116±6	02.03.20	16.8985±7	15.4418±7
28.01.20	0.710251±8	20.02.20	0.512124±6	03.06.20	16.9025±26	15.4466±26
28.01.20	0.710231±8	21.07.20	0.512111±6	23.06.20	16.8958±6	15.4376±7
28.01.20	0.710251±7	08.06.21	0.512097±5	28.05.21	16.8972±10	15.4383±10
11.05.21	0.710255±8	12.08.21	0.512113±5	07.07.21	16.8991±9	15.4290±10
14.07.21	0.710231±7	03.11.21	0.512116±5	29.10.21	16.9031±11	15.4475±10
26.10.21	0.710232±6	24.03.22	0.512124±4	22.03.22	16.9124±11	15.4600±11
28.02.22	0.710245±7	27.10.22	0.512106±5	02.02.22	16.8946±8	15.4357±7
10.03.22	0.710253±5					
10.03.22	0.710250±4					
14.03.22	0.710242±9					

References

Jacobsen, S.B., Wasserburg, G.J., 1980. Sm-Nd Isotopic Evolution of Chondrites. Earth and Planetary Science Letters 50, 139-155.

Nissen, F., Matthiessen, J., Stein, R., 2010. Sedimentary Environment and Glacial History of the Northwest Passage (Canadian Arctic Archipelago) Reconstructed from High-Resolution Acoustic Data. Polarforschung 79, 16.

Stein, R., Nissen, F., Matthiessen, J., 2009. Marine Geology.- In: W.Jokat (ed), The Expedition of the Research Vessel "Polarstern" to the Artic in 2008 (ARK-XXIII/3), Reports of Polar and Marine Research. Alfred-Wegener Institut für Polar- und Meeresforschung, Bremerhaven, Germany, pp. 12-15.

Vare, L.L., Massé, G., Gregory, T.R., Smart, C.W., Belt, S.T., 2009. Sea ice variations in the central Canadian Arctic Archipelago during the Holocene. Quaternary Science Reviews 28, 1354-1366.